INTERFACIAL ASSEMBLY IN AQUEOUS TWO PHASE SYSTEMS

Sarah Danielle Hann

A DISSERTATION

in

Chemical and Biomolecular Engineering

Presented to the Faculties of the University of Pennsylvania

in

Partial Fulfillment of the Requirements for the

Degree of Doctor of Philosophy

2017

Co-Supervisor of Dissertation

_____

Daeyeon Lee

Professor of Chemical and Biomolecular Engineering

Co-Supervisor of Dissertation

_____

Kathleen J. Stebe

Richer & Elizabeth Goodwin Professor of Chemical and Biomolecular Engineering

Graduate Group Chairperson

_____

John C. Crocker

Professor of Chemical and Biomolecular Engineering

Dissertation Committee

Daniel A. Hammer, Alfred G. and Meta A. Ennis Professor of Bioengineering and Chemical and Biomolecular Engineering

Robert A. Riggleman, Associate Professor of Chemical and Biomolecular Engineering

INTERFACIAL ASSEMBLY IN AQUEOUS TWO PHASE SYSTEMS

To Brandon and my family.

ACKNOWLEDGEMENTS

The first people I must acknowledge are my fearless co-advisors, Kate Stebe and Daeyeon Lee. Each time someone asks me who my "real" advisor is, I gratefully reflect on the truly collaborative and inspired team we have become over my five years at Penn. As the original "Stebe-Lee" group member, we didn't know what to expect, but I am so lucky to have been there for the start. Your availability and support have been insurmountable to my development not only as a researcher, but as a person. I strive to be the type of mentor you both have been to me and I will look back on my time as a graduate student fondly due to your diligent leadership.

I would also like to thank my committee members, Dan Hammer and Rob Riggleman, for spirited discussions, brainstorming, and helpful criticism along the way to writing this thesis. I appreciate your openness to share your respective expertise that helped craft our thinking and inspire our next steps in taking on this new project.

My time at Penn would not have been nearly as enjoyable, let alone successful, without the support of the many colleagues and friends I have had the pleasure of interacting with. Being a part of two labs meant I had twice the number of people to brainstorm with and be inspired by, and each one has had an impact on my work. To the many Post-docs, PhDs, Masters, and Bachelors students with whom I have crossed paths: thank you. Thank you to the many people from the Lee and Stebe Labs including: Kwadwo, Lei, Teresa, Sang-Wook, Zaki, Weifeng, Elio, Zach Y., Zach S., Alex, Rohini, Jacob, Yeongseon, Fuquan, Tae Soup, Likai, Miju, Ankit, Martin, Heon-Ho, Harim, Woo-Sik,

Tagbo, Laura, Yuanchi, Katie P., Gang, Jyo Lyn, David, Wei-Han, Zhiwei, Neha, Giuseppe, Syung Han, Renjing, Katie R., Sam, Nima, Francesca, Mohamed, Marcello, Lu, Ningwei, Liana, Iris, Yimin, Lisa, Tianyi, Ali, and Arvind. Especially thanks to Nate with whom I shared an office for five years, an apartment for two, and never turns away from a brainstorming session.

To gain clarity in lab, sometimes one must leave it, and leaving lab to play (and win) various sports leagues has been a particularly memorable opportunity. Thank you to the many teammates in Softball, Kickball, and Frisbee, especially Melissa, Jason, Berger, Cory, Nick, Ben, Mike, Chris, Brad, David, Ian, Julie, Lindsey, and Ellen.

Lastly, I would have never started nor lasted on this journey without the support of my family, Jo Ann, Todd, Bradley and Chris, or fiancé, Brandon. Thank you all for being so understanding of my sometimes difficult schedule and making sure that in between writing papers and being in lab, I never lost sight of the end goal. I appreciate each of you dearly.

ABSTRACT

INTERFACIAL ASSEMBLY IN AQUEOUS TWO PHASE SYSTEMS

Sarah Danielle Hann

Daeyeon Lee and Kathleen J. Stebe

Stabilizing bio-friendly and cyto-mimetic fluid structures has important implications for drug and gene delivery, micro bio-reactors, single cell and microniche studies, and as protocells. The majority of stabilization techniques have been developed for oil-in-water and water-in-oil emulsions, which have limitations in their application to biological systems due to the presence of the oil phase. The structures built in this thesis are therefore made within water-in-water dispersions. These all water dispersions are from aqueous mixtures of two polymers that demix to form two phases, termed aqueous two phase systems (ATPSs). ATPSs are comprised of two water-rich phases and are therefore excellent candidates for hosting or implantation within biological systems. In this thesis, challenges to stabilizing ATPSs are identified and discussed, including the ultra-low interfacial tension characteristic of these systems, and new strategies are developed to overcome such challenges. The first system studied is that of casein and xanthan (a protein and a polysaccharide) which undergoes spinodal decomposition, resulting in a transient bicontinuous structure. Colloids present in this phase-separating mixture attach at the water-water interface owing to capillarity, despite the low interfacial tension. This occurs for both living and passive colloids. The living colloids, *Escherichia coli* and *Pseudomonas aeruginosa* bacteria, ultimately break down and restructure the

bicontinuous matrix, indicating the bacteria can cooperate with the structure. The second system studied is the aqueous mixture of two polymers, poly ethylene glycol (PEG) and dextran. The PEG-dextran system is used to study emulsion stabilization techniques and understand the nuances of building materials at all water interfaces, specifically using polyelectrolyte complexation. In this study, oppositely charged polyelectrolytes are delivered from droplet and continuous phases to form a complex layer at the interface that stabilizes a water-in-water emulsion. Since the polyelectrolytes are soluble in both phases, successful interfacial complexation requires that polyanion and polycation fluxes be balanced such that they meet at, rather than around, the interface. Otherwise, non-stabilizing complexes are formed either inside or external to the droplet, far from the interface. This strategy is utilized to create microcapsules that can support a microbial community within the lumen. Interestingly, when one of the polyelectrolytes is replaced with a charged nanoparticle, the formation of stabilizing complexes is far less dependent on nanoparticle flux, as nanoparticles remain in the phase in which they are originally dispersed. Intriguingly, nanoparticle-polyelectrolyte complexation favors spontaneous double emulsion formation; we name these structures AWE-somes as they are water emulsion bodies. The mechanism for their formation relies on the osmotic pressure imbalance between the droplet and continuous phases. The encapsulated double emulsion structure is reminiscent of membrane-less organelles within biological cells, which comprise internal membrane-less compartments enclosed by a permeable membrane. This motivates the study of transport within the AWE-some structures. Small and large molecules can diffuse into the lumen and selectively partition to the PEG or dextran phases inside the nanoparticle and polyelectrolyte membrane. One drawback of the

nanoparticle-polyelectrolyte shell is less flexible than the membrane formed by the polyelectrolyte pair. To imbue the nanoparticle decorated capsules with both flexible membranes and spontaneous multiple compartments, compound capsules are fabricated in which the continuous phase initially includes both anionic polyelectrolyte and negatively charged nanoparticles. These compound capsules have tunable flexibility and stimulus responsive properties, which are important for fortifying the capsules for various biological environments. Future studies will include the incorporation of biological molecules including DNA and proteins to demonstrate further biological functionality.

TABLE OF CONTENTS

LIST OF TABLES

LIST OF FIGURES

CHAPTER 1. Introduction

1.1 Motivation: Stabilization of Water-Water Mixtures

As a liquid transforms from an initially miscible single phase to a final two phase state, it presents a variety of intermediate structures along the path to complete phase separation. The morphology of such intermediate structures is determined by the path taken into the phase separated region. For example, a binary liquid system that is thermally quenched into the two phase region through the critical point will undergo phase separation by creating a bicontinuous structure, often referred to as spinodal decomposition. Alternatively, two phases can be mixed to create an emulsion with one phase dispersed in the other that would ultimately coarsen over time to form two macroscopically separated phases. By stabilizing these intermediate structures, either kinetically or thermodynamically, multiphasic liquid mixtures with high surface areas can be produced. Such stabilized multiphasic mixtures are important in a number of applications for encapsulation and delivery that range from using encapsulated fluids as microreactors to micro-niche studies for biological cells. Although stabilization techniques are well developed for oil-water based systems, their applicability to many biological or environmental systems can be limited due to the presence of the potentially deleterious oil phase. By replacing the oil phase with another water phase, to create a water-water system, stabilized multiphasic mixtures for applications in drug/gene delivery, micro bio-reactors, nano-cultures, and cell-mimetic studies can be prepared that allow sequestration of delicate cargo. We are therefore motivated to create such high interfacial area

structures in an all-aqueous environment by identifying and addressing key challenges in the stabilization of water-water systems to enable their applications in biologically and environmentally relevant settings.

1.2 Background

1.2.1 Self-Assembly at Fluid Interfaces

Fluid interfaces exist between two phases that are immiscible; the energy associated with these interfaces is characterized by the surface tension. The total energy contribution from the interface scales as the product of the surface tension and the interfacial area. Therefore, to minimize the energy of the system, the lowest energy state is one with the lowest interfacial area, or a macroscopically phase separated state.

Another way to reduce the interfacial area is to introduce a third component before or during phase separation. With the appropriate chemistry, the third component, which can comprise nanoparticles or other colloids, accumulates at the interface between the two immiscible phases, thereby reducing the interfacial area. The thermodynamically-driven accumulation of particles at the interface is one means of self-assembly. The driving force for self-assembly at the interface also scales as the product of the interfacial tension and interfacial area taken up by the colloid, and is known as the trapping energy.

For typical oil-water systems, the trapping energy for individual particles of a range of sizes can be 10^2-10^4 k_BT, and these moieties will therefore be kinetically trapped at the interface. In this trapped state, the interface is considered stabilized. These trapped states are exploited to form particle-stabilized emulsions, known as Pickering emulsions.[1]

When the oil phase is replaced with another water phase to create a water-water interface, the interfacial tension is reduced significantly by up to 3-4 orders of magnitude, therefore reducing the trapping energy. These special low tension interfaces will be the focus of this thesis.

1.2.2 Aqueous Two Phase Systems (ATPS): Water-water interface

Water-water interfaces result from a special class of mixtures known as aqueous two phase systems (ATPSs). ATPSs are aqueous mixtures of two thermodynamically-incompatible, water-soluble components that can comprise two polymers, a polymer and a salt, or a protein and a polysaccharide, among other combinations of hydrophilic materials. The phenomenon was first observed in the late 1890s by microbiologists in a system of gelatin-agar-water[2] and later greatly expanded on in other ATPSs for use in two-phase extraction schemes of biological molecules.[3–5]

The two primary characteristics of ATPS are an ultra-low interfacial tension ($\gamma \leq 10^{-1}$ mN/m) and a broad interfacial width.[5–10] Both of these characteristics complicate interfacial assembly of molecules and colloids. If allowed to equilibrate, ATPS phase separation can take a day to relax; these prolonged timescales, attributable to the ultralow tension and the relatively high viscosity of the mixture, are much longer than a typical oil-water system. As stated in Section 1.2.1, the ultralow interfacial tension reduces the trapping energy, and therefore the driving force, for particle attachment. The broad interfacial width also affects the ability for molecules to self-assemble at the interface

because the two aqueous phases are interpenetrating near the macroscopic interface, resulting in a diffuse interphase layer of about 7-10 nm.

Despite these challenges, researchers have developed a few techniques that enable stabilization of ATPS. Transient stability has been imparted to ATPS to compartmentalize biological materials.[11–16] More stable interfacial assemblies involve chemically distinct tri-block copolymers,[17] flat nanoparticles (that are the approximate width of the interface),[18,19] or protein particles.[20–22] Each of these techniques requires a particular selection of materials based on the ATPS used, and a generalized approach and understanding for stabilization has not yet been achieved.

1.2.3 Polyelectrolyte Complexation

One phenomenon that will be explored in Chapters 3-5 is that of interfacial polyelectrolyte complexation. Polyelectrolytes (PEs) are charged polymers that dissociate in solution; PEs are categorized as either 'weak' or 'strong'. Weak PEs are polymers with degrees of ionization that can be tuned by pH.[23] Strong PEs will remain fully charged in solution, regardless of pH; the PEs used in this thesis are all strong PEs. Polyelectrolyte complexation occurs when two oppositely charged polymers are introduced in solution and they associate driven by the entropy gain upon counter ion release.[24] Once complexed, the PEs form condensed entities whose structure and properties can be tuned by stimuli such as pH (for weak PEs) or salt (for strong PEs).[25–27]

Polyelectrolyte complexation at interfaces has been studied extensively in the production of functional films, in which oppositely charged PEs and/or nanoparticles are

sequentially added in a layer-by-layer process on solid surfaces.[28–31] Recently, water-in-oil emulsions generated within microfluidic devices have also been stabilized by PE complexes to create PE microcapsules.[32–34] Given their ionic nature, however, the delivery of PE from the oil phase can present a major challenge, as charged species in non-polar media require particular selection of material and potentially extra processing steps, limiting the applicability of this technique.[35]

Here we introduce a nomenclature, PE/PE, in which any membrane-forming components before the slash are introduced in the droplet phase, while those after the slash are introduced in the external phase.

1.3 Objectives and Outline

The main objective of this thesis is to stabilize water-water interfaces, both bicontinuous and emulsion-based, by understanding the interfacial phenomena associated with ATPS, and in turn to fabricate biologically and environmentally friendly functional materials using ATPS. This thesis explores the interaction of live bacteria with water-water interfaces. Additionally, interfacial complexation of polyelectrolytes and nanoparticles is explored to impart stability within an ATPS emulsion and to produce novel compartmentalization systems. Lastly, a combination of techniques is used to modulate capsule properties and demonstrate control over stabilized microcapsules.

Chapter 2 addresses the feasibility of assembling either microbes or microparticles at the interface in a bicontinuous ATPS. This chapter describes and compares how live bacteria and inert colloids interact with all aqueous interfaces.

Chapter 3 describes the polyelectrolyte complexation within ATPS and, in particular, addresses the objective of understanding the nuances with working in these all-water phases. Relevant transport effects are investigated and general rules for using PEs within ATPS are described. Additionally, bacteria-containing microcapsules are created to demonstrate the feasibility of using PE microcapsules as micro-niches or delivery vehicles.

Chapter 4 builds on the PE/PE complexation in *Chapter 3* by replacing one PE with a nanoparticle (NP) (PE/NP). The change in complexing agent significantly changes the structure and properties of the microcapsules; this chapter presents a mechanistic scheme to explain these results. The potential of using these nanoparticle-containing (PE/NP) microcapsules as protocells is demonstrated.

Chapter 5 combines the materials and mechanisms of *Chapters 3* and *4* to show that distinct structural and functional control over the all-aqueous microcapsules based on ATPS can be achieved. We demonstrate that the structures and properties can be precisely controlled and augmented through the inclusion of both PE and NP in the continuous phase during capsule formation.

Chapter 6 summarizes the conclusions of this thesis and identifies opportunities and open questions for future investigation of the field.

CHAPTER 2. Trapping and Assembly of Living Colloids at Water-Water Interfaces

Reprinted (adapted) with permission from S. D. Hann, M. D. Goulian, D. Lee, K. J. Stebe. Trapping and assembly of living colloids at water-water interfaces. Soft Matter, 2015, 11, 1733-1738. Copyright (2015) Royal Society of Chemistry.[36]

2.1 Introduction

Fluid interfaces provide excellent environments to locate and organize particles, as evidenced by the rich and rapidly evolving literature focusing on the interaction and assembly of particles at interfaces.[37–43] Pieranski's seminal work demonstrated the ability of interfaces to trap colloids, and the ability of the colloids at interfaces to form phases and structures which can be modulated by tuning interparticle interactions.[44] This work has spawned numerous studies in which capillary interactions and packing constraints are exploited to induce organization of particles into two- and three-dimensional structures.[42,45,46] When colloids are present in systems of two immiscible fluids, they attach to the interface to lower the interfacial area, thereby lowering the total system energy. In the case of conventional oil-water systems, this interfacial energy is significant and leads to a high trapping energy.[44] Depending on the nature of interactions between the immiscible fluids and the concentration of colloids, such systems can be stabilized in a range of states ranging from Pickering emulsions[1] and foams,[47] to non-spherical droplets stabilized by particle monolayers.[48,49]

Interfaces with far lower interfacial tension, formed, for example, by spinodal decomposition, also trap particles at the interface, as has been exploited to form bicontinuous interfacially-jammed emulsion gels (bijels).[50,51] We are particularly interested in studying colloidal behaviour in all aqueous systems. Interactions within these systems can be tuned to achieve a wide range of phase transitions, including phase separated systems in which the two phases form via spinodal decomposition.[52] The resulting interfaces have an interfacial tension, albeit one which is orders of magnitude lower than that in the more conventional oil-water systems.[7] Our interest stems from the potential for these systems to sustain living species, opening the door to creating three dimensional structures using living colloids such as bacteria cells.

The development of non-trivial structures to confine and organize living colloids can have significant impact not only from a materials viewpoint, but also from a fundamental perspective in the study of the dynamics of living colloids in confinement. A rich literature is developing on the collective dynamics and self-organization of bacteria swimming in confined systems, including quasi-2D systems[53], 3D confining systems[54], and for bacteria trapped at/near fluid interfaces.[55–57] Aqueous two phase systems, such as those studied here, can allow us to create soft, topographically complex, or, in the case of bicontinuous systems or systems with interconnecting pathways, topologically complex systems in which to confine bacteria to study their dynamics.

In this chapter, we have successfully trapped living bacteria at the interface between casein-rich and xanthan-rich phases. Our results, for both living and inert

colloids, strongly suggest that these bacteria attach to the interface to lower the interfacial area. These experiments serve as a proof of principle for this new domain of materials which can be used as dynamic, phase separating vehicles for studies in food science, medicine and materials science.

2.2 Materials and Methods

2.2.1 Stock Solution Preparation

Stock casein and xanthan were prepared following the procedures described in the numerous phase separation studies.[52,58,59] The casein, obtained from Fisher, was used to prepare a 10 wt% solution; the casein was stirred with 0.1 wt% NaOH in water at 55°C for 2 hours then stirred at room temperature for another 2 hours. The stock xanthan, generously supplied by CP Kelco, (Keltrol – food grade xanthan gum) was used to make a 0.2 wt% solution by mixing 0.1 M NaCl with the xanthan in water and stirring at 70°C for one hour before stirring overnight at room temperature. Both stocks were then kept at 4°C.

2.2.2 Sample Cell Preparation

The solutions were placed in a well formed within a polydimethylsiloxane (PDMS) slab by using a rectangular mold, suitable for placement on a microscope stage. The well holds 50 μL of solution, and is approximately 500 μm deep. It was filled with the solution to be observed, and immediately sealed using a coverslip as a lid, as depicted in Figure 2.1. When the wells were not being imaged, they were kept

in a 100% humidity chamber to prevent evaporation, and wrapped in a protective foil to prevent photo bleaching of fluorophores used to label various constituents.

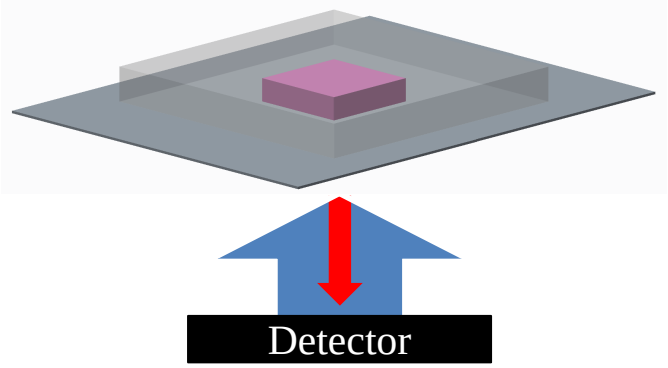

Figure 2.1. Schematic of experimental setup. Casein-xanthan suspension was enclosed in a PDMS cell on top of a coverslip. Total sample thickness was 500 μm. Imaged on inverted confocal laser scanning microscope (CLSM).

2.2.3 Bacteria Preparation

Four species of bacteria were used in this study: *Pseudomonas aeruginosa* (PA01), *Pseudomonas sp.62*, non-motile GFP-labelled *Escherichia coli* (MDG10 – a derivative of MC4100), and motile WT *E. coli* (MG1655). All species were cultured at room temperature in LB broth for 2 days. The bacteria were all harvested in stationary phase and then stored at 4°C for 1 day. These bacterial suspensions were then centrifuged and the pellet was re-suspended in phosphate buffered saline (PBS) before adding to the sample solution.

We monitored both WT and GFP *E. coli* strains during various periods throughout the phase separation at 20 μm above the coverslip for short periods of time. These movies (Supplementary Information of Ref 36, movies S1-S3) reiterate the free motion that the WT *E. coli* has immediately after mixing versus

24 hours after mixing. Once trapped at the interface, they do not swim. This lack of motility is either because they are trapped at the interface and cannot move or they have turned off their motility gene. No additional verification was done investigating the gene expression through time. The lack of motion of the GFP *E. coli* in Movie S3 is shown as verification that we have used a non-motile strain.

2.2.4 Solution Preparation

The solutions and suspensions used in experiments were mixed approximately 20 min before $t = 0$. In all studies, the casein concentration was kept constant at 2 wt%. Xanthan was added at 0.08 wt% and the bacterial suspension was added at about 0.01% solids. PBS was added to achieve the desired wt% after addition of the stock solutions. 5 μL of a 0.05 wt% Rhodamine B (Fisher) solution was added per 1 g sample. Green fluorescent polystyrene (PS) beads (1 μm diameter) from Sigma were used for the non-bacteria experiment, also at 0.01% solids. For the non-fluorescent bacteria, a 3 μL/100 mL SYTO 9 solution was also added at 50 μL/1 g solution. The solution was mixed on the vortex mixer for 3 pulses and added to the PDMS cell. The final pH of the solution was approximately 6.3.

2.2.5 Sample Imaging

Solutions were imaged using confocal laser scanning microscopy (CLSM) on an Olympus IX81. The 512 x 512 pixel images were taken using a 40X water immersion lens excited by 488 nm and 543 nm lasers and collected through EGFP and Rhod 2 filter sets. Images were compiled using ImageJ Software.

2.3 Results and discussion

2.3.1 Living colloids at the interface

We exploit the aqueous phase separating system of casein and xanthan, which can be tuned by varying the relative concentrations of each component.[52,59] This system is relatively well studied, as it is widely exploited in the formulation of foodstuffs such as dairy products.[60] It is particularly interesting as a model system to investigate the interactions between living colloids and interfaces because these components are known to undergo spinodal decomposition under certain conditions, in particular when the casein is a part of skim milk powder (SMP).[52,58] We are working with solely casein and xanthan at concentrations near the previously reported spinodal point; Rhodamine B dye was added to the mixture to directly visualize the casein phase. Under these conditions, the system visually resembles an interconnected, bicontinuous structure. Furthermore, the protein phase has the potential to serve as a nutrient source for the bacteria in the system if the bacteria possess the correct enzymes, which allows the possibility for the bacteria to degrade and consume the structure over time.

We chose a wild type (WT) *E. coli* [MG1655] stained with SYTO 9 to ascertain whether living colloids attach to the interface of this phase separating casein-xanthan mixture. WT *E. coli* serves as an ideal model bacterium, as it has been widely manipulated and exploited in the study of recombinant DNA technology and as a host for production of recombinant proteins such as insulin.[61] Initially, as shown in Figure 2.2A, the bacteria are scarce and are only observed

swimming in the casein-void regions, indicating that they are not immediately driven to the interface (Movie S1). Following the progression shown in Figure 2.2B – D, the bacteria attach to the interface within 16 h. Their accumulation at interfaces continues as the phase separation of the casein-xanthan mixture progresses; after 40 h, they have filled a large portion of the casein-xanthan interface. Figure 2.2F, a projection of the compiled 3-D scan taken with a confocal laser scanning microscope (CLSM), gives clear evidence of bacteria at the interface of the interconnected casein-xanthan phases. By allowing the system to continue to evolve over one week post-mixing, we can see in Figure 2.2E that there is barely any detectable red fluorescence remaining in the solution, indicating a loss of localization of the casein phase. Since the samples are kept at room temperature, the growth dynamics of the bacteria are slower than their typical growth at 37 ˚C, which allows our system to evolve and the bacteria to interact with its changing environment. At the end of one week, there were still live bacteria, as verified by agar plating. The progression from Figure 2.2A-E indicates the live bacteria are actively interacting with the matrix due to the segregation of the casein phase. As a control, the SYTO 9 dye was added to the casein-xanthan system devoid of bacteria; no increase or decrease in green or red fluorescence, respectively, was observed over time.

An important question arises regarding the mechanism for the localization of the bacteria at the interface. Since the bacteria may consume casein, it is plausible that bacteria may swim toward the casein-rich interface via chemotaxis.[62] To test whether such cell motility is critical in inducing the attachment of bacteria to the

interface between casein-rich and xanthan-rich phases, we use non-motile GFP *E. coli* [MDG10] as our living colloids in the same phase-separating system.

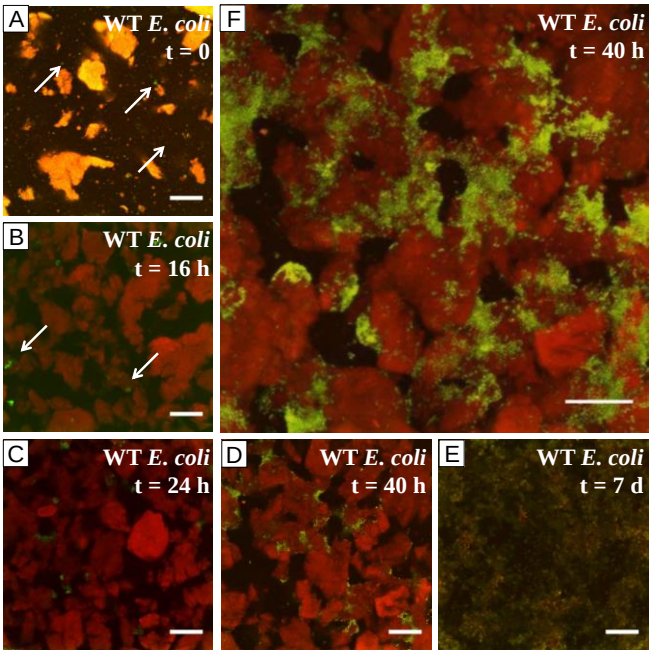

Figure 2.2. WT *E. coli* in casein-xanthan. Casein is stained red with Rhodamine B and *E. coli* is stained in green with SYTO 9. (A) Immediately after mixing, arrows showing free bacteria. (B) 16 h after mixing. (C) 24 h after mixing. (D) 40 h after mixing. (E) 7 d after mixing. (A-E) 20 μm above cover slip. (F) Projection of scan from top, 40 h after mixing. All scale bars 50 μm.

As shown in Figure 2.3, the non-motile bacteria attach to the interface within 24 h, and the density of interface-trapped bacteria increases with time. When the system was allowed to evolve for longer times, in addition to densifying, the casein-rich region fluorescence again diminished as in the motile WT *E. coli* case. We confirm that these non-motile GFP *E. coli* can survive on the casein by culturing them in a casein-added PBS solution, where the casein serves as the only possible carbon and nitrogen sources. As seen in Figure 2.3E, the bacteria have a slight increase in growth in the initial hours in

the casein solution and are able to maintain a relatively constant number over a week. In contrast, the bacteria are not able to survive on the xanthan alone. Thus, once bacteria are trapped at the interface, their ability to slightly degrade the casein likely contributes to the subsequent long-time restructuring of the matrix.

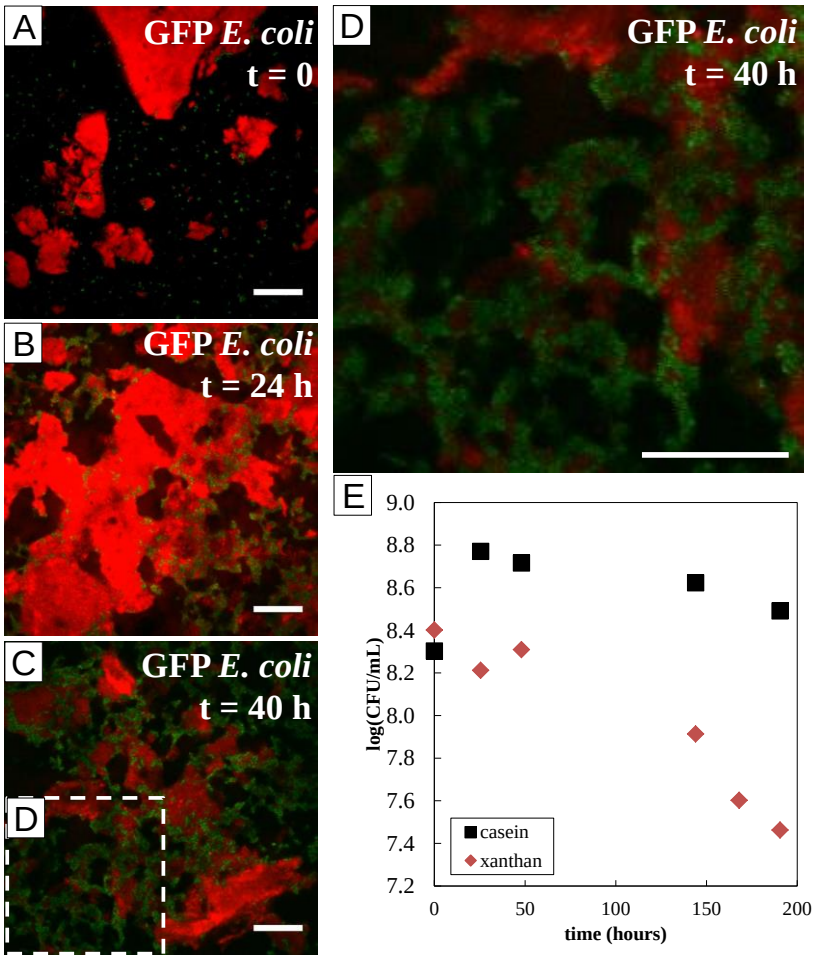

Figure 2.3. Non-motile, GFP E. coli in casein-xanthan mixture. Casein is stained red by rhodamine B and the E. coli is green. (A) Immediately after mixing. (B) 24 h after mixing. (C) 48 h after mixing. (D) Inset of (C). (E) Growth curve of GFP E. coli in 2 wt% casein solution (■) and 0.08 wt% xanthan (♦) in PBS, at 22 °C, measured by agar plating method. (A-D) taken 20 μm above cover slip, scale bar 50 μm.

We also observe interfacial attachment of other bacteria, including *Pseudomonas aeruginosa (*PA01) and *Pseudomonas sp.62* in this casein-xanthan system. For both species, the bacteria become trapped at the interface after ~16 h, and the phase separated mixture coarsens. A key difference is that *P. sp. 62* and PA01 can actively break down and consume casein at higher rates than *E. coli*, so the casein region diminishes more rapidly, Figure 2.4 and Figure 2.5. These results clearly demonstrate that phase separating aqueous mixtures can induce attachment of living colloids and sustain life, and that choosing specific bacteria strains affects the lifetime and dynamics of the matrix.

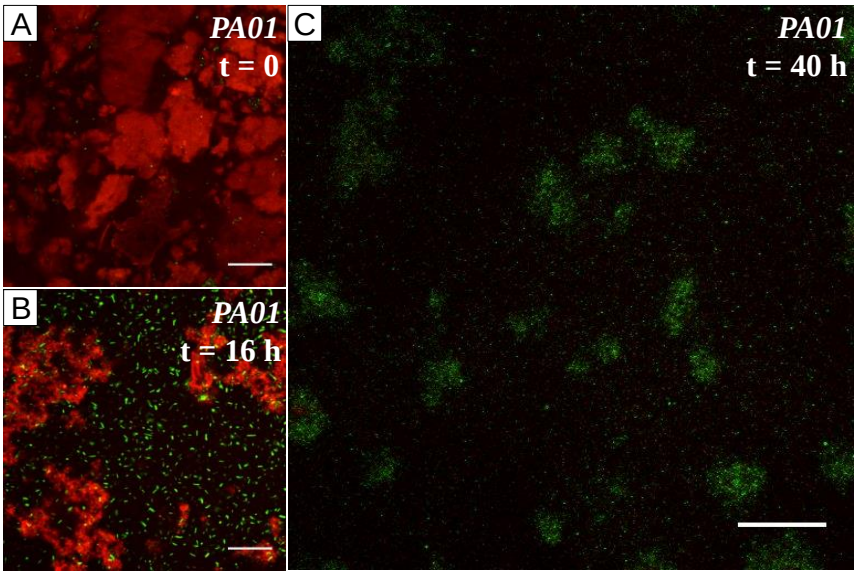

Figure 2.4. Time progression of *P. aeruginosa* (PA01) imaged in CLSM 20 μm above coverslip. Casein is stained with Rhodamine B and PA01 is stained with SYTO 9. (A) Immediately after mixing (B) 16 hours after mixing (C) 40 hours after mixing. All scale bars are 50 μm.

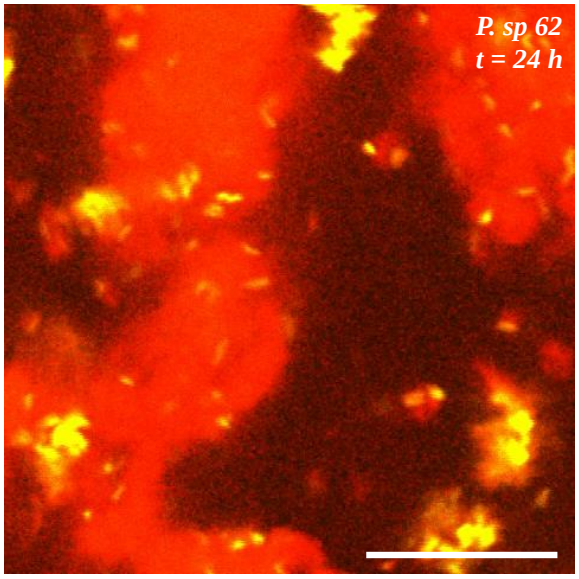

Figure 2.5. Image of *Pseudomonas sp. 62* in 2 wt% casein, 0.08 wt% xanthan solution 20 μm above coverslip. Scale bar 20 μm.

2.3.2 Inert colloids at the interface

Our results based on motile and non-motile *E.coli* suggest that chemotactic motility is not necessary to induce the attachment to the interface. To ascertain whether capillarity could be a likely mechanism, we estimate trapping energies owing to capillarity, *i.e.*, the energy associated with the reduction in the interfacial energy owing to particle attachment. The trapping energy of a colloid particle from an interface (ΔE) can be estimated as $\Delta E \sim \gamma A$, where γ and A denote the interfacial tension and the area of interface eliminated by particle attachment, respectively. A recent report has shown that interfacial tension between two aqueous phases made of poly(ethylene glycol) and dextran can be as low as 0.012 mJ/m^2.[7] Using this value along with the typical size of bacteria (~ 1 μm), we estimate that the trapping

energy at such an interface can exceed $10^3 k_B T$; this value is significant and indicates that once bacteria attach to the interface it may be extremely difficult to detach themselves from the interface. If, as this estimate suggests, capillary forces can account for the interfacial trapping of bacteria, then similar behaviour should be observable for inert colloids.

To confirm that the casein-xanthan system possesses sufficient interfacial energy to trap inert colloids at the interface, we added 0.01% green fluorescent polystyrene (PS) beads (*i.e.*, inert colloids) to the mixture at t = 0, Figure 2.6. After 24 h (Figure 2.6B), the beads are found only at the interface between the casein and xanthan regions. After 40 h, shown in Figure 2.6C, the phase separation has continued to progress and most of the casein regions within the viewing window are connected. This phase separation progression has occurred at room temperature and is nearly bicontinuous after 40 h as shown in Figure 2.6E. After this time point, the casein continues to densify and all components settle to the bottom. During the transition, however, we can see the inert colloids indeed remain trapped at the interface. Similar results have been reported recently for inert colloids in a phase separated system of gelatin and maltodextrin; the inert colloids were indeed trapped at the interface in a manner similar to oil-water-colloid three component systems.[63]

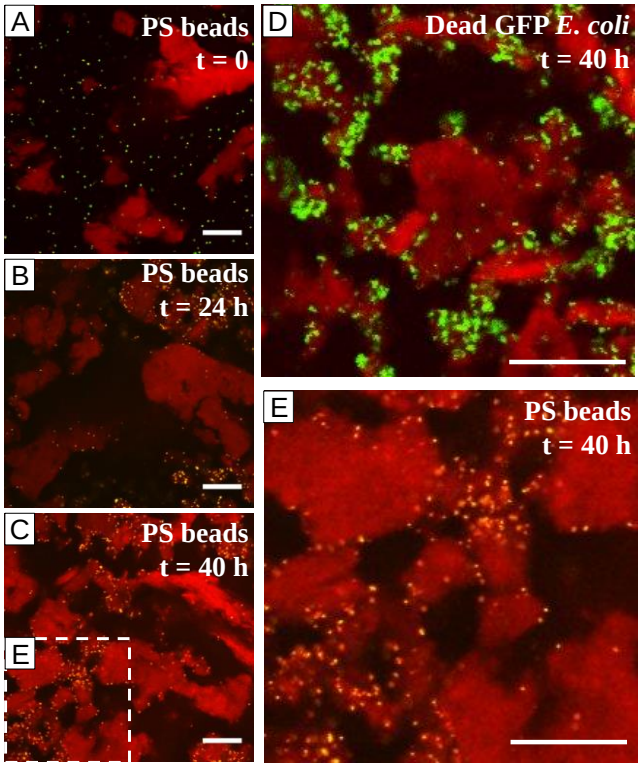

Figure 2.6. Inert colloids in casein-xanthan phase separating system imaged by CLSM. Casein is stained red by Rhodamine B, green are green fluorescent polystyrene (PS) beads (A,B,C,E) or spectinomycin-killed GFP *E. coli* (D). (A) PS beads immediately after mixing. (B) PS beads 24 h after mixing. (C) PS beads 40 h after mixing. (D) Dead GFP *E. coli* 40 h after mixing. (E) Inset of (C). All slices from 20 μm above glass, scale bars 50 μm.

To complement the PS bead study with inert colloids that more closely match the shape and surface chemistry of live *E. coli*, we repeated this experiment with antibiotic-killed GFP *E. coli*, with similar results. Within 24 h, the dead bacteria were trapped at the interface and remained so as the system evolved, as seen in Figure 2.6D. These results demonstrate that even weak interfacial tension can exert significant trapping energies, leading to attachment and trapping of particles at interfaces between two aqueous phases. The prolonged time required for the colloids to find the interface may be attributed to the highly viscous nature of the

xanthan phase. The colloids have significantly dampened Brownian motion in this two phase system.

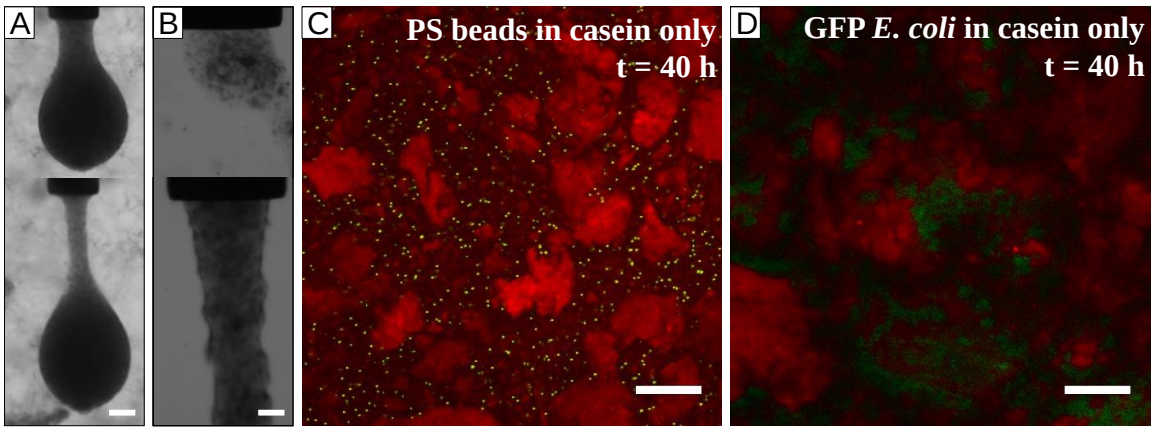

Figure 2.7. (A) Sequence of pendant drop experiment, drop fluid is 10 wt% casein, bulk fluid is 0.1 wt% xanthan, both filtered with 5 μm filter, scale bar 200 μm. (B) Sequence of pendant drop experiment, drop fluid is 10 wt% casein; bulk fluid is DI water, scale bar 200 μm. (C) PS beads in 2 wt% casein solution (no xanthan) 40 h after mixing. (D) GFP *E. coli* in 2 wt% casein solution (no xanthan) 40 h after mixing. (C) and (D) taken 20 μm above cover slip; casein is red, colloids are green; scale bar 50 μm.

It would be interesting to directly quantify the interfacial tension in this system. We attempted this measurement by performing a simple pendant drop experiment. When a casein solution (10 wt%) was injected slowly into a xanthan solution (0.1 wt%) through a tube, we observed the formation of a transient pendant drop which elongated continuously as shown in Figure 2.7A. In contrast, when xanthan was removed from the continuous phase, it was not possible to form a cohesive drop no matter how slowly we injected the casein solution, as shown in Figure 2.7B. These observations indicate that the presence of the casein-xanthan system leads to the development of interfaces that have a finite interfacial tension.

Our conclusion regarding the importance of surface tension in the interfacial attachment of living and inert colloids is further corroborated by adding bacteria to a casein-only solution. Figure 2.7C-D demonstrate that in the absence of xanthan, living and inert colloids do not attach to the blobs of casein phase even after 40 h post mixing, indicating that surface tension, albeit extremely small, is critical in making the particles attach to the interface. We were unable to determine a value for this tension, however, owing to the complex rheological nature of this system; the significant elasticity of the bulk phases can play a role in determining the shape of the droplet. This is particularly evident in the movies of pendant drop elongation (Movies S9-10), and in Figure 2.8 in which one side of the droplet is torn away. Even after continued elution, the torn drop edge remains jagged, a form that is not consistent with an interface dominated solely by interfacial tension. These non-Newtonian aspects preclude a comparison of the pendant drop shape to solutions of a Young-Laplace equation to extract the interfacial tension.

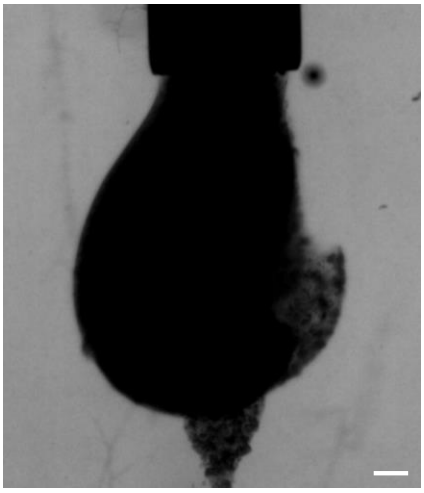

Figure 2.8. Frame from pendant drop experiment in which 10 wt% casein was eluted into 0.1 wt% xanthan. Scale bar is 200 μm.

2.4 Conclusions

We have demonstrated that living and inert colloids attach to the interface between two aqueous phases, including motile and immotile bacteria. Our results strongly indicate that the attachment of these colloids is due to the presence of appreciable capillary trapping energies owing to the weak but finite interfacial tension between the two aqueous phases. This system, which uses only biologically compatible components, has potential for the development of novel biomaterials and bioreactors that take advantage of bacterial interfacial assemblies. Furthermore, these results can be recapitulated in other aqueous-aqueous systems, (e.g. PEG-dextran), opening new possibilities to biologically-inspired materials research.

The organization that we observe may also be an important mechanism underlying the development of spatially structured microbial communities in natural settings, such as mixed-species biofilms. Bacteria synthesize numerous extracellular macromolecules, including polypeptides, polysaccharides, and nucleic acids, that form a protective matrix; xanthan gum secreted by the soil bacterium *Xanthomonas campestris* is one example. Macromolecules produced by distinct species may phase separate and drive specific bacterial populations to the interfaces, while the bacteria in turn control their localization by modulating the macromolecules anchored to their surface or by transforming the surrounding matrix. Thus, the interplay between the physicochemical properties of the fluid interfaces and the microbes' response to their environment may lead to complex

spatial ordering that enables species to occupy distinct niches and optimize efficient cross-feeding or protection from competitors.

CHAPTER 3. One-Step Generation of Cell-Encapsulating Compartments via Polyelectrolyte Complexation in an ATPS

Reprinted (adapted) from S. D. Hann, T. H. R. Niepa, K. J. Stebe, D. Lee. One-Step Generation of Cell-Encapsulating Compartments via Polyelectrolyte Complexation in an Aqueous Two Phase System, 2016, ACS Applied Materials & Interfaces DOI: 10.1021/acsami.6b07939. [64]

3.1 Introduction

The encapsulation of delicate, functional cargo within biocompatible capsules is central to diverse fields including the targeted drug delivery of pharmaceutical actives,[65–67] and live cell encapsulation,[68,69] with applications ranging from fundamental study of microbes[70–72] to the development of artificial organs.[73] Ideally, capsules should protect, store, and allow delivery of their cargo; the encapsulating membrane should be versatile in composition and function, and the entire capsule should not comprise materials that are potentially deleterious to the contents or the spaces into which they might be implanted or introduced.

Emulsion-templated capsule formation is one widely adopted, robust technique for achieving these goals. This method exploits microdroplets in an external, immiscible liquid phase; cargo can be placed in the drop internal phase as the drops are formed, and encapsulating membranes are formed by interfacial stabilization at the drop surface. The vast majority of these systems exploit water droplets in oil, often in the form of water-in-oil emulsions; the aqueous drop interior can sequester water soluble molecules or

aqueous suspensions, and the oil-water interface provides a robust site for membrane formation via chemical crosslinking,[65,74,75] interfacial trapping of particles,[1,76–78] or interfacial complexation and polymerization.[32–34,79–82] This method has several attractive features. The finite interfacial tension of the oil-water interface allows particles, surfactants and macromolecules to readily adsorb, where they can be further manipulated or reacted. Thus, interfacial assembly, in principle, allows diverse, functional contents to be incorporated by assembly into the membrane, and asymmetric membrane formation should be straightforward by selective assembly from either the drop interior or exterior phases. Finally, these methods can be adopted in scalable processes.

In order to make these techniques more biologically relevant, this chapter focuses on the fabrication of such multiphasic dispersions without the potentially deleterious oil phase, through the use of ATPS. In such systems, living cells have been successfully sequestered. However, the encapsulation of living cells in stable ATPS-based microcapsules, rather than hydrogel particles, has not been demonstrated to date, to our best knowledge. We investigate the potential of using ATPS to form cell-viable capsules with fluid interiors and robust, tunable, stimuli-responsive membranes via interfacial complexation of polyelectrolytes. To imbue our capsules with these features, we are inspired by the extensive work on the fabrication and application of microcapsules and microparticles formed via complexation of oppositely charged polyelectrolytes, achievable via layer-by-layer (LbL) assembly,[83–87] via thermal quench of heated microdroplets with polyelectrolyte complexes,[88] coacervates of polymers and nucleotides for protocell-mimetic structures,[89,90] or via interfacial complexation at oil-water

interfaces.[32–34] Polyelectrolyte complexes respond to various environmental factors, such as solution pH and ionic strength, which affect their physical properties, including their permeability and structural integrity. Recently, polyelectrolyte complexation has been demonstrated in an ATPS to create salt- and pH-responsive microcapsules and microgel particles.[91]

Here, we investigate the interfacial complexation of two oppositely charged polyelectrolytes in the ATPS of poly(ethylene glycol) (PEG) and dextran, a widely studied ATPS known to be biologically friendly.[92] We develop an improved understanding of factors that influence structure formation within ATPS of molecules that are, at best, only weakly trapped at the interface, and identify critical conditions that affect the final complexation structure. Based on this framework, we form ATPS-capsules. Within the fluid core, we sequester live bacteria cells, and demonstrate that the viability and proliferation of encapsulated cells can be interrogated by taking advantage of the permeability of the polyelectrolyte shell. Encapsulation of living cells in stable and tunable ATPS systems represents a potentially transformative advance that will enable the use of these compartments in the screening of antibiotics,[93,94] the development of food and pharmaceutical products[95] and the fundamental investigation of microbial interactions[70–72] in the complex environments of biofilms.[96]

3.2 Materials and Methods

3.2.1 Materials

Poly(ethylene glycol) (PEG, MW = 20,000 g/mol), dextran from Leuconostoc spp. (MW = 450,000 – 600,000 g/mol), poly(diallyldimethylammonium chloride) (PDADMAC, 20 wt.% MW = 200,000 – 350,000 g/mol and MW = 400,000 – 500,000 g/mol), and poly(sodium 4-styrenesulfonate) (PSS, MW = 70,000 g/mol) were purchased from Sigma-Aldrich. Fluorescein-labeled PSS (f-PSS) was synthesized based on a previous report.[97] Rhodamine B-tagged dextran (RD70, MW = 70,000 g/mol) was purchased from ThermoFisher Scientific. All chemicals were used as received.

3.2.2 Solution preparation

All solution composition % are given in wt%. A stock solution of 20% dextran was prepared by stirring (DI) water from a Millipore Milli-Q unit (> 18.2 MΩ·cm) with the appropriate amount of dextran on a stir plate overnight. This stock solution was subsequently mixed with aqueous solutions of either 20% PDADMAC, or 20% PSS, to which the remaining mass of DI water was added to achieve the desired polyelectrolyte (PE) concentration. A similar process was followed for the continuous PEG phase; a stock solution of 15% PEG was prepared by overnight mixing with DI water, and the respective amounts of PE and water were added to achieve the desired PE concentration. Osmotic pressures were measured with The Micro Osmometer Model 3000 (Advanced Instruments Inc.) courtesy of Prof. Hammer's laboratory at the University of Pennsylvania.

3.2.3 Polyelectrolyte complexation in pendant drops

Pendant drops were injected using an Attension Theta optical tensiometer. A needle of 0.85mm diameter injected 1 μL of 15% dextran/0.5% PDADMAC (MW 400,000 – 500,000) at a rate of 1 μL/s into a cuvette containing 3 mL of 10% PEG/PSS solutions. Recording of the drop was started as the drop was being injected at a rate of 6 frames/sec.

3.2.4 Capsule formation via electrospray

Capsules were made using an all-aqueous electrospray technique.[98] Briefly, 15% dextran droplet phases were prepared with either 0.5% PDADMAC (MW 200,000 – 350,000) or 0.64% PSS. This solution was loaded into a syringe and connected to tubing which is, in turn, connected to a tapered capillary with a tip diameter of 130 μm. The dextran solution was charged by connecting the inlet needle to one electrode from a high voltage power source. The opposite electrode was connected to a 2 cm-diameter copper ring placed 1 mm from the tip of the tapered capillary. This arrangement applies the complimentary electric force which pulls the micron-scale droplets out of the capillary. The droplets were fabricated at a flow rate of 1 mL/hr with an applied voltage of 4.8 kV. For encapsulation of bacteria, the diameter of the capillary tip was 70 μm, and droplets were fabricated at a flowrate of 4 mL/hr with an applied voltage of 4 kV. These droplets were sprayed into the 10% PEG solution with the oppositely charged polyelectrolyte. Polyelectrolyte concentrations are defined based on molar charge ratios of the two polyelectrolytes. Both polyelectrolytes used in this study contribute one charge per repeat unit. For example, the molar charge ratio of a 1:1 solution corresponds to one mole of each polyelectrolyte, 207 g PSS:161.5 g PDADMAC, or 1.28 g PSS:1 g PDADMAC. In

this example, for a dispersed phase of 15% dextran/0.5% PDADMAC, the continuous phase is 10% PEG/0.64% PSS to achieve the 1:1 molar charge ratio.

3.2.5 Triggered release tests

Experiments were performed within microdialysis cells to probe the release properties of capsules in response to changes in the ionic strength of the solution. In order to gently change the solvent conditions around fabricated microcapsules, all solvent exchanges performed on the capsules were made within microdialysis cells, Figure 3.1. The large membrane pores (1 μm) allow easy exchange of solvent, allow PEG to be removed, and allow salt to be added.

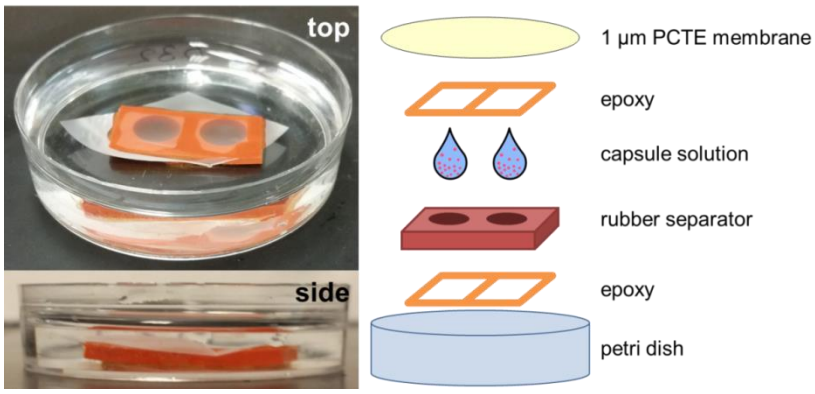

Figure 3.1. (left) digital images of microdialysis cell (right) Schematic depiction of microdialysis cell used to dialyze water against capsules to remove wrinkles.

Polycarbonate track-etched (PCTE) membranes (1 μm pores) were used to allow passage of water and salt solutions between the two chambers of the microdialysis cell. Total intensity loss of RD70 was measured by averaging the fluorescent intensity of monitored capsules in ImageJ at different time points and normalizing by initial time intensity.

Initial time t = 0 marks the time at which the bulk solution within the microdialysis cell was exchanged.

3.2.6 Bacterial culture capsules

Capsules containing bacteria were created by mixing 15% dextran, 0.64% PSS, 20 μL/mL *Pseudomonas aeruginosa* (PAO1; OD 0.02; ~ 10^7 CFU/mL), and cell culture medium. The cell culture medium was added to the polymer mixture to achieve a total concentration of 0.64% PSS and 15% dextran. The medium is 2% glucose and 1% minimum medium supplement (MMS); MMS components are listed in Table A1.1. After electrospraying into 10% PEG, 0.5% PDADMAC solution, the capsules were moved to a separate bath of 15% dextran, 25% medium by pipetting. These capsules were then incubated at 37°C overnight to assess growth of PAO1. When imaging, 2 mL aliquots of capsule solution were moved to a coverslip-bottom petri dish and 1.5 μL of 3.34 mM SYTO® 9 and 20 mM propidium iodide dyes were added to the solution. These dyes were purchased from ThermoFisher Scientific. All imaging of bacterial capsules were done with an Olympus Confocal Laser Scanning Microscope (CLSM). Bacterial cells were counted using the Analyze Particles function within ImageJ.

3.3 Results and Discussion

3.3.1 Polyelectrolyte complexation in aqueous two phase system (ATPS)

We study the complexation of two oppositely charged strong polyelectrolytes, poly(styrene sulfonate) (PSS); and poly(diallylmethyl ammonium chloride) (PDADMAC). Each polyelectrolyte is initially present in either the drop phase, comprising a solution of 15% dextran in water, or the external phase, comprising a

solution of 10% PEG in water. The drop and external phase compositions are quite close to one of the equilibrium conditions in the ternary phase diagram of this ATPS (15.54% dextran, 0.55% PEG and 9.51% PEG, 0.05% dextran), so that, when the two solutions come in contact, chemical potential gradients driving intermixing of the PEG and dextran solutions is weak. The phase diagram of the PEG-dextran system used in this work is presented in Figure 3.2. The black lines are previously reported equilibrium tie lines based on the black dot initial compositions. This work uses two phases comprised of 10 wt% PEG and 15 wt% dextran, which is close to the 4th tie line from the top in the phase diagram.

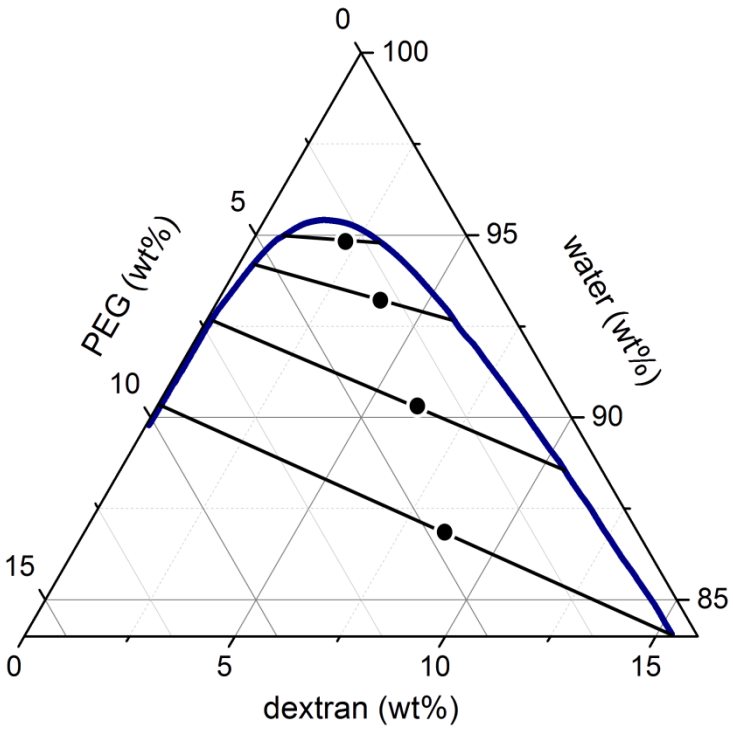

Figure 3.2. Ternary phase diagram of MW 20,000 PEG–MW 500,000 dextran–water: Adapted with permission from Diamond, A. D. and Hsu, J. T. "Phase Diagrams for Dextran-PEG Aqueous Two-Phase Systems at 22C". *Biotechnology Techniques.* 1989, *3* (2), 119–124. Copyright 1989 Springer.

The strong polyelectrolytes dissociate fully in aqueous solution, and remain fully ionized regardless of the solution pH and ionic strength, facilitating the systematic investigation of their complex formation. We study complex formation on drops containing a fixed concentration of 0.5% PDADMAC in external PEG solutions containing various % PSS selected to achieve charge ratios of PSS:PDADMAC ranging from 0.5:1 to 3:1, where 1:1 corresponds to 0.64% PSS.

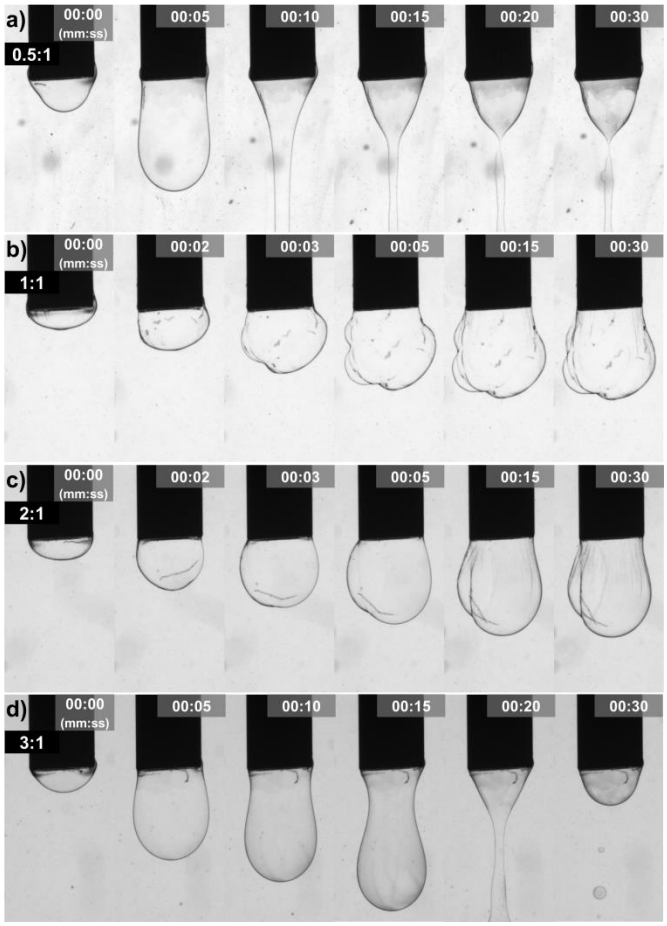

Figure 3.3. Injection of 1 μL 15% dextran/0.5% PDADMAC into 10% PEG with various concentrations of PSS. a) 0.5 PSS:1 PDADMAC ratio injected over 30s. b) 1:1 c) 2:1 d)3:1. Needle diameter = 0.85 mm.

While we are ultimately interested in the formation of microcapsules, to illustrate the rich behaviors within this system, we first record complexation on pendant drops of the dextran solution formed in the external PEG solution from a needle 0.85 mm in diameter. As the drops are injected, they are recorded at a rate of 6 frames/sec. Snapshots from these video series, presented in Figure 3.3, reveal highly non-monotonic changes in interfacial complexation with charge ratio. The 0.5:1 drop elongates and detaches. The Bond number $Bo = \frac{\Delta\rho g R_N^{\ 2}}{\gamma}$ characterizing the importance of gravitational forces to interfacial forces is greater than 10^2, where g is the gravitational acceleration constant, $\Delta\rho$ is the density difference between the phases, R_N is the characteristic length scale (i.e., droplet size), and γ is the interfacial tension. This indicates that, absent the formation of a complexed elastic structure to stabilize the drop interface, the drop will elongate and detach from the needle rather than attain a stable shape. This suggests that, at this charge ratio, any complex at the interface is too weak to stabilize the drop. At higher charge ratios (1:1 and 2:1), a complex layer at the interface stabilizes the drop within the first frames, and the drops remain stably attached to the tip of the needle. Also, the irregular shapes of these drops suggest the formation of elastic layers stabilizing the interfaces. By increasing the charge ratio even further to 3:1, however, the dextran drop is no longer stabilized, and again falls off due to gravity.

To understand these trends, it is important to note that, in our system, not only are there very weak trapping energies at the interface, both polyelectrolytes are miscible in both phases. This is a strikingly different feature than in the oil-water systems, in which

interfaces trap the film forming components, and components of differing solubilities in drop and external phases are commonly exploited. In our system, a polyelectrolyte in one phase can freely diffuse into the other phase, unless it is captured by the counter-polyelectrolyte to form a stable complex. This suggests that complexation may not be limited to the water-water interface. The location at which the polyelectrolytes meet to form complexes in this dynamic process is explored here. We propose that the relative fluxes of the two polyelectrolytes determine the location of complex formation, and that this location can be tuned to form stable interfacial complexes, Figure 3.4.

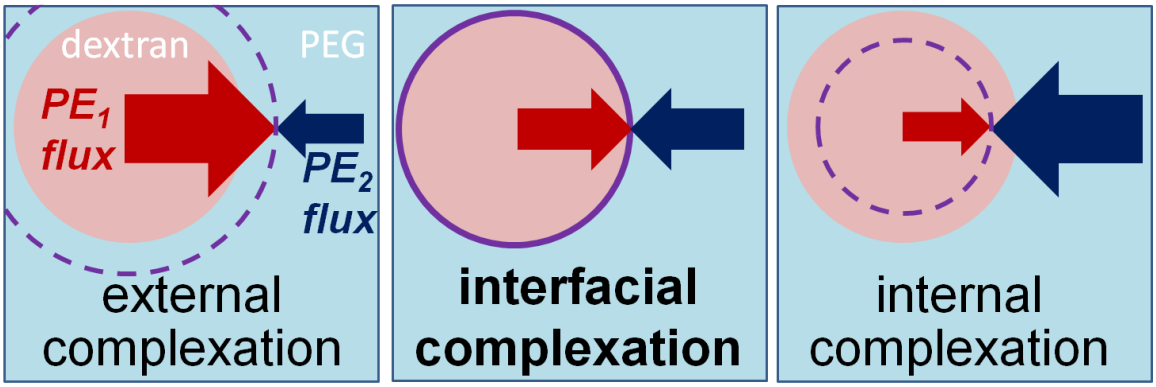

Figure 3.4. Schematic of flux balances near the PEG-dextran interface.

If they are imbalanced, complexation can occur in either the drop or external phases. In Figure 3.3, this suggests that the fluxes of the two polyelectrolytes is optimum between 1:1 and 2:1, resulting in a stabilized film, whereas the charge ratios of 0.5:1 and 3:1 have imbalanced polyelectrolyte fluxes, allowing complexes to form out of and into the drop, respectively. Mass transport within this system is determined by both convection and diffusion and quantitative modeling is required to diagnose the specifics of the transport

mechanisms that influence the formation of microcapsules and particles, which is beyond the scope of this report. By systematically varying the relative concentrations of the polyelectrolytes, the importance of the relative fluxes is evident in determining the final structure of the complex.

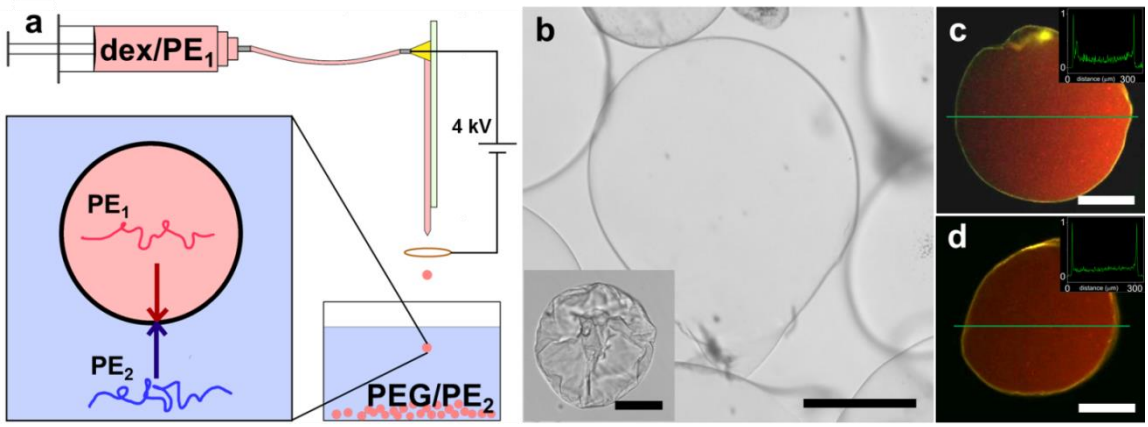

Figure 3.5. (a) Schematic illustration of electrospray setup. 15% dextran with polyelectrolyte(1) (PE_1) is injected into a capillary device which is connected to (+ or -) electrode of a high voltage supplier. Droplets are pulled out of the capillary tip toward a 2 cm diameter copper ring that is connected to the opposing electrode. These drops are sprayed into a bath of 10% PEG with PE_2, and the two PEs meet at the interface (zoom in). (b) A typical capsule made by electrospray with PE_1 = 0.5% PDADMAC and PE_2 = 0.64% PSS and dialyzed against water to fully inflate, inset is the capsule as made in original 10% PEG/0.64% PSS solution before dialysis. (c) PE_1 = 0.5% PDADMAC, PE_2 = 0.64% fluorescein-PSS (f-PSS) and encapsulated RD70 dye (red signal) imaged with confocal microscopy; inset is the fluorescence intensity of the f-PSS across the capsule along the green line. (d) PE_1 = 0.64% f-PSS (green signal), PE_2 = 0.5% PDADMAC and encapsulated RD70 dye (red signal) imaged with confocal; inset is the fluorescence intensity of the f-PSS across the capsule along the green line. All scale bars 100 μm.

With this premise to provide guidance, we now focus on the relevant case of microcapsule formation around small droplets. Dextran containing aqueous droplets roughly 200 μm in diameter are formed by all aqueous electrospray (AAE)[98] into an external bath containing PEG (See Figure 3.5); the drop phase contains one

polyelectrolyte, the PEG phase the other. AAE relies on the formation and break-up of aqueous jet under a high voltage,[98] allowing for the pre-formed droplets to meet the continuous phase with neat interfaces between the two phases (Figure 3.5a). Under appropriate conditions, which we describe below, hollow microcapsules with many wrinkles can be formed (inset, Figure 3.5b).

The formation of wrinkles on the as-made microcapsules is likely due to the mismatch of osmotic pressures between the two phases (Table 1) and can be removed by dialyzing the capsules against DI water to induce an influx of water, as shown in Figure 3.5b. The integrity of the microcapsules and their ability to encapsulate molecules can be demonstrated by adding rhodamine-labeled dextran (MW = 70,000) in the droplet phase of the ATPS as shown in Figure 3.5c. Moreover, robust hollow microcapsules encapsulating rhodamine-labeled dextran are also formed by switching the initial placement of the polyelectrolytes in the two phases of the ATPS (Figure 3.5d). In both cases, there is a slightly higher rhodamine signal around the interface of the capsule, indicating some dextran, likely entangled, is in the shell. The localization of PSS in the microcapsule shells is also confirmed by the strong fluorescence signal resulting from fluorescently labeled PSS (f-PSS) in the shell (Figure 3.5c-d, insets). Interestingly, we find that PSS is always present in the interior of the capsules regardless of its initial placement, consistent with the partitioning behavior of PSS observed by Ma et al.[91] This result also suggests that PSS is able to diffuse through the shell during complexation and that the shell composition is likely to be uniform throughout its thickness.

Table 1. Osmotic pressure measurements for relevant solutions used within this study.

Solution Description	Osmolarity (mOsm)
15 wt% dextran	59
10 wt% PEG	97
15 wt% dextran + 0.5 wt% PDADMAC	93
10 wt% PEG + 0.32 wt% PSS	117
10 wt% PEG + 0.64 wt% PSS	143
10 wt% PEG + 1.28 wt% PSS	189
10 wt% PEG + 1.92 wt% PSS	229
10 wt% PEG + 2.56 wt% PSS	292
5 wt% PEG + 0.64 wt% PSS	53
7 wt% PEG + 0.64 wt% PSS	73
15 wt% dextran + 0.64 wt% PSS	119
10 wt% PEG + 0.5 wt% PDADMAC	95

To test our flux-dependent complexation hypothesis at this smaller, sub-millimeter scale, the charge ratio of PSS:PDADMAC is again varied, but over a greater range. We first study capsule formation with PDADMAC fixed at 0.5% in the dextran phase, and PSS at concentrations from 0.01 to 2.56% in the external PEG phase, corresponding to molar charge ratios of 0.07:1 to 4:1. As shown in Figure 3.6a, when the charge ratio of PSS:PDADMAC is 0.07:1, the dextran droplet is not completely contained as evidenced by the satellite drops and nonuniformity of the interface complex. This droplet represents the case in which the PDADMAC flux is too rapid, allowing complexation to occur just outside the droplet interface. For molar charge ratios of 0.5:1 and 1:1, the fluxes are balanced so that complexation occurs near the interface, resulting in wrinkled microcapsules. As shown in Figure 3.5b, these wrinkles can be removed by osmotically

swelling the capsules. Increasing the PSS concentration further to ratios of 2:1 and 4:1 again creates imbalanced fluxes, but the imbalance this time allows PSS to enter the droplet and complex with PDADMAC in the internal drop space, resulting in a loosely complexed drop (2:1) and a coacervate structure within the droplet (4:1). Similar trends are observed if the initial placement of the polyelectrolytes is reversed; (Figure 3.6b), supporting the importance of mass transport in determining the location of complexation, and the need to tune the fluxes to form complex films at the interface of the ATPS. The ability to create both microcapsules and microgel particles with the same four components is consistent with a prior study using a similar system in which the higher affinity of PSS toward the dextran phase resulted in microgel particles when PSS is originally in the dextran phase and microcapsules when PSS is introduced from the PEG phase.[91]

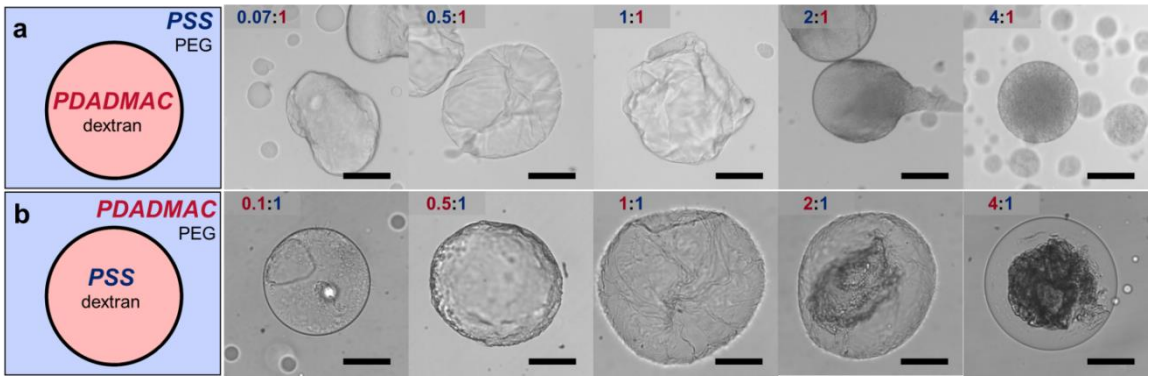

Figure 3.6. a) Capsules/droplets made by electrospray with 15% dextran/0.5% PDADMAC in dispersed phase with varying amounts of PSS in the continuous 10% PEG phase. The molar charge ratios of PSS:PDADMAC are varied from 0.07:1 to 4:1 as labeled from left to right. b) Capsules/droplets made by electrospray with 15% dextran/0.64% PSS in the dispersed phase with varying amounts of PDADMAC in the continuous 10% PEG phase. The molar charge ratios of PDADMAC:PSS are varied from 0.1:1 to 4:1 as labeled from left to right. All scale bars are 100 μm.

Although our results clearly demonstrate the importance of balancing the fluxes of the two polyelectrolytes, the role of the interface that exists in the ATPS requires a closer examination. Here we probe whether proper balancing of the fluxes of the two polyelectrolytes could allow complexation and capsule formation in the absence of an interface. To test this possibility, we perform a study without either PEG or dextran; an aqueous solution of PDADMAC is simply electrosprayed into an aqueous solution of PSS (Figure 3.7b). In this case, we do not observe capsules, but rather see elongated complexes that may bear structures related to the impingement of a jet as the miscible droplet contacted the bath surface. To mimic the viscosities of the original PEG and dextran phases in a miscible system, glycerol is added to the PDADMAC solution, which is electrosprayed into the glycerol and PSS solution. Again, coacervates are formed, but no encapsulating membranes are observed. These experiments suggest that finite interfacial tension plays an important role in capsule formation. These results are consistent with the literature pertaining to the hydrodynamics of drops of miscible fluids compared to those with finite tension.[99–101] These studies suggest that together, finite tension and high internal phase viscosity allow the drop to persist over time scales that allow the complexation to occur without loss of drop integrity. As such, interfacial tension is a key component to maintaining the droplet interface for templating complexation.

To gain further insight into the effect of the interfacial tension and at the same time to balance the osmotic pressures of the two phases, the continuous PEG phase concentration is varied. In an ATPS in equilibrium, as the compositions of the two phases move closer

to the critical point, the interfacial tension decreases.[5] Likewise, by decreasing the concentration of PEG in the continuous phase, we expect the interfacial tension between the two aqueous phases to decrease. These variations in the PEG concentration are shown on the phase diagram in Figure 3.7a. As the continuous PEG phase concentration is decreased down to 5%, the resulting structures show less wrinkles and appear more inflated than those prepared with a 10% PEG solution (Figure 3.6), as expected due to the lower continuous phase osmotic pressure. However, below 5% PEG, intact capsules are no longer observed, as the RD70 is no longer detected (fluorescence inset). This effect is likely due to the diminishing interfacial tension, which may alter the hydrodynamics as the drops are formed, and impedes the formation of encapsulating shell via complexation of PDADMAC and PSS. These observations indicate that the interfacial tension of the ATPS, albeit small, is necessary for templating the formation of microcapsules via complexation.

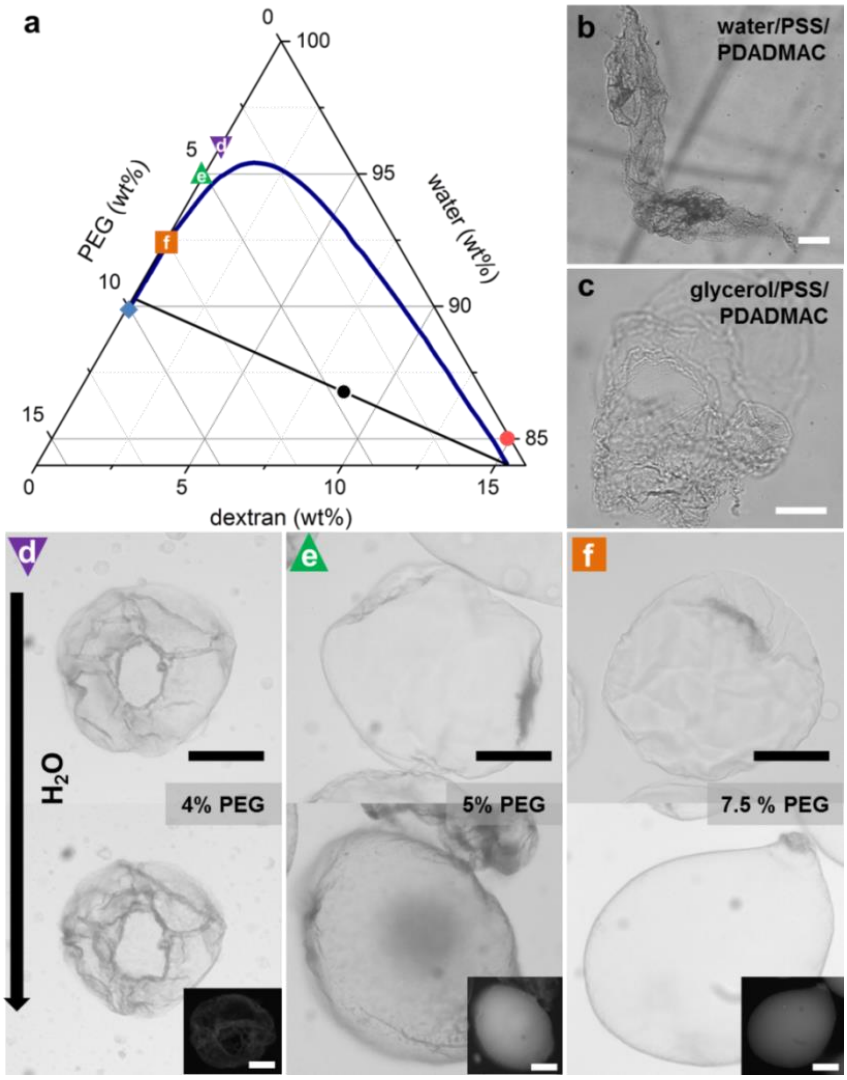

Figure 3.7. a) Ternary phase diagram of MW 20,000 PEG and MW 500,000 dextran in water, with the binodal line represented by a blue solid curve. Data adapted from Diamond and Hsu.[8] Black dot and line drawn are based on reported tie line compositions. Blue diamond (◆) and red circle (●) are the PEG continuous phase and dextran dispersed phase compositions, respectively, that were used for Figures 1-3. Colored symbols (▼,▲,■) labeled d, e and f are the continuous phase compositions of the corresponding letters in this figure. b) Removing PEG and dextran from the ATPS, the complex structure created by spraying 0.5% PDADMAC into 0.64% PSS. c) Dispersed phase of 81% glycerol/0.5% PDADMAC sprayed into continuous phase of 64% glycerol/0.64% PSS, which have the same approximate viscosities of 15% dextran and 10% PEG, respectively. d-f) 15% dextran/0.5% PDADMAC sprayed into varied% PEG/0.64% PSS continuous phases. Top row images are the capsules/drops as made in their respective PEG phases. Bottom row images are these capsules/drops dialyzed against pure water. e-f) insets are fluorescence microscopy images showing encapsulated RD70 dye. All scale bars are 100 μm.

3.3.2 Stimuli-responsive properties of polyelectrolyte microcapsules

A hallmark of polyelectrolyte microcapsules is their stimuli-responsiveness. A number of studies based on layer-by-layer assembly, for example, have shown that polyelectrolyte microcapsules undergo drastic changes in their permeability and/or shape when the ionic strength or osmotic pressure of the solution is changed.[27,83,85] To confirm that our encapsulating polyelectrolyte membranes exhibit this behavior, the coacervates and capsules presented in Figure 3.6a are both osmotically- and ionically-stressed and monitored over time. To monitor the release of encapsulated materials, 1 mg/mL RD70 is mixed in 15% dextran along with 0.5% PDADMAC and electrosprayed into the corresponding molar charge ratio PSS and 10% PEG continuous solutions. The resulting structures are dialyzed against pure water, which subjects the capsules and coacervates to a net negative osmotic pressure, resulting in their expansion. Over time, the capsules with 0.07:1 to 1:1 ratios of the two polyelectrolytes retain their shape while the 4:1 coacervate droplets lose their integrity and begin to disassemble as shown in Figure 3.8a i-iii. After 24 h of net negative osmotic stress, 0.5:1 and 1:1 capsules retain 80% of the original dye, 0.07:1 and 2:1 capsules retain only 50%, and the 4:1 coacervate droplets have released all encapsulated dye. Different abilities to encapsulate dextran molecules are consistent with the visual trend observed in Figure 3.3 and Figure 3.6 in which there appears to be a structural optimum based on fabrication conditions. The microcapsules that are created with 0.5:1 and 1:1 charge ratios are more mechanically resilient than ones made with 0.07:1 and 2:1 in their ability to retain encapsulated cargo because the capsules are formed while the fluxes of the two polyelectrolytes are delicately balanced.

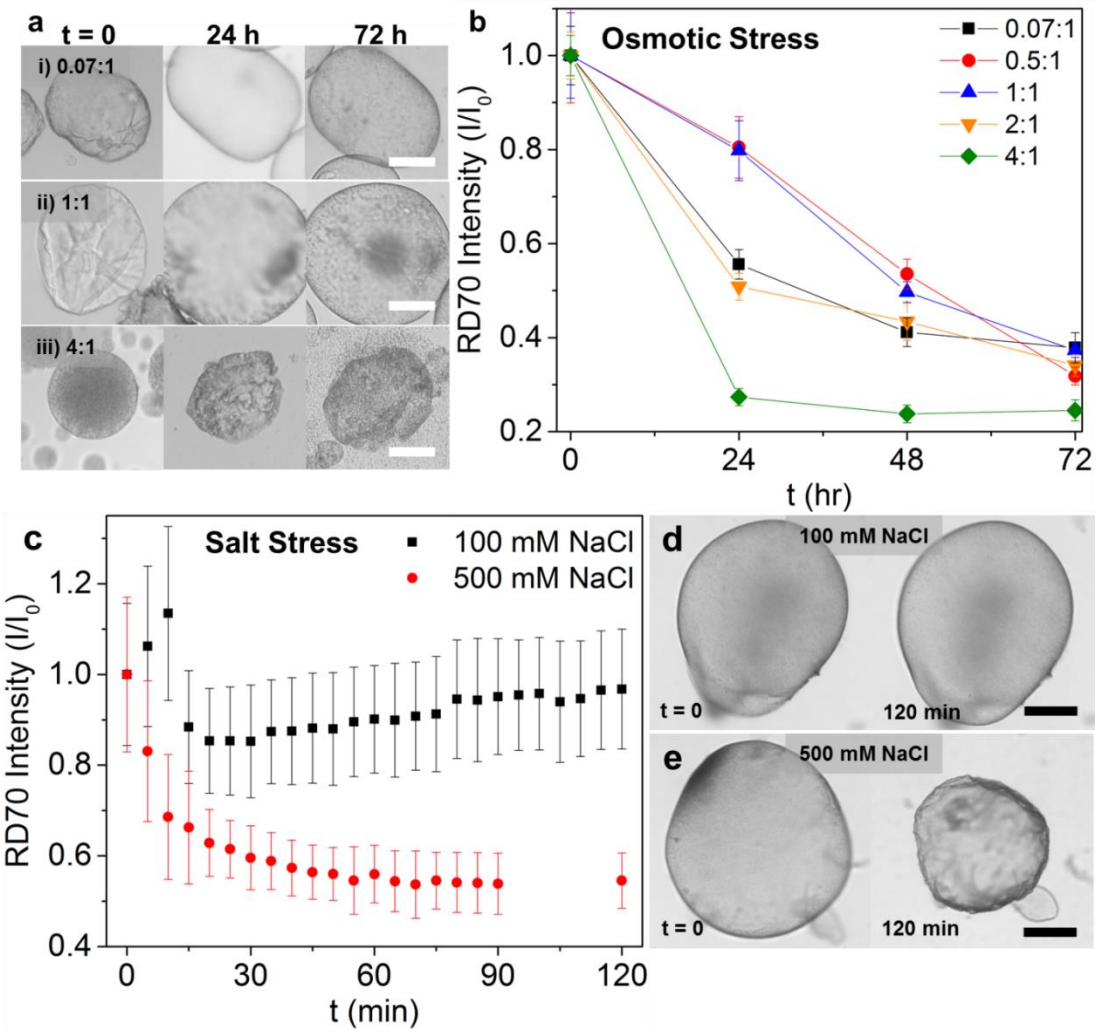

Figure 3.8. a) Bright field images of capsules/droplets made by electrospraying 15% dextran/0.5% PDADMAC into 10% PEG with varying amounts of PSS. i-iii) dialyzed against pure water from t = 0 – 72h. b) Measured intensity loss of RD70 dye over time due to net negative osmotic stress. Error bars are standard error of average intensities of at least 8 capsules per time point. c) 0.5:1 capsules, dialyzed in water, salt added at t = 0. d) Time lapse of 0.5:1 capsule due to exposure to 100 mM NaCl. e) Time lapse of 0.5:1 due to exposure to 500 mM NaCl. Error bars are standard deviation of average fluorescent intensity from the single capsules shown. All scale bars 100 μm.

We also test the response of the microcapsules to changes in the ionic strength by exposing capsules made under 0.5 PSS:1 PDADMAC charge ratio to 100mM and 500mM NaCl. RD70 is encapsulated in the lumen of the capsule to enable monitoring of

the triggered release. While little changes in the shape and fluorescence intensity are observed in the case of 100 mM NaCl treatment, significant release of the RD70 as well as shrinkage of microcapsules are observed within 60 min for the higher salt concentration, Figure 3.8c. The shrinkage and release of the encapsulated dye suggest that an increase in the ionic strength induces change in the permeability of the microcapsule shell through dissociation of polyelectrolyte complexes. These results confirm that polyelectrolyte microcapsules and coacervates formed via complexation in ATPS indeed exhibit stimulus-responsive properties and imply that microcapsules that respond to different stimuli such as pH or temperature can potentially be assembled using different types of polymers.

3.3.3 Encapsulation of live bacteria in polyelectrolyte microcapsules

One of the most significant advantages of the ATPS is its inherent bio-compatibility. We recently developed nanocultures, semipermeable microcapsules with internal volume of nanoliters, for use in sequestering and interrogating microbes and their microcolonies in contact with growth media, antibiotics, and in interaction with other kingdoms.[96] Encapsulation of living cells in a stable ATPS, in particular, could offer unique opportunities by maintaining cell viability and at the same time interrogating cells by diffusing analytical probes from the continuous phase. To demonstrate that our system is relevant in this context, bacteria are encapsulated within the polyelectrolyte capsules made under 1:1 charge ratio of PDADMAC and PSS to create all aqueous nanocultures, i.e. all aqueous nL-scale compartments that can host microbial cells. To create these capsules, the droplet phase of 15% dextran and 0.64% PSS is mixed with 20 μL/mL

stationary phase *Pseudomonas aeruginosa* (PAO1; OD 0.02) and a mixture of glycerol and vitamins. The continuous phase consists of 10% PEG and 0.5% PDADMAC. Upon the formation, the bacteria-containing capsules are moved to a continuous phase consisting of 15% dextran with the glycerol and vitamins to maintain a consistent media environment, and incubated at 37°C, see Section 3.2.6 for details. Initially after loading or after 24 h, the capsules are exposed to a Live/Dead staining assay and imaged under a confocal microscope as shown in Figure 3.9. By comparing the total number of cells (live and dead, green signal) within the pictured area, there is an order of magnitude increase in total cells/μm^2 from 1.7 x 10^{-3} at t = 0 to 1.9 x 10^{-2} at t = 24 h, indicating that the scarce-nutrient polyelectrolyte microcapsules enable cell growth and the viability of the cell can be probed by taking advantage of the permeability of the shell. Control growth studies indicate that PSS slightly retards the growth of the PAO1, but does allow proliferation, as seen in Figure 3.9. The growth of PAO1 bacteria in this minimalist media was measured by mixing 15% dextran, 25% MMS/glycerol mixture, 20 μL OD 0.02 PAO1 per 1 mL dextran/media mixture. PSS and PDADMAC were added at different concentrations to show the effects of free polyelectrolyte on bacterial growth. These mixtures were incubated at 37°C and their absorbance was measured at 630 nm. Higher absorbance corresponds to higher bacterial numbers. These results are presented in Figure 3.10. The following chapters will include other complexing moieties, and future work will include the identification of other polyelectrolyte pairs that may further promote bacterial growth.

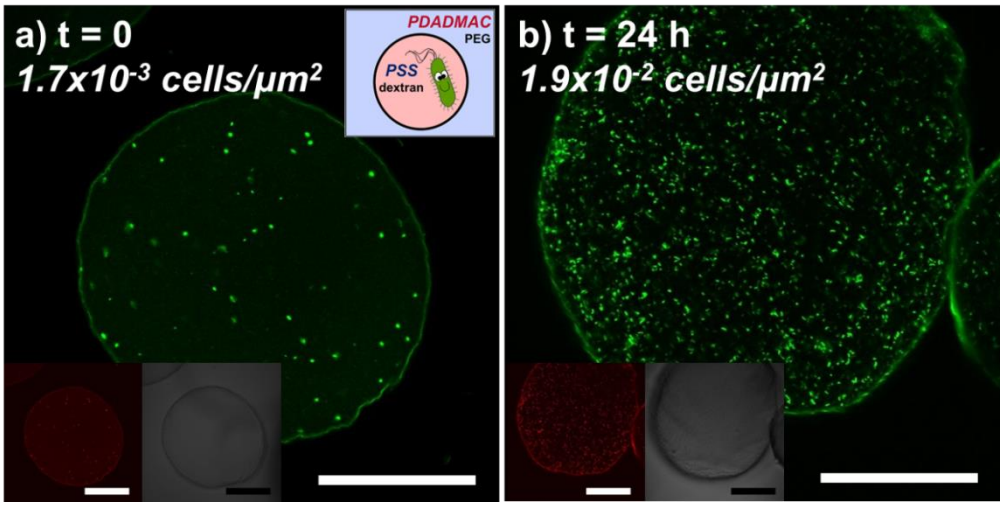

Figure 3.9. 15% dextran, 0.64% PSS, PAO1 culture, and media were electrosprayed into a 10% PEG, 0.5% PDADMAC solution, then moved to a 15% dextran, 25% media bath and incubated at 37°C. Cells are stained with SYTO 9 (green signal, all cells) and propidium iodide (red signal, dead cells) per the Live/Dead staining protocol. a) Initial time scan imaged with CLSM, areal cell density of $1.7x10^{-3}$ cells/μm^2. b) Bacterial microcapsule imaged 24h post incubation, areal cell density of $1.9x10^{-2}$ cells/μm^2. All scale bars 100 μm.

The flexibility to choose the placement of the two polyelectrolytes in the two aqueous phases is extremely useful because PDADMAC is known to display antimicrobial properties.[102,103] By simply switching the initial location of the PDADMAC to the drop phase, and performing the cell encapsulation experiment described above, we confirm that no cell growth occurs (Figure 3.10). Thus, by placing the PDADMAC in the continuous phase, microbes are viable, whereas if it is in the drop phase, the microbes in the nanocultures are not. The latter configuration could be useful in encapsulation applications that require sterile conditions.

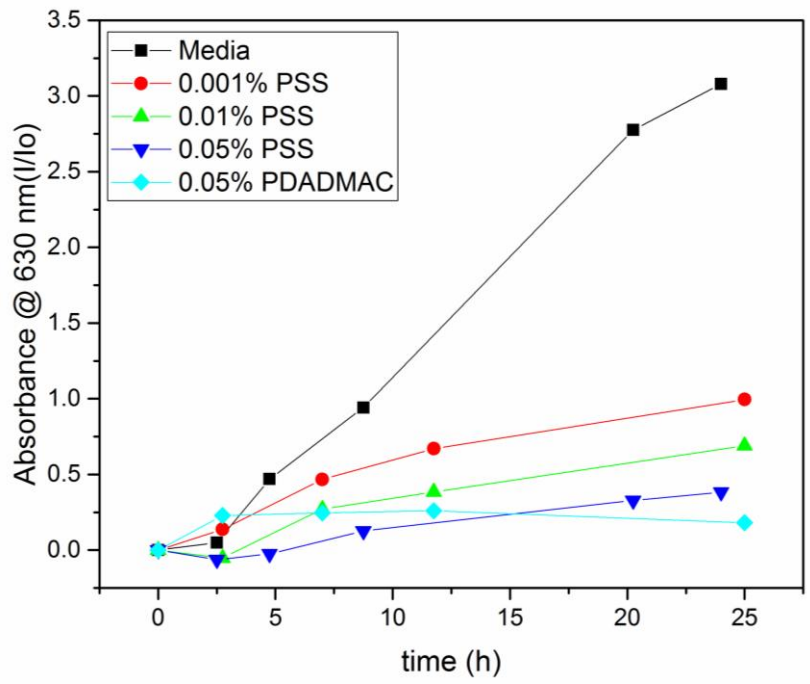

Figure 3.10. Absorbance measured at 630 nm of PAO1 cultures with varying amounts of PSS or PDADMAC, normalized by initial intensity, I_o. Black square curve has no polyelectrolyte.

3.4 Conclusion

We have formed robust capsules via interfacial templating on droplets containing dextran in external PEG phases via interfacial complexation of the strong polyelectrolytes PSS and PDADMAC. Owing to their high solubility in either the dextran-rich or PEG-rich phases, the polyelectrolytes can interact in either the drop or external phase, posing challenges for interfacial complexation. To form fluid filled capsules, the fluxes of the polyelectrolytes must be tuned to meet at the interface; an excess of polyelectrolyte in the external phase leads to complexation and gelation within the capsules core. The encapsulating membrane displays strong changes in permeability and integrity at high

ionic strength and under osmotic stress, an important feature for stimuli-responsive membranes that can potentially enable triggered release of encapsulated cargo. This study also demonstrates the encapsulation and incubation of live bacteria. The encapsulated cells were interrogated by taking advantage of the permeability of the microcapsule shell. This droplet stabilization and encapsulation scheme represents a significant advance on current ATPS stabilization technologies, as microcapsules made through this approach are rapidly formed, stimuli-responsive, and allow cell-viability to be maintained. This method paves the way to the formation of a broad variety of versatile functional components in such encapsulating membranes. The fundamental insights on which this method relies, i.e. the tuning of fluxes of complexing species to interact at the interface, and the important role played by interfacial tension, can be applied to other complexing charged moieties such as nanoparticles, proteins, and even DNA, which we explore in the next chapter.

CHAPTER 4. All Water Emulsion-bodies (AWE-somes) with Permeable Shells and Selective Compartments

Reprinted (adapted) from S. D. Hann, K. J. Stebe, D. Lee. All Water Emulsion-Bodies (AWE-somes) with Permeable Shells and Selective Compartments, 2017, ACS Applied Materials & Interfaces DOI: 10.1021/acsami.7b05800. [104]

4.1 Introduction

Nature exploits compartmentalization for spatial and temporal control of reactions and pathways in living cells. In the past decade, membrane-less organelles have been identified as an important class of compartments. These fluid-like bodies are formed by condensation of proteins and RNAs in the cytoplasm or nucleus of a eukaryotic cell. Diverse organelles coexist, localizing proteins and reagents that are released or exchanged between them, with partitioning rules regulated by solution conditions and local composition that continue to be revealed.[105,106] These observations have inspired research into cell mimics containing phase separated domains. Examples include systems based on phase separated polymers contained in lipid vesicles[107–109] and multiple emulsions formed using microfluidic techniques.[110,111] While promising, such methods typically require multiple fabrication steps,[107] the use of potentially deleterious organic solvents,[112,113] or feature domains that lack long term stability.[110,111] Furthermore, membranes (e.g., lipid bilayers) surrounding these cell mimics impede the transport of small and large molecules between the interior and exterior of these structures, limiting the supply of reagents and removal of waste.

One class of systems that has shown great promise in recapitulating some of the features found in living cells is aqueous two phase systems (ATPSs), comprising mixtures of two water soluble polymers that phase separate to form two distinct phases. Since these systems are intrinsically bio- and environmentally friendly, they are of particular interest for encapsulation and manipulation of delicate, protein-based materials,[21,114] low-fat foodstuffs,[115,116] or living cells.[78] Furthermore, proteins, enzymes, and RNA partition and react within ATPSs,[107–109] making ATPSs excellent systems for exploration of biomolecule manipulation. However, effective stabilization of ATPS multiple emulsions poses a challenge due to their physicochemical properties and the nature of the formation techniques. Single water-in-water emulsions, let alone double water-in-water-in-water emulsions, are notoriously difficult to stabilize compared to their oil-in-water counterparts due to their characteristically ultra-low interfacial tension and broad interfacial width.[5,8,9,18] In Chapter 3, we presented a facile route to stabilizing these all-aqueous interfaces via complexation of two oppositely charged polyelectrolytes (PEs).[64,91,117] The resulting PE/PE microcapsules are remarkable for their ease of production, stability, response to stimuli like pH and salt, and ability to support living microbes.

In this chapter, we present a new approach to creating double emulsion all-water emulsion-bodies (AWE-somes) using interfacial complexation in ATPS. We find that by replacing one of the PEs with charged nanoparticles (NPs), which can afford the microcapsules with useful functionality such as catalytic, optical, or responsiveness to external fields, rigid PE/NP membranes or shells can be formed by the same all-aqueous

route, and that these membranes can indeed encapsulate droplets, with membrane permeability that allows communication with the external phase. Remarkably, under certain conditions, an encapsulated double emulsion forms spontaneously; that is, all water emulsion bodies (AWE-somes) form, comprising an encapsulated droplet that has within it internal droplets. We elucidate the mechanism for this surprising phenomenon and demonstrate control over the inner droplet size in the AWE-somes and demonstrate membrane permeability. Moreover, we show that the internal droplets can selectively compartmentalize molecules and perform simple yet critical functions. For example, a simple reaction within the internal droplets can be triggered by an agent that diffuses through the rigid shell, and molecules can be partitioned and stored in these internal droplets, similar to the basic functions that are performed by membrane-less organelles found in living cells.[106]

4.2 Experimental Section

4.2.1 Materials

In addition to the materials identified in Section 3.2.1, LUDOX® TM-50 colloidal silica (nominally 22 nm diameter, 50 wt% suspension in water), LUDOX® SM colloidal silica (nominally 8 nm diameter, 30 wt% suspension in water), rhodamine B (≥95%, HPLC grade), fluorescein sodium salt, tetramethylrhodamine isothiocyanate mixed isomers (TRITC), 3-aminopropyl)triethoxysilane (APTS), and tetraethyl orthosilicate (TEOS) were purchased from Sigma-Aldrich. Sodium hypochlorite (bleach, 8.25% solution), ammonia, and ethanol (200 proof) were purchased from ThermoFisher Scientific. Rhodamine-tagged PEG (f-PEG, MW = 20 000 g/mol) was purchased from Creative

PEGWorks. Fluorescent silica nanoparticles (f-NP, 18 nm diameter) were synthesized according to a previously published report.[118] Briefly, 2 mg TRITC was mixed with APTS at a 50:1 molar ratio in ethanol and stirred in the dark for 12 hours to make the fluorescent cores. Next, 2 vol% TEOS in ethanol was added drop-wise over 20 min. The remaining TEOS was added over 40 min in a solution of ammonia, water, and ethanol and then stirred in the dark overnight to build the silica shell. The final concentrations of each component were 0.2 M [NH_3], 1.494 M [H_2O], and 0.155 M [TEOS], respectively, to achieve a nominal particle size of 25 nm. This solution was dialyzed against DI water for 2 days. The f-NPs were imaged with TEM and have an average particle diameter of 18 nm. All chemicals were used as received.

4.2.2 Solution Preparation

Solutions are prepared in the same way as Section 3.2.2. Again, all concentrations expressed in % are wt%, unless otherwise noted. The PEG-silica continuous phases were made by adding 15% PEG by mass, then silica solution by volume, then DI water to achieve the desired concentration. These solutions were vortex mixed and sonicated at least two times each for at least 2 min each time. The pH of the PEG phase was measured to ensure a pH > 9.5, else the pH was adjusted with 0.1 M NaOH. The PEG-silica solutions were used within 12 hr of mixing.

4.2.3 Pendant Drop

0.5 μL drops of 15% dextran and 0.25% PDADMAC drops were injected at a rate of 1 μL/s into a 3 mL cuvette of 10% PEG and silica. The needle diameter is 0.85 mm in all

experiments. Images were recorded from the time that the drop was injected. Images were recorded at 1.5 fps.

4.2.4 AWE-some Fabrication

AWE-somes were fabricated using the same all-aqueous electrospray setup as described previously and in Section 3.2.4.[64,98] The 15% dextran-0.5% PDADMAC phase was injected from a 5 mL syringe at a rate of 500 μL/h. The glass capillary device has an opening of approximately 150 μm. The voltage drop across the glass capillary device was adjusted between 3000 – 4000 V to achieve microcapsules of approximate 100-200 μm diameter. The 10% PEG-silica phase was gently stirred at 200 rpm.

4.2.5 Fluorescent PEG Permeation

Microcapsules were made without any fluorescent molecules, then 5 mL of these solutions were placed in a new petri dish and approximately 2.5 mg of f-PEG was added to the continuous phase. These solutions were swirled and gently mixed with a micropipette tip for 2 min, then imaged under an Olympus confocal laser scanning microscope (CLSM) at the noted times. In between imaging, the petri dishes were kept wrapped in foil and in a 100% humidity container, to minimize photo-bleaching and evaporation.

4.2.6 Small Molecule Diffusion

AWE-somes were made without any fluorescent molecules, then 50 μL aliquots were placed in small wells on the microscope. The respective small molecule solutions

(fluorescein sodium salt, rhodamine B, or sodium hypochlorite) were added at 10 μL; for fluorescence quenching, sodium hypochlorite was added about 1 cm away from the imaged capsule. The capsules were monitored with CLSM.

4.3 Results and Discussion

4.3.1 Spontaneous Double Emulsion AWE-some Formation

Using the same method to form PE/PE microcapsules in ATPS as described in Chapter 3, we electrospray drops of dextran-rich phase containing a positively charged PE, poly(diallyldimethylammonium chloride) (PDADMAC), into a PEG-rich phase with 22 nm SiO_2 NPs. The PEG phase is prepared at pH 9-10, which ensures the SiO2 NPs are highly negatively charged.[119] Upon encountering each other, the NP and PE likely undergo complexation by the entropic liberation of counter ions.[24] The concentrations of NPs in the PEG phase are adjusted such that a wrinkly skin is formed, indicating interfacial complexation and successful microcapsule formation. Unexpectedly, we observe internal droplets within these PE/NP AWE-somes. However, they are distinctly different from typical double emulsions in that the outer interface clearly shows the presence of a rigid shell, and the internal droplets appear to have fluid interfaces, like droplets dispersed in an immiscible liquid. Another interesting observation is that the size of internal droplets depends on the NP concentration; drop size decreases with an increase in the concentration of 22 nm NPs in the PEG-rich phase as shown in Figure 4.1a-c.

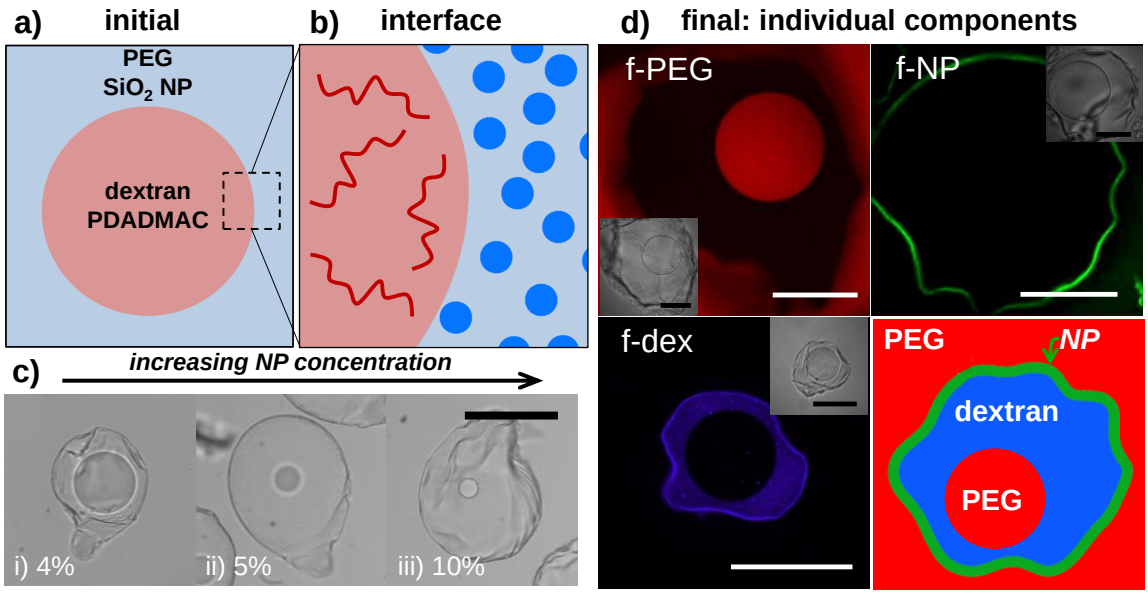

Figure 4.1. Schematic of spontaneous double emulsion AWE-some formation. (a) Initial placement of NP and PE in ATPS. PEG- and dextran-rich phases form the exterior and dispersed phases of ATPS. (b) Schematic of interface from (a). (c) Optical micrographs of microcapsules made with 22 nm diameter SiO_2 at i) 4% ii) 5% and iii) 10%. The concentration of PDADMAC in the dextran phase is kept constant at 0.5%. (d) Fluorescently-labelled components are included during formation of double emulsion microcapsules. *f-PEG*: Rhodamine tagged PEG (MW = 20 000). *f-dex*: False colored, Rhodamine tagged dextran (MW = 70 000). *f-NP*: False colored, 18 nm diameter TRITC core-SiO_2 NPs. Insets are corresponding bright field images. *Bottom right*: Illustration showing the final location of each component upon formation of AWE-somes. All scale bars 100 μm.

While the two phases within the irregularly shaped shell are likely related to those used to form the AWE-some, the exact nature and placement of these phases is not clear from these images. To confirm the make-up of the two phases within the microcapsules and to visualize the NP location, we use fluorescently labeled PEG, dextran and NPs, Figure 4.1d. These results confirm that the internal droplet is PEG-rich, the continuous droplet phase is dextran-rich, and the NPs are located only in the encapsulating

membrane; that is, the inner droplet interface is indeed that of PEG-dextran without NPs. The shell thickness is approximately 2-4 μm, according to SEM (Figure 4.2), which is similar to thicknesses that were reported for microcapsules prepared via interfacial complexation of alumina silica and sulfonated copolymer at the oil-water interface.[33]

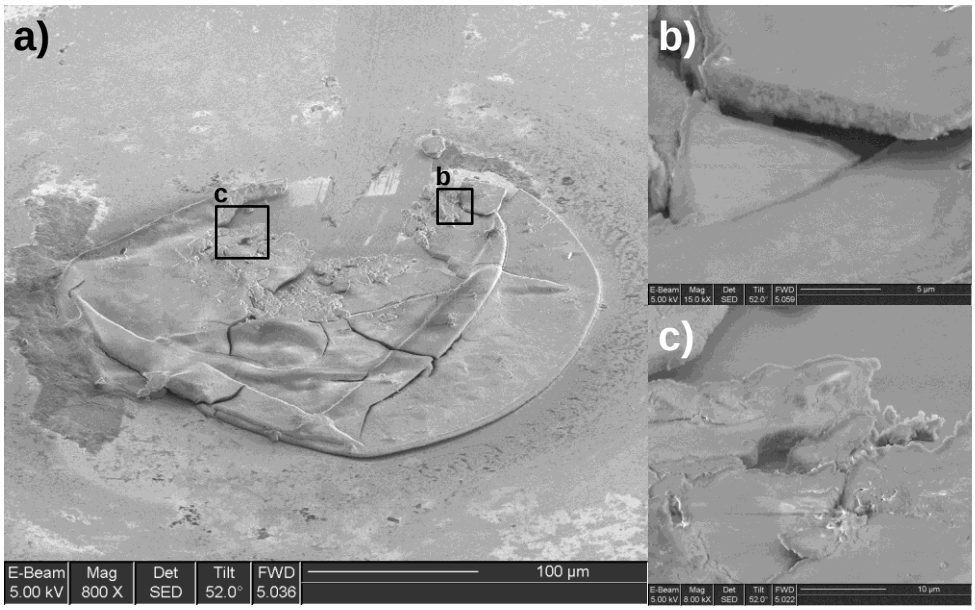

Figure 4.2. SEM micrograph of 0.5% PDADMAC/4.5% NP microcapsule. (a) Scale bar 100 μm, insets indicated by boxes. (b) Inset of cracked wall, shell thickness 2.1 μm, scale bar 5 μm. (c) Inset of cracked wall, shell thickness 2.0 μm. Scale bar 10 μm.

To understand the mechanism for the spontaneous formation of AWE-somes, we use the pendant drop method to enable direct visualization of morphology evolution.[64] We inject 0.5 μL of a solution of 15% dextran and 0.25% PDAMDAC into solutions of 10% PEG and two concentrations, in wt%, of 22 nm diameter NP, Figure 4.3. Without complexing agents, a dextran drop injected into an external PEG phase detaches due to the low interfacial tension and the density difference between the two phases. However,

when NPs are present in the external PEG phase, as depicted schematically in Figure 4.3a, the final structure is a dextran drop stabilized with a PE/NP membrane that ultimately includes distinct PEG drops, Figure 4.3d. Intriguingly, we find that the size of the internal PEG droplet depends on the concentration of NPs in the external PEG phase, Figure 4.3b-c. Furthermore, the internal PEG droplets form at the membrane and detach into the capsule interior. For example, at 2 wt% NP, Figure 4.3b, large PEG drops form on the NP-PDADMAC membrane, detach, and migrate upwards due to their buoyancy. Some of these droplets will undergo coalescence. Doubling the NP concentration, Figure 4.3c, results in smaller drops formed along the membrane that similarly detach and float towards the needle.

Based on these observations, we propose a mechanism behind the formation of internal droplets inside the PE/NP AWE-somes and their dependence on the NP concentration. At the initial introduction (t = 0) of dextran-PE droplets to the PEG-NP external phase, there exists a clean interface across which there is an osmotic pressure imbalance ($\Pi_{PEG} > \Pi_{dex}$) likely due to the highly concentrated NP suspension (Figure 4.4a).[120,121] When the first NPs flux toward the interface and begin to complex with the PE from the dextran phase, the initial membrane is both rigid and highly permeable (Figure 4.4b). Prior studies have indeed shown that complexes of NP and PE form porous materials.[122] Furthermore, the NPs have a near complete affinity for the PEG phase and do not enter the dextran phase.[123] Water leaves the dextran phase, and is replaced by PEG, devoid of NP, from the continuous phase, Figure 4.4b. This exchange continues until

enough NPs are included in the membrane to significantly reduce the membrane permeability, at some representative time, t_f (Figure 4.4c). The formation of a droplet of PEG within the dextran phase, rather than a thin film of PEG wetting the shell, suggests that the PEG phase prefers to contact the dextran rather than to wet the shell. The smaller droplets formed at higher NP concentration are consistent with more rapid reduction in the permeability of the shell due to faster flux of NPs to the shell.

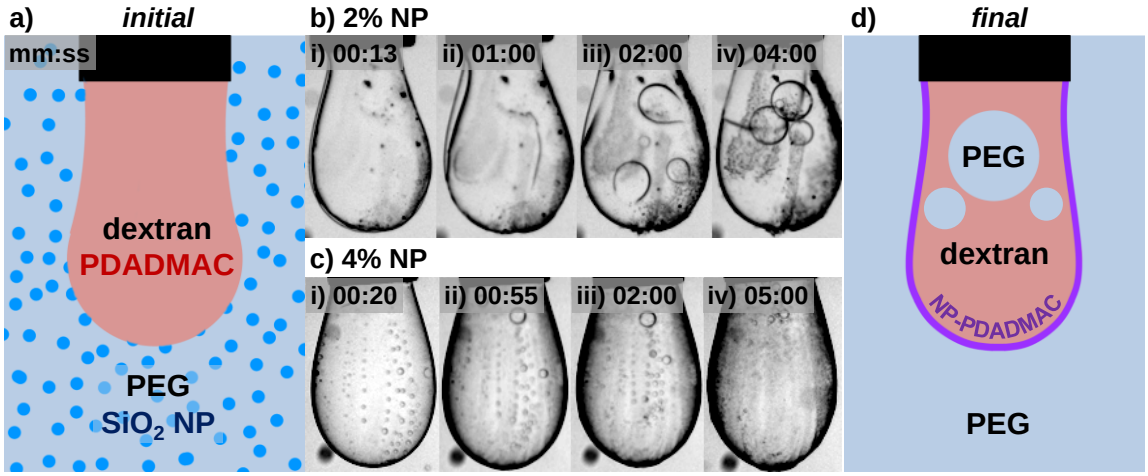

Figure 4.3. In situ observation of encapsulated double emulsion formation using the pendant drop method. Injection of 0.5 µL 15% dextran/ 0.25% PDADMAC drop at a rate of 1 µL/s into 10% PEG/22 nm NPs. (a) Schematic of initial state. (b) Time evolution of hanging drop with 2% SiO_2 in the PEG phase up to 4 minutes post-injection. (c) Time evolution of hanging drop with 4% SiO_2 in the PEG phase up to 5 minutes post-injection. (d) Schematic of final state of hanging drops. Needle diameter = 0.85 mm.

To test these ideas, PE/NP AWE-somes are generated with SiO_2 NPs of different sizes (8 and 22 nm) at various wt% while keeping the concentration of PE constant in the dispersed phase. For a given wt%, the number density of particles scales as the cube of the ratio of radii. Thus, both the osmotic pressure of the nanoparticle suspension[120] and

the rate of NP transport toward the shell are changed strongly when the particle size is reduced, which in turn influence the AWE-some structure. The relative projected areas of inner and entire droplets are plotted as a function of NP concentrations (Figure 4.4d). For the smaller NPs (8 nm diameter), a lower concentration in wt% is required to achieve the internal droplet sizes similar to the 22 nm case; for example, we see that 1.33% 8 nm NP and 4.5% 22 nm NP result in inner drop projected area fractions of 0.15 and 0.2, respectively. Furthermore, the size of the internal droplets decreases with concentration of the NPs, suggesting that t_f is reduced by their rapid incorporation into the shell. The final size of the inner drop depends on a complex interplay of osmotic stress, NP incorporation, and shell permeability. Despite these open issues that invite further study, these data support the proposed mechanism for encapsulated double emulsion formation. The higher number density means the permeability of the shell decreases sharply in a short period of time, resulting in smaller drops than the same wt% larger NP.

The formation of the internal droplets also depends on the initial placement of the charged moieties. For example, if the NPs are initially placed in the interior dextran phase, and the PE is placed in the exterior PEG phase, a NP/PE shell forms; however, because the osmotic pressure is higher in the droplet phase, water from the exterior phase diffuses in and swells the dextran phase (Figure 4.5 and Figure 4.6). The hollow shells end up inside the swollen dextran phase.

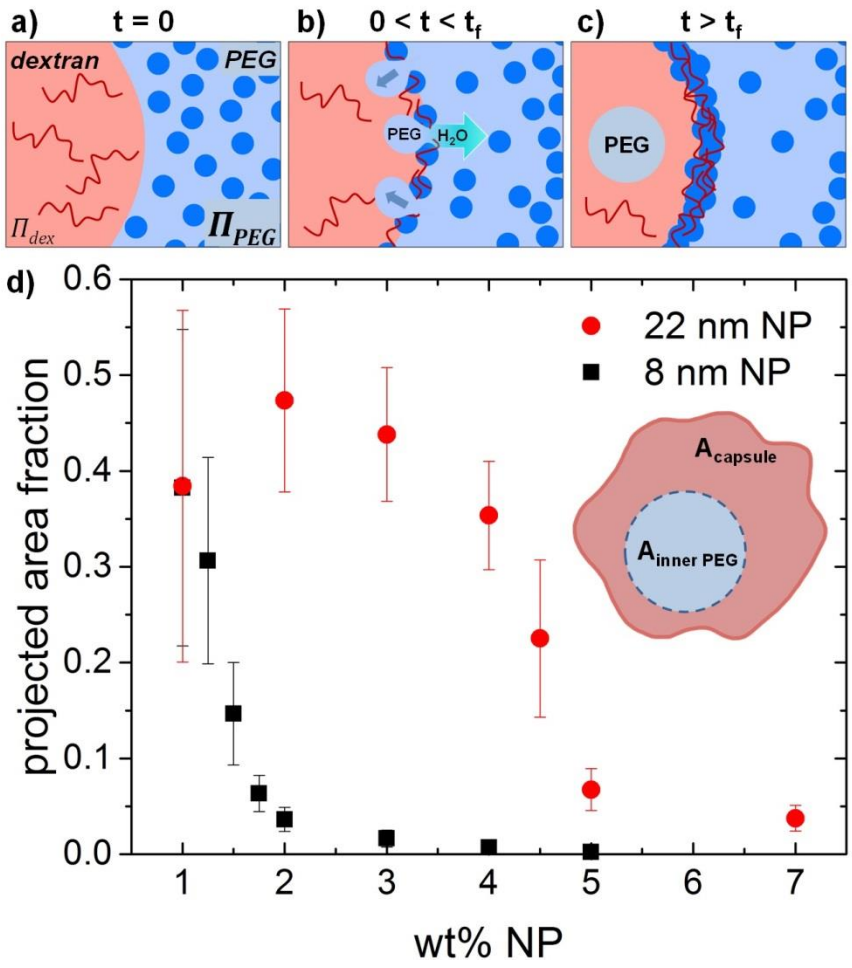

Figure 4.4. Hypothesized mechanism behind PEG drop inclusion and projected areal fraction of PEG drop inside AWE-some. (a) Initial state of dextran drop containing only PDADMAC and has osmotic pressure, Π_{dex}. PEG phase initially contains only SiO_2 NPs and has osmotic pressure, Π_{PEG}, where $\Pi_{PEG} > \Pi_{dex}$. (b) Short times post-introduction, NPs and PDADMAC form a porous, rigid complex at the interface. In this initial stage, water is driven out of the dextran phase due to the osmotic pressure gradient, which drives the PEG-phase inward due to the incompressibility of each phase on either side of the rigid membrane. (c) This exchange occurs until a later time, t_f, where permeability is drastically reduced. (d) Plot of projected area of included PEG drop normalized by the projected are of the capsule as a function of NP concentration in the PEG phase. More than 100 AWE-somes are averaged for each data point and error bars are standard deviation.

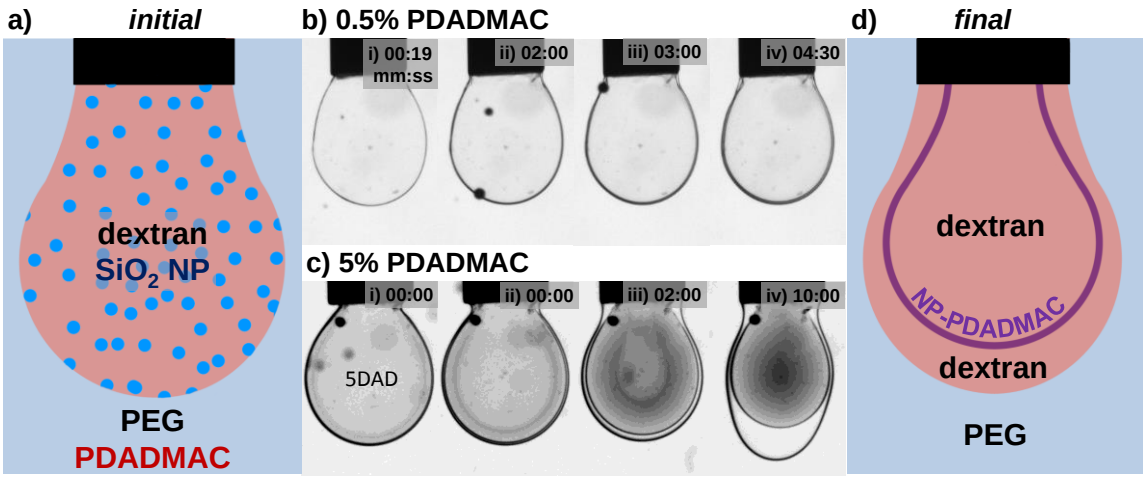

Figure 4.5. Injection of 0.5 µL 15% dextran/4% 22 nm silica NPs at a rate of 1 µL/s into 10% PEG and PDADMAC. (a) Schematic of initial state. (b) Time evolution of hanging drop with 0.5% PDADMAC post injection. (c) Time evolution of hanging drop with 5% PDADMAC up to 10 min post injection. (d) Schematic of final state of hanging drops. Needle diameter = 0.85 mm.

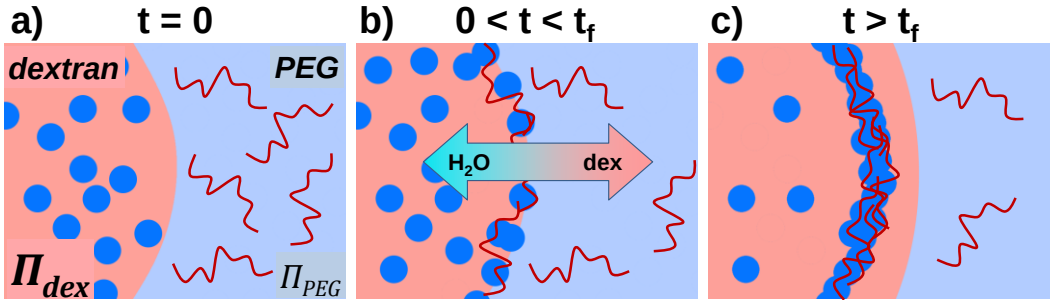

Figure 4.6. Schematic of osmotic driving force for NP/PE microcapsules.

4.3.2 AWE-some Shell Permeability and Compartmentalization

This research was inspired by the manner in which living cells exploit both compartmentalization within organelles, and transport through the cell membranes to maintain their function and induce chemical reactions. We test the potential of performing these basic functions using double emulsion AWE-somes. To test shell

permeability, we use both large and small molecules. For large molecule transport, fluorescently labeled-PEG (f-PEG, MW = 20 000) is added to the external phase of the encapsulated double emulsions prepared with 8 nm or 22 nm SiO_2 NPs, which have PEG inner droplets of similar sizes. Fluorescence intensity of the inner droplet slowly increases over time and saturates after ~24 hr, Figure 4.7a-d, indicating that there is a continuous and gradual exchange of PEG between the inner PEG droplet and the external phase. Interestingly, the size of NPs does not seem to affect the rate of exchange as shown in Figure 4.7d. The PEG permeability behavior presented in Figure 4.7 is consistent for different size PEG drops, capsules of different ages, and different NP sizes. Furthermore, the discrete value represented on the y-axis of Figure 4.7 is seen to be a function of the amount of f-PEG added to the solution and can be normalized for all data to superpose onto the same curve, Figure 4.8. This superposition suggests that the permeability of the membrane is very similar for all cases studied here.

In contrast to PEG, small molecules, such as fluorescein salt and Rhodamine B, transport through the shell instantly allowing for rapid partitioning, Figure 4.9a-b. Excitingly, these two small molecules show different partitioning behavior; fluorescein salt prefers the dextran phase within the AWE-some, whereas Rhodamine B favors the PEG inner phase. Analogous partitioning has previously been observed in ATPS of PEG and dextran.[3,114] In these works, biomacromolecules partition preferentially to either the PEG-rich or dextran-rich domains due to the distinct chemical environment within these domains. The partition coefficient can be altered by changes in solution conditions including pH, salt, or temperature. These results provide important evidence that different

molecules can flux across the shell to partition preferentially within the AWE-some compartments, similar to partitioning into different organelles within the living cell.

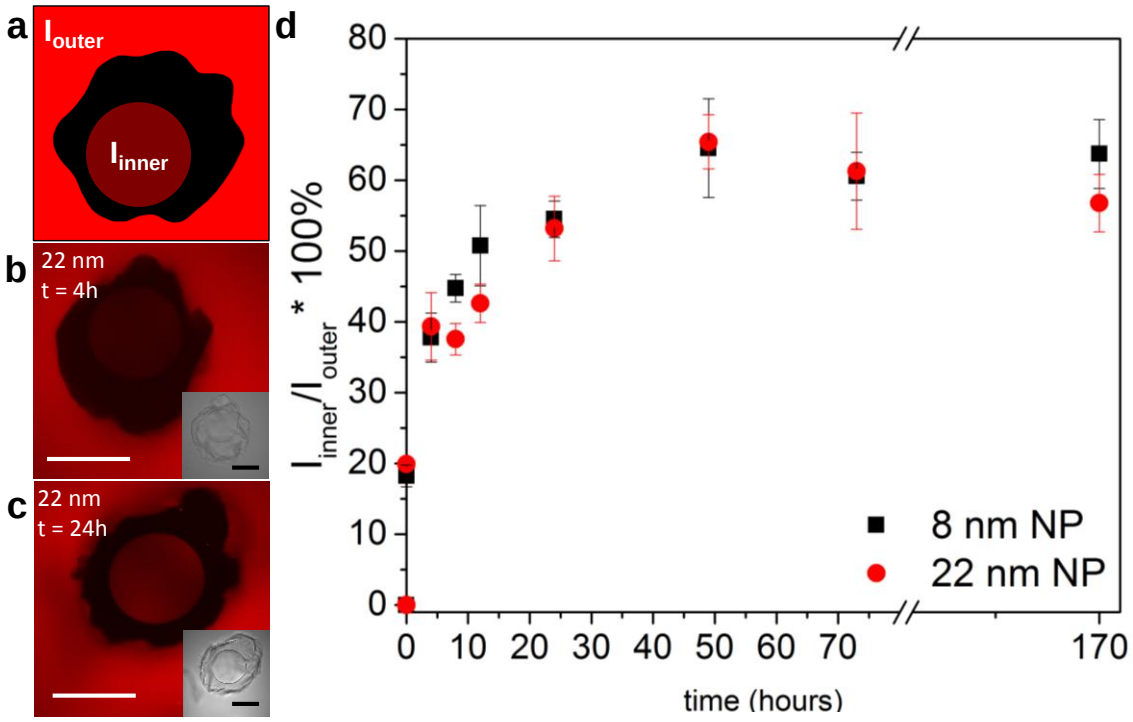

Figure 4.7. Permeation of f-PEG (MW = 20 000) into AWE-somes. (a) Schematic of measurement geometry. (b) Representative fluorescent image of PDADMAC/22 nm NP AWE-somes measured 4 h after addition of f-PEG. (c) A different AWE-some measured after 24 h. Insets are corresponding bright field images. (d) Plot of concentration of f-PEG in the inner PEG drop normalized by that in the outer PEG phase as a function of time for AWE-somes made with 8 nm and 22 nm NP. All scale bars 100 μm.

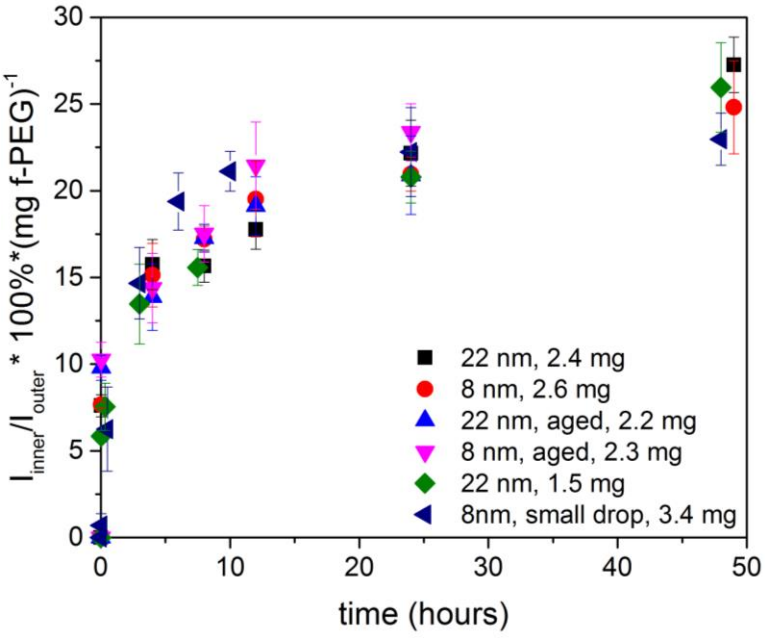

Figure 4.8. Additional data to previous figure; measurement of PEG permeation into capsules by adding f-PEG to 5 mL continuous PEG phase and normalized by the mass of f-PEG. Legend descriptions indicate the size of silica NP used to form the capsule (nm) and the amount of f-PEG added to the 5 mL solution (mg). All capsules were made for inner PEG drop fractions of 0.25 except (◀), which is made to a fraction of 0.05. Data designated as 'aged' (▲,▼) are capsules that were made 1 week prior to adding f-PEG. Mass 'mg' in legend refers to the amount of f-PEG added to the 5 mL continuous PEG phase.

4.3.3 AWE-some Compartmentalized Reaction

One of the key functions of organelles in the living cell is to compartmentalize and induce specific reactions triggered by agents that are delivered from outside the cell or organelle, such as ribosome biogenesis within the nucleolus.[105,106] Taking advantage of the permeability of the encapsulating shell and the partitioning of molecules within the AWE-somes, we demonstrate that a reaction can be performed within the inner PEG phase, triggered by a reactive component that diffuses into the AWE-some from the

external PEG phase. Encapsulated double emulsions are fabricated with f-PEG, which partitions into the inner PEG droplets. Sodium hypochlorite is subsequently introduced to the outer phase, which diffuses into the microcapsules without disturbing their structural integrity, and quenches the fluorescent signal of f-PEG in the inner droplets within 2 minutes as shown in Figure 4.9c-d.

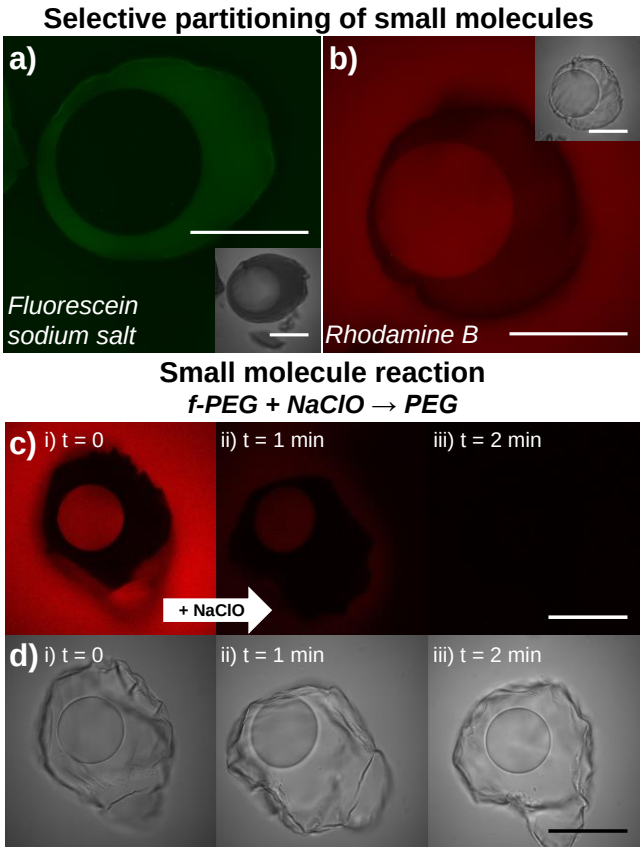

Figure 4.9. Small molecule diffusion and reaction. (a) Fluorescein sodium salt added to continuous PEG phase, found predominantly in the dextran phase of AWE-some. (b) Rhodamine B added to PEG phase, found predominantly in PEG phases. Insets are bright field. (c) 10 µL NaClO is added to 500 µL of outer PEG phase approximately 1 cm away from monitored capsule. Within 2 minutes, signal from f-PEG is quenched inside the AWE-some. (d) Bright field images of AWE-some in (c). All scale bars 100 µm.

4.4 Conclusion

In this chapter, we have demonstrated spontaneous formation of encapsulated double emulsions by inducing interfacial complexation in ATPS. Encapsulated double emulsions emerge due to rapid formation of PE/NP membranes via interfacial complexation, followed by osmotic pressure driven transport of water from one phase to the other. Like cells containing membrane-less organelles, double emulsion AWE-somes support features such as permeation, selective compartmentalization and compartmentalized reaction. Because of the ease of processing, this platform has significant potential for creating functional, biocompatible and biomimetic structures. For example, incorporation of pH-sensitive weak polyelectrolytes will confer pH-sensitive permeability in the shell. The shell can also be functionalized with catalytic NPs to create the framework to induce reactions at the interface.[124,125] Moreover, proteins with different functionalities can be incorporated using their native charge. We have already successfully incorporated lysozyme, a known antibacterial protein, in the shell using this scheme (Figure 4.10). Incorporating a gene network or other cellular machineries into the encapsulated double emulsions will enable recapitulation of key cellular functions in artificial systems, which could potentially impact the area of biosensing and synthetic biology.[126] Our future investigations will focus on elucidating molecule transport properties through the shell, decoupling the effect of transport and osmotic effects on the structure of AWE-somes, and also incorporating various biologically functional materials in AWE-somes.

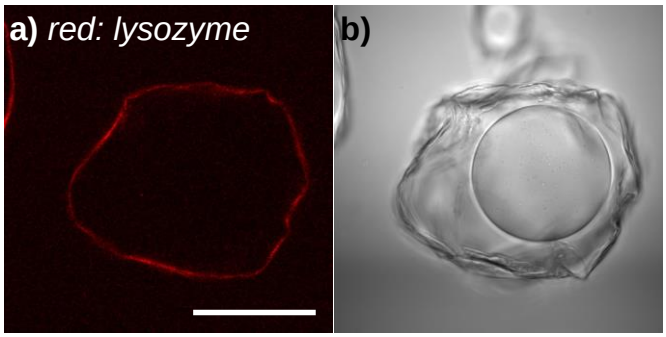

Figure 4.10. Confocal image of microcapsule fabricated with 15% dextran/0.5% PDADMAC/1μM rhodamine tagged lysozyme into 10%PEG/4.5% 22 nm silica NPs. (a) Fluorescent image, where red is the rhodamine tagged lysozyme. (b) Corresponding bright field image. Scale bar is 100 μm**.**

CHAPTER 5. Tuning Interfacial Complexation in ATPS with Polyelectrolytes and Nanoparticles for Compound AWE-somes

Reprinted (adapted) from S. D. Hann, D. Lee, K. J. Stebe. Tuning Interfacial Complexation in Aqueous Two Phase Systems with Polyelectrolytes and Nanoparticles for Compound All Water Emulsion Bodies (AWE-somes), 2017, Physical Chemistry Chemical Physics. DOI: 10.1039/c7cp02809a. [127]

5.1 Introduction

The mechanism of interfacial complexation in ATPS is dependent on the transport of the two species as well as the partitioning of the charged moieties in the two phases, as evidenced by the variety of structures achieved in Chapters 3 and 4. The PE/PE microcapsules (Chapter 3) exhibit stimuli-responsive properties and are able to sustain bacterial growth. The PE/NP microcapsules (Chapter 4) provide additional functionality due to the presence of NPs and the spontaneously formed double emulsion structures. Such AWE-somes, with basic features that resemble model cells with membraneless organelles, enable sequestration and segregation of chemically distinct molecules within the lumen, and the exchange of materials with the outer phases. However, unlike PE/PE microcapsules, which can be stressed without losing structural integrity, PE/NP AWE-somes are extremely brittle, likely due to dense packing of nanoparticles in the shell, making them mechanically fragile under osmotic stress and mechanical loading. We are intrigued by the potential to combine properties of the two schemes to imbue NP-

laden membranes with mechanical robustness while enabling the formation of double emulsion AWE-somes.

In this chapter, interfacial membranes are formed in ATPS by introducing cationic PE-containing droplets into continuous baths containing both anionic PE and NP. We show that the structure and properties of microcapsules fabricated using this method can be tuned by systematically varying the concentrations of NPs and PEs in the outer phase. This tunability, accompanied by the potential for scale-up production, makes interfacial complexation in ATPS a truly versatile platform to induce the fabrication of functional microcapsules for applications in encapsulation, microreaction/separation and controlled release.

5.2 Experimental Methods and Materials

5.2.1 Materials

All materials used are the same as in Sections 3.2.1 and 4.2.1.

5.2.2 Solution Preparation

Solutions are prepared as in Sections 3.2.2 and 4.2.2. For continuous phase solutions, 15% PEG, 50% NP, and water are combined to achieve target composition, and alternatingly vortexed and sonicated until a homogeneous mixture is made. Then, if required, 10% PSS is added to achieve final composition. These solutions are used within 12 h of mixing. For droplet phase solutions, 20% dextran, 20% PDADMAC, and water are mixed until homogenous.

5.2.3 Microcapsule Fabrication and Characterization

An all-aqueous electrospray[98] setup is used to generate monodisperse dextran droplets in PEG continuous phases. A 5 mL syringe of dextran is injected at a rate of 1 mL/h through a capillary with tip diameter 170 μm. The voltage drop is varied between 3500-4000 V to achieve approximately 100 μm diameter drops. The capsule production rate is approximately 1 Hz. For fluorescent capsules, f-NP or f-PSS are incorporated at 1-10% of their respective components, and imaged with a confocal laser scanning microscope (CLSM). Fabricated microcapsules are placed in 250 μL wells and dialyzed through 1 μm polycarbonate track etched (PCTE) membranes, as in Figure 3.1.[64] Microcapsule response to pH change is monitored by taking a 100 μL aliquot of capsule suspension (approx. 20 capsules) and adding 7 mL of pH adjusted 15% PEG. The pH is adjusted using 0.1 M HCl or NaOH while stirring and monitored by pH meters.

5.3 Results and Discussion

5.3.1 Microcapsules via Interfacial Complexation in ATPS

Complexation of two oppositely charged species at the interfaces between two immiscible water phases leads to the formation of functional microcapsules with unique properties and structures.[64,91,117,104] As described in Chapter 3, when two oppositely charged polymers are present, one in each of the phases of an ATPS, robust PE/PE microcapsules can be formed by balancing the flux of each PE from its respective bulk phase toward the water-water interface. Imbalanced fluxes leads

to the complexation in one of the two bulk phases, since the PEs are soluble in both phases. Balanced fluxes result in PE/PE microcapsules, Figure 5.1a.[64] As introduced earlier, we will use the following nomenclature to describe the composition of microcapsules: A/B where A and B denote the materials present in the dispersed droplet phase and the continuous phase, respectively. When there is more than one complexing species present in one phase, we will use (B,C) to describe the species present. When necessary, we will also use subscripts after symbols to describe wt% concentration of each species. For example, $PE_{0.5}/(PE_{0.1},NP_2)$ corresponds to a microcapsule made with 0.5% PE in the dispersed dextran phase and 0.1% PE and 2% NP in the external PEG phase.

As described in Chapter 4, replacing one of the two PEs with NPs results in a distinctly different mechanism for film formation due to the strong affinity of the NPs for one of the two phases, in which internal water droplets spontaneously form to create AWE-somes (Figure 5.1b).[104] Due to the NP strong preference for the PEG phase, the NP remain at the interface and undergo complexation with the PE sequestered in the dextran phase. However, as the rigid NP-PE complex begins to form at the water-water interface, PEG is osmotically exchanged into the dextran droplet as water is extracted until the membrane permeability is sufficiently reduced, resulting in an encapsulated double emulsion. While PE/PE microcapsules are mechanically pliable, as evidenced by their tendency to inflate in a hypotonic solution without losing their structural integrity, PE/NP AWE-somes are very brittle, rupturing upon exposure to a solution of low osmotic pressure. Thus, while the incorporation of NPs could potentially broaden the

functionality of these membranes, and the formation of the internal droplet could provide an interesting platform for reaction and selective compartmentalization, the fragility of the capsules potentially limit their applications. We are inspired by the possibility of tuning the structure and mechanical robustness by including both NP and PE of the same charge in the continuous phase to create compound PE/(PE,NP) AWE-somes.

We use the aqueous two phase system (ATPS) of poly(ethylene glycol) (PEG) and dextran to create the templating interface. Droplets of dextran with a cationic PE, poly(diallyldimethylammonium chloride) (PDADMAC), are dispersed into PEG solutions with anionic 22 nm SiO_2 NPs and/or an anionic PE, poly(sodium 4-styrenesulfonate) (PSS), using the all-aqueous electrospray method.[98] To illustrate the structural effect of NP and PSS, we keep the concentration of PDADMAC in the dextran (dispersed) phase constant at 0.5%, while changing the concentrations of NP and PSS in the PEG (continuous) phase (Figure 5.2). Without any NPs and/or PE in the continuous phase, the dextran/PDADMAC droplets remain perfectly spherical, and droplets undergo coalescence, indicating a lack of stabilizing membrane.

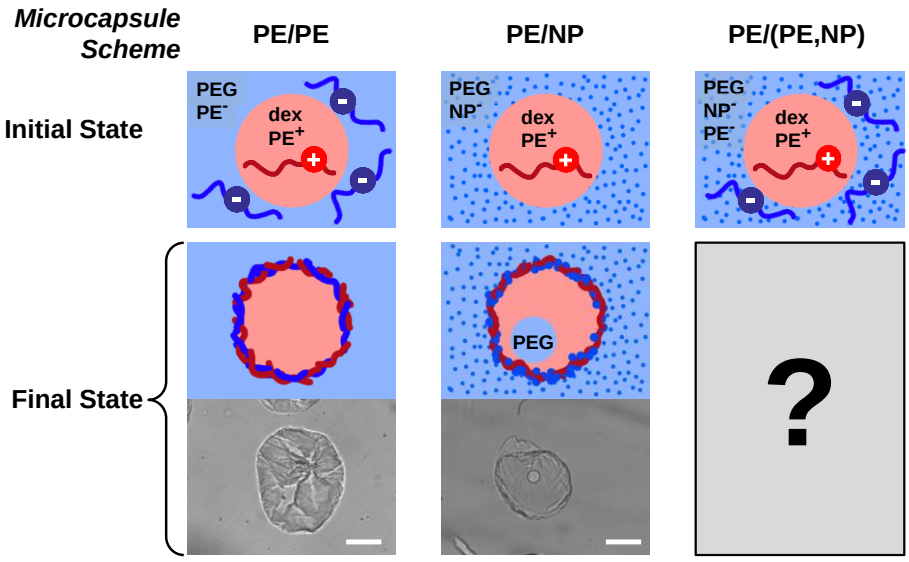

Figure 5.1. Schematic of initial and final configurations of PE/PE, PE/NP, and PE/(PE,NP) (compound) capsules. All droplet phases are 15% dextran and 0.5% PDADMAC. *Left column*: PE/PE capsules, as presented in Chapter 3. Outer phase is 10% PEG and various concentrations of PSS. *Center column:* PE/NP capsules (AWE-somes), as presented in Chapter 4. Outer phase is 10% PEG and various concentrations of 22 nm SiO_2 NP. *Right column:* Schematic of compound PE/(PE,NP) capsules presented in this chapter. Outer phase is 10% PEG and various concentrations of both PSS and SiO_2 NP. Scale bars are 100 μm.

Once small amounts of either PE or NP are added to the continuous phase, the droplet morphology changes markedly owing to the formation of interfacial films. For $PE_{0.5}/PE_{0.1}$, complexation occurs predominantly in the continuous phase, as evidenced by the large number of globules and dark patches along the interface. As the concentration of PSS in the continuous phase is increased to 0.5-1%, complexation occurs at the interface, resulting in interfacial films with wrinkles. When the concentration of PSS is further increased to 2%, a dark condensed phase emerges inside the droplets due to complexation between the two PEs. The majority of PDADMAC undergoes complexation with PSS inside the dextran

droplet and thus no robust complex layers are formed at the interface. Therefore, despite the osmotic pressure difference no wrinkles are observed at the interface, consistent with the findings presented in Chapter 3.[64]

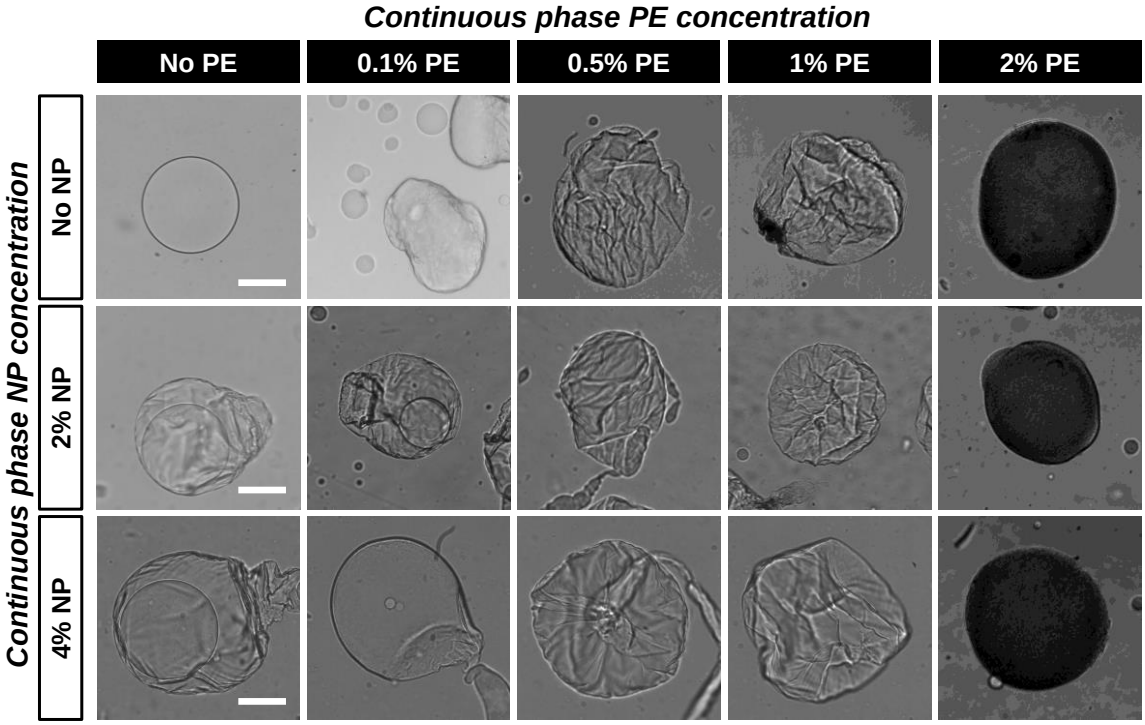

Figure 5.2. Optical images of microcapsules made with varying outer phase compositions. All droplet phases are 15% dextran and 0.5% PDADMAC. The outer phase is 10% PEG with 0, 0.1, 0.5, 1%, or 2% PSS (*columns, left to right*) and 0, 2, or 4% 22 nm diameter SiO_2 NP (*rows, top to bottom*). Wrinkly capsules indicate good membrane formation (wrinkles are due to osmotic compression of the capsule). Double emulsion AWE-somes [$PE_{0.5}/NP_2$, $PE_{0.5}/(PE_{0.1},NP_2)$, $PE_{0.5}/NP_4$, $PE_{0.5}/(PE_{0.1},NP_4)$] contain included PEG drop in the lumen of the capsule. Scale bars are 100 μm and apply to all images.

For $PE/(PE,NP_2)$ microcapsules, the inner PEG drop size is decreased and eventually eliminated as PSS concentration is increased, with a wrinkled microcapsule without an internal droplet at [PSS] = 1%. A similar trend is

observed for PE/(PE,NP_4) microcapsules; the inner PEG drop size is reduced and then eliminated as the concentration of PSS is increased. At high concentrations of PSS (> 1%), the PE/PE structure ultimately dominates; complexation, likely between the two PEs, occurs within the dextran-PDADMAC droplets, regardless of NP concentration. Visually, the PE/(PE,NP) microcapsules adopt structures that have some characteristics of both PE/PE (Figure 5.2, top row) and PE/NP (Figure 5.2, left column) structures; that is, encapsulated double emulsions are generated for the PE/($PE_{0.1}$,NP) series (similar to PE/NP microcapsules) and the microcapsules with wrinkles but without internal droplets are formed for the PE/(PE_1,NP) series (similar to PE/PE microcapsules). These results suggest including both anionic species during fabrication enables fine control of the accessible structures.

To discern which species make up the shells of PE/(PE,NP) microcapsules, fluorescently tagged PSS (f-PSS) or fluorescent core-shell SiO_2 NP (f-NP) are added to the continuous phase and the resulting structures are imaged with confocal microscopy. $PE_{0.5}$/($PE_{0.1}$,NP_2) contain both PE and NP in the shell, as shown in Figure 5.3a-b. Moreover, PSS is present in the microcapsule interior, but not in the internal PEG droplet, consistent with the slightly greater affinity of PSS for the dextran phase.[91] At higher PSS and NP concentrations, $PE_{0.5}$/(PE_1,NP_4) (Figure 5.3c-d), the shell is primarily composed of PSS and possibly a small amount of NP, as evidenced by the weak signal when the laser intensity of the confocal microscope is increased, Figure 5.3e. These observations suggest that the anionic species, PSS and NP, compete to complex with the sole cationic species,

PDADMAC. The presence of NP in the continuous phase promotes interfacial complexation, as it reduces the flux of PDADMAC out of the dextran drop by associating with it at the interface. As PSS concentration is increased, the structure is increasingly dominated by the PSS flux and its complexation with the PDADMAC. Including both anionic species enables tuning of the microcapsule formation by exploiting both mechanisms. By tuning PSS and NP concentrations in the continuous phase, we are able to vary the size of the internal droplets and tune the relative makeup of the shell.

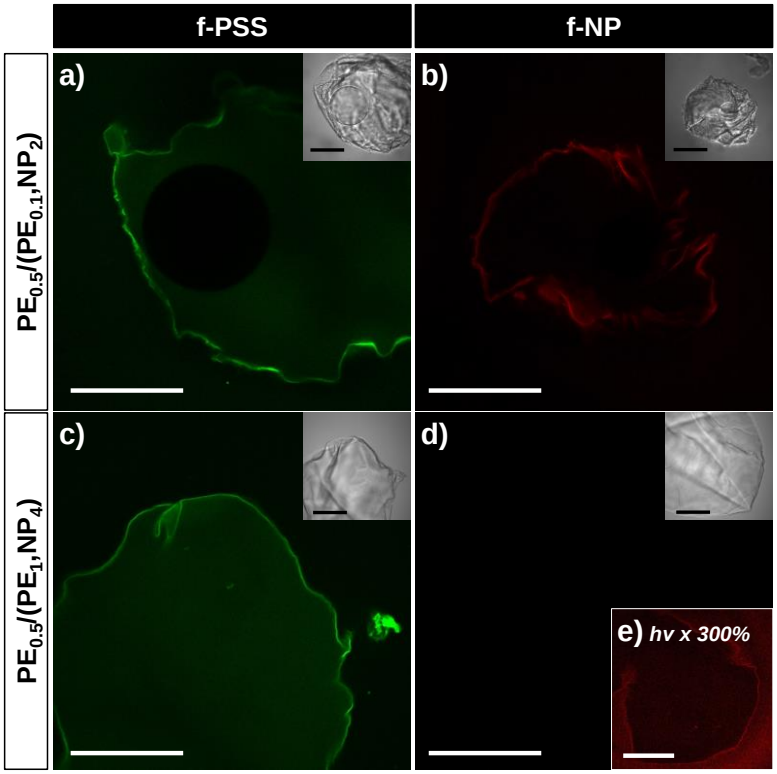

Figure 5.3. Representative compound microcapsules fabricated with fluorescently labelled PSS and TRITC-core SiO_2 NPs. $PE_{0.5}/(PE_{0.1},NP_2)$ microcapsules with (a) f-PSS and (b) f-NP. $PE_{0.5}/(PE_1,NP_4)$ microcapsules with (c) f-PSS and (d) f-NP. (e) Laser intensity of (d) increased 300%. Insets (a-d) are corresponding bright field images. Scale bars are 100 μm.

5.3.2 Tuning the Mechanical Robustness of the Shell

The ability to tune the makeup of the shell by changing the concentrations of PE and NP in the continuous phase potentially enables the control of the mechanical properties as well. The PE/PE microcapsules are easily reinflated without losing the structural integrity when subjected to pure water (i.e., negative osmotic stress) (Figure 5.4b). The PE/NP microcapsules, in contrast, rupture when exposed to pure water, likely due to the brittleness of the shell made of a high concentration of NPs (Figure 5.4c). Although the physical mechanism for the fragile nature of PE/NP shells is not yet known and is a focus of ongoing work, the high packing density of SiO_2 may contribute to such brittleness. It has been shown that dense packings of SiO_2 NPs are quite brittle.[128,129] By incorporating a small amount of PE in the microcapsule shell in the PE/(PE,NP) microcapsules, the robustness of the shell is dramatically improved against osmotic stress. The microcapsules can be reinflated to remove the wrinkles, similar to PE/PE microcapsules, indicating that they are likely softer and more flexible (Figure 5.4d-f).

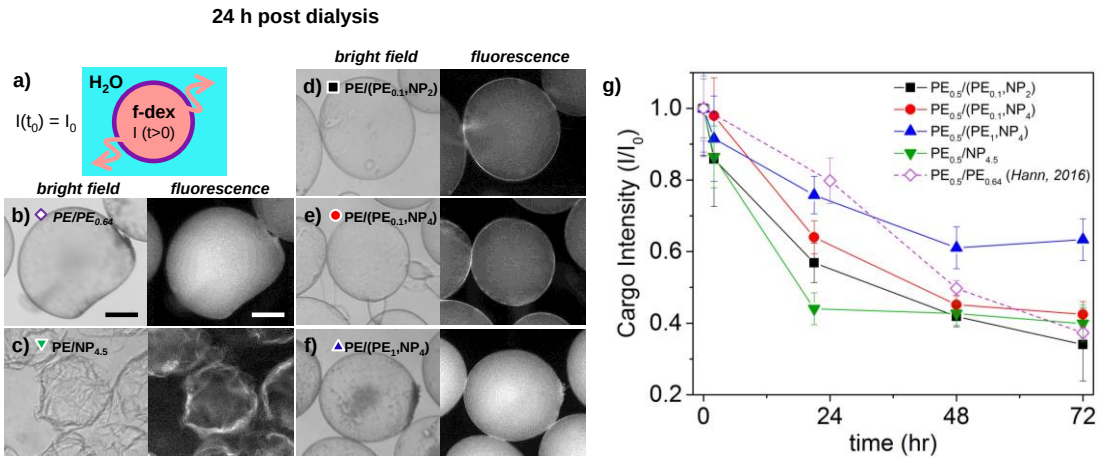

Figure 5.4. Release of encapsulated dextran in response to negative osmotic stress. Microcapsules fabricated with fluorescent dextran (f-dex, Cargo) are washed with pure DI water through microdialysis cells. (a) Schematic of experiment geometry. (b-f) Optical micrographs of capsules after 24 h dialysis. Scale bar is 100 μm and applies to all images. (g) Measured release of f-dex normalized by initial intensity over time. Decrease in intensity indicates loss of encapsulated dextran. Final intensity (I/I_o) of 0.4 is the equilibrium final signal of an empty shell (residual signal is from f-dex incorporated in the shell.

The integrity of the shell under osmotic stress is further probed by monitoring the retention of an encapsulated macromolecule. Microcapsules are prepared by electrospraying fluorescent dextran (MW = 70 000)-0.5% PDADMAC droplets into the PEG phase with 2 or 4% NP and 0.1 or 1% PSS. The resultant microcapsules are subsequently subjected to negative osmotic stress by exposing them to DI water. The evolution of the intensity of the encapsulated fluorescent dextran is monitored for each population; a loss in relative intensity indicates release of the encapsulated dextran. While the relatively robust PE/PE microcapsules slowly release dextran under osmotic stress, PE/NP microcapsules lose close to 60% of dextran within the first 24 hours. The remaining 40% of the dextran appears to be incorporated into the shell, as the shell's intensity remains

approximately constant after 24 h. Additionally, dextran incorporated in the shell may aid in the retention of encapsulated dextran, contributing to the remaining signal. Release profiles from the PE/(PE,NP) microcapsules resemble the profiles obtained for PE/PE microcapsules. Comparing the fluorescence intensities of different microcapsules after 24 h, in general, the higher the ratio of PE to NP, the smaller amounts of dextran are released from the capsules. $PE_{0.5}/(PE_{0.1},NP_2)$ and $PE_{0.5}/(PE_{0.1},NP_4)$ capsules have released about 40% dextran, while the $PE_{0.5}/(PE_1,NP_4)$ capsules have released only 20%, similar to the 1:1 $PE_{0.5}/PE_{0.64}$ microcapsules. Interestingly, the $PE_{0.5}/(PE_1,NP_4)$ microcapsules have a slower release profile than that of the other capsules. After longer times, these capsules do ultimately release the dextran, as shown in Figure 5.5. These observations again clearly suggest that the mechanical robustness of microcapsules against osmotic stress can be tuned and enhanced by varying the concentration of PE and NP in the continuous phase during electrospraying, which in turn allows for tuning of the release properties of these microcapsules.

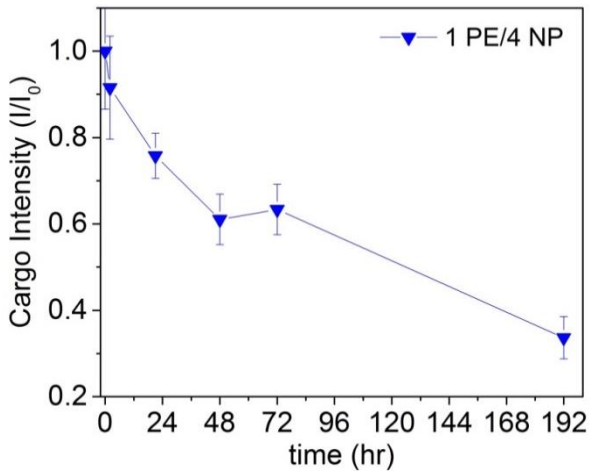

Figure 5.5. Release of encapsulated fluorescent dextran for $PE_{0.5}/(PE_1,NP_4)$ compound microcapsule.

5.3.3 Tuning the pH Responsive Properties of Microcapsules

The PE/PE and PE/NP microcapsules disassemble under high salt and low pH conditions, respectively. By including both anionic species in the PE/(PE,NP) microcapsules, the stimuli-responsive properties can also be tailored. PE/PE microcapsules do not respond to changes in the solution pH as they are made of two strong PEs which have permanent charges along the backbone.[24] In contrast, PE/NP microcapsules disassemble upon exposure to a low pH (pH <5) likely due to SiO_2 NPs losing their anionic charge, and thus their ability to maintain association with PDADMAC. Even with a small amount of anionic PE included as in the $PE_{0.5}/(PE_{0.1},NP_2)$ microcapsule, the disassembly of the microcapsule is suppressed when the capsules are placed in pH 3 PEG, while the internal droplets are maintained over at least 30 min, Figure 5.6. Interestingly, confocal microscopy of the $PE_{0.5}/(PE_{0.1},NP_2)$ microcapsules indicates that some NP are liberated from

the shell (green arrows) during the pH decrease; however complexation between the two PEs is apparently sufficient to maintain the shell structure and keep some NPs incorporated in the shell (white arrows). This ability to tune the stimuli-responsive properties is a feature that could be exploited in the application of these capsules. For example, it will be possible to enable selective partitioning and conversion of molecules in different compartments within these modified AWE-somes in various solution conditions while maintaining the structural integrity of the microcapsules.

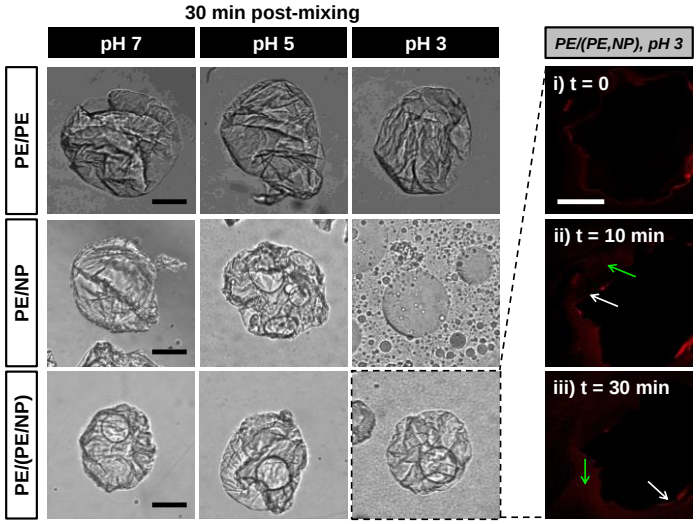

Figure 5.6. PE/PE, PE/NP, and compound PE/(PE,NP) microcapsule response to pH stimulus. Microcapsules (fabricated at pH 9) were washed with 15% PEG to remove external complexing agents, then subjected to different pH 15% PEG solutions (columns, left to right). $PE_{0.5}/PE_{0.5}$ capsules (*top row*). $PE_{0.5}/NP_2$ AWE-somes (*middle row*). $PE_{0.5}/(PE_{0.1},NP_2)$ AWE-somes (*bottom row*). Complete capsule dissolution occurs for $PE_{0.5}/NP_2$ capsules at pH 3. Rightmost column is confocal image series of f-NP in $PE_{0.5}/(PE_{0.1},NP_2)$ capsules at pH 3. Some NP remain in shell (white arrows) while some NP are dissolved off the shell (green arrows). Scale bars 100 μm.

5.4 Conclusions

In this chapter, we have presented the basic framework for fabricating tunable, multi-functional microcapsules via interfacial complexation in ATPS. We demonstrate that the structure and properties of microcapsules formed via interfacial complexation in ATPS can be tuned by inducing assembly between the external phase containing PE and NP of the same charge and an internal phase containing an oppositely charged PE. Mechanical robustness and the flexibility of the membrane surrounding the microcapsules can be varied by changing the relative amount of PE and NP present in the continuous phase. This approach potentially enables the formation of membranes with functionality afforded by NPs, the formation of encapsulated double emulsions typical for the PE/NP AWE-somes, and the enhancement of the mechanical properties typical of the PE/PE microcapsules. This ability to tune the structure and properties of microcapsules over a wide range will be especially beneficial for tailoring their properties for specific applications including cell mimicry, foodstuffs stabilization, cell encapsulations and controlled release. These applications may require capsules of different size ranges; the extension of these methods to making capsules of different size ranges is a focus of ongoing work.

CHAPTER 6. Summary and Outlook

The insight provided within this thesis develops the framework for interfacial assembly in ATPS and the special considerations that must be taken with regards to the transport processes at and around the all water interface. The next steps for this thesis work will build on the fundamental understanding established here. This chapter identifies a key application space in which we are well suited to impact. This chapter is in preparation for submission for publication.

6.1 Introduction: Compartmentalization in nature

Throughout biology, temporal and spatial coordination of components of various scales is needed to perform complex functions. This coordination is achieved, in part, by compartmentalization, to confine components or entities, control local environment, and regulate material fluxes and reactions. Fundamental studies that address the formation, structure and roles of such compartments in nature have inspired materials scientists to create complex structures to recapitulate their important features and functions. If these bio-inspired compartmentalized structures are used to manipulate proteins or other delicate cargo, they must be formed from materials that minimize deleterious effects. Such a requirement has spurred interest in aqueous two phase systems (ATPSs) which provide a rich platform for structure formation and are gentle hosts to bio-active components. ATPSs are aqueous mixtures of hydrophilic materials that demix into two water-rich phases. There are a number of pairs of polymers and proteins/polysaccharides that undergo this phenomenon; a commonly used pair is that of poly(ethylene glycol)

(PEG) and dextran.[130] Historically, ATPSs were explored as biological two phase extraction media[2,131] and exploited as diagnostic tools.[132] Their inherent biocompatibility makes them particularly attractive for their use as hosts to compartmentalize various biological and/or non-biological components.

6.2 Molecular confinement: self-assembly within cells

Cells are the smallest form of life and subcellular compartmentalization is central to life itself. The interior space of cells is divided into organelles or compartments in which specific tasks are executed and coordinated, ranging from DNA sequestration, to energy production and lipid and protein formation. To perform these tasks, molecules must partition, react, and re-distribute selectively from one organelle to another. Organelles can be membrane-bound, that is, they are encased in lipid bilayer membranes and bound to the cell membrane itself. Membrane-bound organelles are stable entities that are resistant to environmental fluctuations, can isolate cytotoxic reactions, and retain ions due to the presence of the lipid membranes.[133] These stably confined entities have inspired a wide and well established body of work on lipid or polymer vesicles,[134,135] which have been shown to support broad ranges of cell-mimetic processes such as DNA transcription,[136] encapsulation,[137] and RNA catalysis.[108]

There are other organelles that are not encased within a lipid bilayer. These membrane-less organelles are fluid droplets comprised of biomolecular condensates that are thought to form by phase separation processes within the cell cytoplasm, and are found in both prokaryotic and eukaryotic cells. Membrane-less organelles are dynamic

entities, sensitive to fluctuations in pH, temperature, and local concentration of other biomolecules. Fundamental studies have begun uncovering mechanistic insights into their formation and function within the cell.[133,138] Membrane-less organelle formation is understood in terms of biopolymer or protein solution thermodynamics; above a critical concentration, the system phase separates into protein-rich and protein-poor phases when enthalpic penalties overcome the entropic driving force for mixing,[133,138,139] resulting in a protein-rich aqueous compartment surrounded by an aqueous medium that is not bound by a membrane, surrounded by an aqueous medium. This compartment can selectively partition molecules in the protein-rich phase and exchange them with the cytoplasm in the cell interior. Related solution thermodynamic arguments apply to the phase separation of polyelectrolyte coacervate phases in aqueous solutions, which are also able to host proteins.[140,141] Furthermore, in this context, stable ATPS droplets are prime candidates as vehicles for protocells or bio-inspired cell mimics. Such systems could serve as models for the membrane-less organelle formation process and could aid in elucidation of responses to cues such as curvature, compartmentalization, pH, temperature, and ionic strength.

The Keating group has made seminal contributions in this arena. They exploit the ATPS system of PEG and dextran encapsulated within giant uni-lamellar lipid bilayer vesicles (GUVs) to serve as model cytoplasm within a synthetic cell. Both PEG and dextran serve as model biopolymers that mimic the crowded cytoplasm. Furthermore, under appropriate conditions, domains rich in dextran or PEG form, which serve as model membrane-less organelles within this model cytoplasm, Figure 6.1.[107,142,143] These

synthetic cells, or protocells, are powerful tools for modeling cell functions. Additionally, the formation of dextran-rich phases can be modulated based on the initial composition of ATPS and solution conditions. This modulation is important as a protocell model system, in which induced crowding can also be ‘turned on’ or ‘off’ based on external stimuli. Proteins partitioning from one phase into the other can be tuned in response to external stimuli such as pH and temperature, Figure 6.2.[21,108,109] Such protein partitioning studies provide insights into related biological processes like the partitioning and reaction of RNA in membrane-less organelles. This research firmly establishes ATPSs as systems that are appropriate models to study and mimic membrane-less organelles.

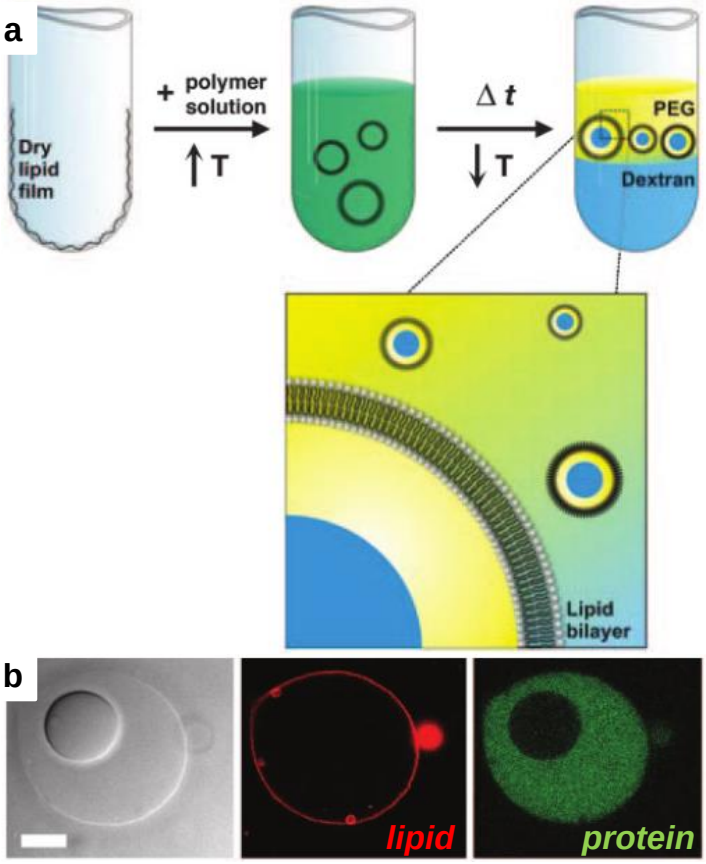

Figure 6.1. Lipid stabilized PEG/dextran ATPS emulsion. (a) Emulsion formation scheme. (b) Transmitted light (Left) and fluorescent images of emulsion droplet, prepared with rhodamine-tagged lipid (center) and fluorescein-tagged streptavidin (right). Scale bar = 10 μm. Reprinted with permission from Ref 142.

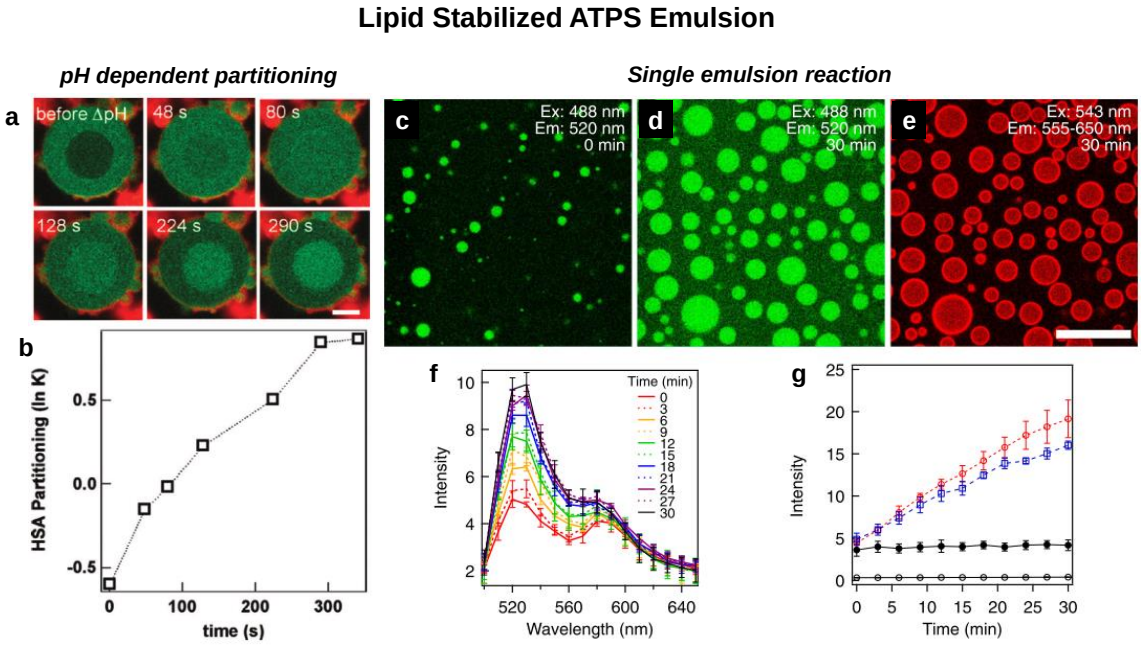

Figure 6.2. Demonstrated protein partitioning and RNA cleavage reaction within liposome-stabilized ATPS. (a) Fluorescent human serum albumin (HSA, green channel) is localized in the PEG-rich phase at pH 6.5 and partitions to the dextran-rich phase upon an increase to pH 12. Red fluorescence is rhodamine-tagged lipid. Scale bar is 5 μm. (b) Measured partitioning coefficient (ln K) with respect to time after pH change, negative ln K indicates PEG-phase affinity, positive ln K indicates dextran-phase affinity. (a)-(b) Reprinted with permission from Ref 108. (c) Initial fluorescein channel image and (d) 30 min after reaction has started, demonstrating an increase in donor intensity in the PEG-rich phase. (e) Rhodamine channel at t = 30 min, includes acceptor fluorescence and liposome tags. Scale bar is 25 μm, applies to (c)-(e). (f) Fluorescence emission spectra (Ex: 488 nm) from PEG-rich phase, which come both from a decrease in quenching (due to the reaction) and an increase in PEG-phase concentration due to re-partitioning. (g) Reaction progress monitored in PEG-rich phase by summing intensity from 520 and 530 nm to capture donor peak, without lipid-membranes (red data), with lipid membranes (blue data), and without enzyme degradation (no reaction, black line). (c)-(g) Reprinted with permission from Ref 21.

In addition to this research, which exploits GUVs filled with ATPS, there has been significant activity focused on other ATPS droplets or capsules with differing levels of complexity, with increasing control over the size, shape, and composition of the final structure as well as the transport properties of the shell that encapsulates ATPS-based

structures. Moreover, the protocell concept has inspired materials science research to imbue these assemblies with functionalities that go beyond biology by incorporation of synthetic materials such as nanoparticles and other non-biological materials.

6.2.1 Creating ATPS droplets and dispersions

To exploit ATPS droplets, reliable means to form them with control over their size and morphology are required, a task that presents unique challenges due to the ultra-low tension of aqueous-aqueous interfaces.[5,144,145] Unfortunately, microfluidic methods that rely on jet break up for drop formation that have proven robust for immiscible fluids like oil and water systems are not well suited to this purpose.[113] The physics of drop formation by jet break up relies on a balance of the viscous/inertial forces that form the jet and the interfacial tension that drives its break up into droplets.[146–148] For very low tensions, the viscous and inertial forces dominate, and the jet remains intact.

To overcome this challenge, a number of techniques have been developed to introduce new effects to create water-water droplets based on ATPS as summarized in Figure 6.3.[130] A simple flow focusing device that relies on gravity to drive the dispersed phase through the device at low flow rates and generate weak viscous and inertial forces enables water-in-water drop formation.[149] Despite the low droplet generation rate, the device creates monodisperse droplets with a coefficient of variation (CV, i.e. polydispersity) of 1-10% (Figure 6.3a). Higher droplet generation rates in microfluidic devices are enabled by perturbing the inlet stream of the dispersed phase periodically to induce droplet breakup with the Rayleigh-Plateau instability (Figure 6.3b-c). In this

scheme, the stream can be pulsed (Figure 6.3b),[150] or distrubed mechanically[151,152] or piezo-electrically[111,153] (Figure 6.3c) to create monodisperse droplets.

There is a particularly ingenious method that bypasses the challenges associated with ultra-low interfacial tensions to create water-in-water emulsions from ATPSs. In the all-aqueous electrospray (AAE) technique,[98,130] the drop-forming aqueous phase is sprayed into air, taking advantage of the elevated surface tension of the air-water interface to form dispersed droplets; once formed, the droplets fall through air into a bath containing the external aqueous phase (Figure 6.3d). AAE relies on charging the dispersed phase, and placing an electrode of opposite charge away from a capillary; a jet forms that rapidly disintegrates into discrete droplets smaller than those formed in a simple gravitational dripping regime. Like other microfluidic techniques, the droplet size and the rate are highly controllable based on a number of variables such as the field strength, capillary dimeter, and injection rate. The AAE technique was used for capsule formation in Chapters 3-5.

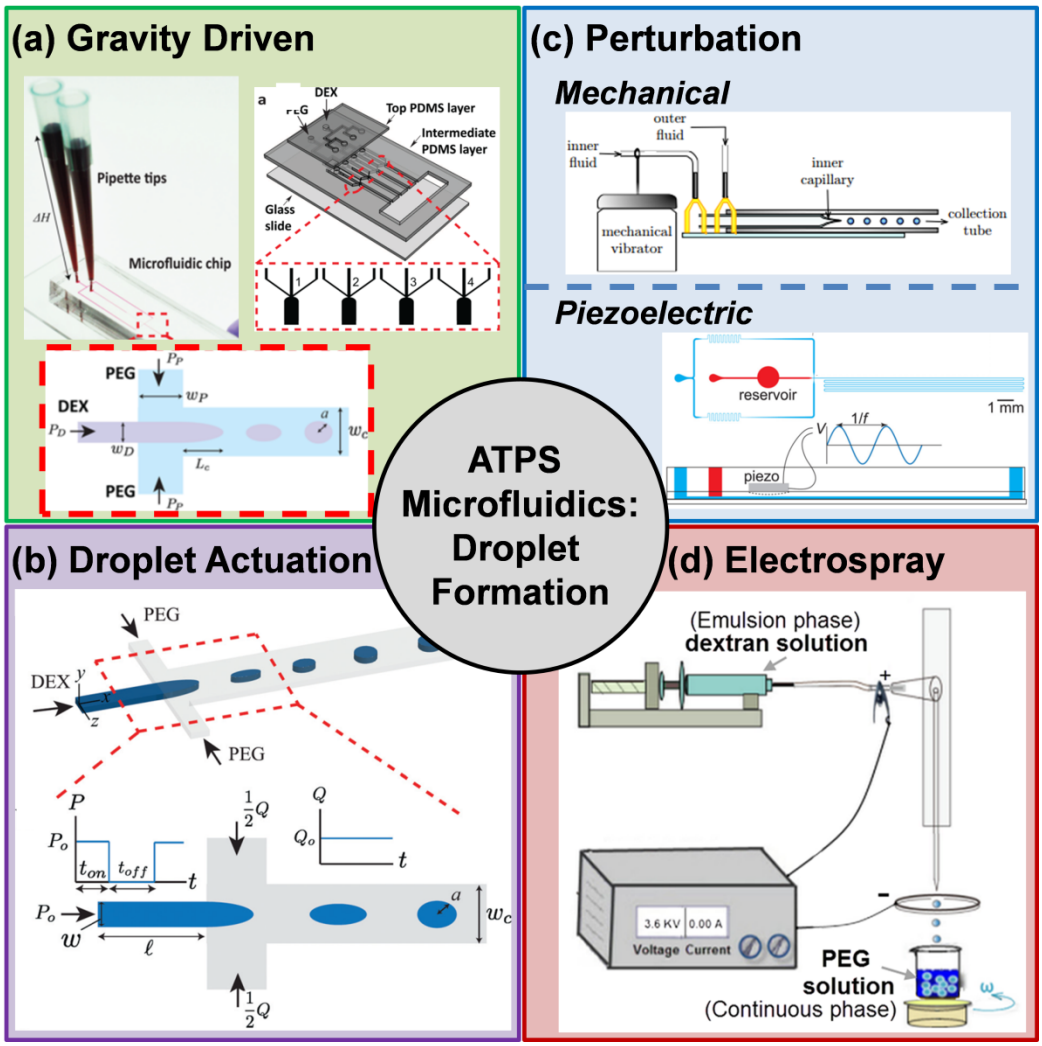

Figure 6.3. Summary of ATPS microfluidic techniques to create monodisperse water-in-water droplets. (*a, Gravity Driven)* PDMS device in which inlet pressure is controlled by hydrostatic pressure of fluids in inlet reservoirs. Low inlet pressure enables droplet breakup due to lower viscous/inertial forces. Reprinted with permission from Ref 149. *(b, Droplet Actuation)* The inner phase (DEX) is pulsed periodically to induce droplet breakup. Reprinted with permission from Ref 152. *(c, Perturbation) (Mechanical)* The tubing of the inner fluid is perturbed with a mechanical vibrator to induce droplet breakup within a glass capillary device. Reprinted with permission from Ref 151. *(Piezoelectric)* A piezoelectric bending disc is positioned at the inlet channel into the PDMS device. Sinusoidal voltage is applied, to which the bending disc periodically contracts and relaxes, resulting in a constricted and relaxed channel width, leading to droplet breakup. Reprinted with permission from Ref 153. *(d, Electrospray)* Emulsion phase is charged and injected into a glass capillary device, which is then pulled out into the continuous phase through an oppositely charged electrode. Reprinted with permission from Ref 98.

6.2.2 Stabilizing ATPS droplets

Once generated, to prove useful as biological hosts for substantial times, the all aqueous drops must be stabilized. Once again, the ultra-low tension of the ATPSs poses unique challenges, as most stabilization strategies developed for oil-water systems rely on the appreciable interfacial tension between the two phases and exploit the distinct chemical differences of the dispersed and continuous phases.[9] These include the adsorption of surfactants, macromolecules or stabilizing ligands, or the trapping of dense layers of particles at the interface to impart repulsion and suppress coalescence. To stabilize all-water emulsions, more careful material selection is typically required due to lack of strong driving force to induce adsorption of molecules and materials to the interface. Here, we focus on the interfacial complexation of oppositely charged species to stabilize these ATPS-based emulsions. While there have been some successes in creating ATPS Pickering emulsions,[18–20,78,154] and the aforementioned studies in which ATPS droplets are formed within GUVs, this thesis has focused on artificial membrane-like materials including polyelectrolyte-polyelectrolyte shells, and nanoparticle-polyelectrolyte shells.

Chapter 3 developed a powerful approach to stabilize ATPS via polyelectrolyte complexation. In this approach, oppositely charged polyelectrolytes (PEs) are introduced from the two aqueous phases, which meet and complex at the interface. Due to the all-aqueous nature, PEs are soluble in both phases, affording great flexibility in material choice. Due to the inherent miscibility of the complexing agents however, the flux of the PEs must be balanced to create stable microcapsules, and partitioning of the two PEs in the two phases need to be taken into account. If the flux of two PEs from respective

phases toward the interface is unbalanced, complexation occurs away from the interface, either within the dispersed droplets or in the continuous phase as shown in Figure 3.4 and Figure 3.6. The composition of these particles can be influenced by the equilibrium partitioning in each phase, as illustrated in Figure 6.4.[64,91] PSS, which favorably partitions to the dextran phase, originally placed in the continuous phase (Figure 6.4a-c) results in microcapsule formation, and fluorescently tagged PE is found only at the PEG-dextran interface. In contrast (Figure 6.4d-f), microgel particles will form if the PSS is originally placed in the droplet-phase all else constant, and fluorescently tagged PE is found throughout the droplet phase. Complexation of two oppositely charged PEs has also been induced in the middle phase of water-in-water-in-water double emulsions prepared using a microfluidic device. In this scheme, one polyelectrolyte is added to the outer phase, and an oppositely charged PE is added to the inner phase; the middle aqueous phase serves as a 'complexation zone', Figure 6.5.[117] While this drop formation mechanism is more complex, it affords control of the complexation location without relying as heavily on balancing the fluxes of the two PEs.

These stabilization techniques based on interfacial complexation have several advantages, including rapid complexation, diverse materials options, and scalable single-step processing. The PE/PE microcapsules have flexible and elastic membranes that can support pressure differences, as evidenced by their ability to wrinkle and expand under osmotic stresses. The polyelectrolyte complex layer is also permeable, allowing chemical exchange between the interior and exterior of the microcapsule. Finally, these capsules

are stimuli-responsive; the electrostatic interactions can be modulated using external stimuli such as pH and ionic strength.

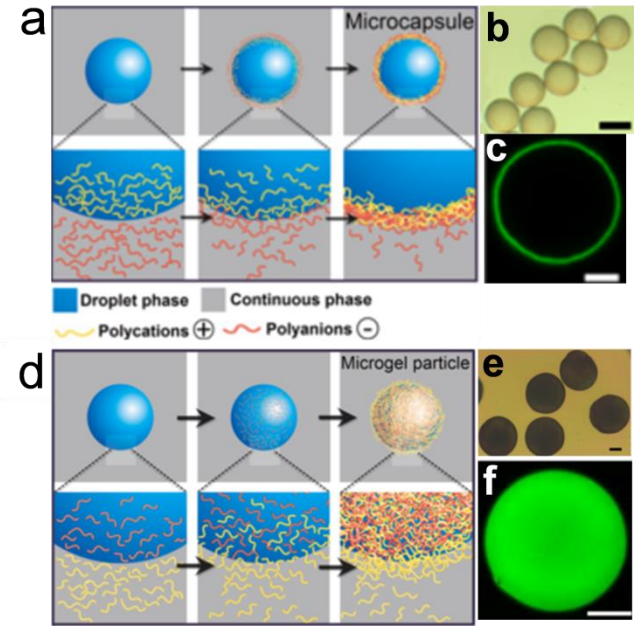

Figure 6.4. Microcapsule and microgel formation from strong and weak polyelectrolytes generated by AAE. (a) Schematic of microcapsule formation from interfacial complexation. (b) Optical and SEM images of *(1-2)* PSS and poly(allylamine hydrochloride) (PAH) and (3-4) PSS and PDADMAC. Scale bars 300 μm. (c) Confocal images of PSS-PAH capsules with varying shell thicknesses based on varying PE concentration, plotted in (d) Fluorescent signal is from FITC-PAH. Scale bars 50 μm. (e) Schematic of microgel particle formation based on internal complexation. (f) Optical micrograph of PAH-PSS microgel particle. (g) Confocal image of PAH-PSS particle fabricated with FITC-PAH. Scale bars 100 μm. Reprinted with permission from Ref 91.

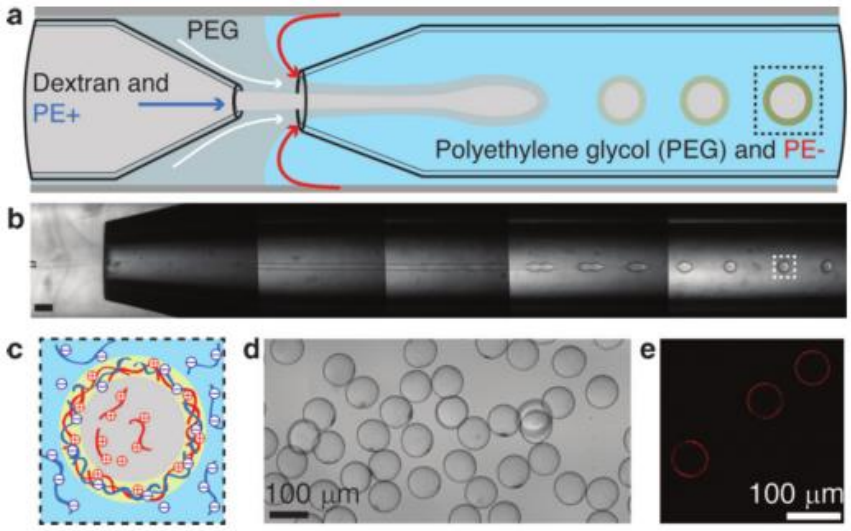

Figure 6.5. Polyelectrolyte complexation in middle aqueous phase within a water-in-water-in-water double emulsion. (a) Schematic of glass capillary microfluidic device used to fabricate microcapsules. (b) Optical micrograph of droplet breakup. (c) Illustration of complexation of PDADMAC and PSS occurring in the middle water phase, the 'complexation zone'. (d) Optical micrograph of final capsules. (e) Fluorescent image of capsule shells labeled with ethidium homodimer. Reprinted with permission from Ref 116.

As demonstrated in Chapter 4, the functionality of these ATPS-derived capsules can be further enhanced via the introduction of nanoparticles (NPs) in the shell, in which the NPs can provide catalytic, luminescent, magnetic or other useful properties. Incorporation of NPs in the shell can be accomplished by inducing interfacial complexation between a PE of one charge and an oppositely charged NP, as presented in Chapter 4. The inclusion of SiO_2 NPs results in brittle outer shells rather than flexible membranes as evidenced by their rupture under osmotic stress and the mechanical properties of the NP-laden shell can be modulated, as discussed below.

Not only does the incorporation of NPs change shell mechanics and afford new functionality, but it also provides an unexpected pathway to scalable formation of

encapsulated all aqueous double emulsions. When a PE is added to the droplet (dextran) phase and SiO_2 NPs to the continuous (PEG) phase, the formation of a PE/NP microcapsule was accompanied by the spontaneous inclusion of a droplet made of the outer aqueous phase (PEG) within the PE/NP microcapsule. The formation of such encapsulated double emulsions results from rapid formation of PE/NP complex layer (Figure 4.4a), followed by displacement of water from the inner phase and concomitant influx of the continuous phase through the PE/NP shell due to osmotic pressure imbalance (Figure 4.4b), until the permeability of the PE/NP shell is significantly reduced (Figure 4.4c). These all water emulsion-bodies, or AWE-somes, have several features that resemble the basic structure and functionality of the cell. The spontaneously formed droplets within the AWE-some do not have membranes, like the membrane-less organelles found in the cell. Molecules can be selectively compartmentalized in the included droplet and undergo reaction in response to an agent that permeates through the PE/NP shell, as described in Section 6.2.3.

The structure and properties of AWE-somes can be further enhanced and tailored for applications requiring mechanical and chemical robustness and integrity. As noted above, the AWE-somes formed via interfacial complexation of oppositely charged NP and PE are surrounded by rigid shells that are prone to brittle rupture upon mechanical or osmotic perturbation. The possibility of modulating the shell properties while maintaining the spontaneous formation of AWE-somes was explored by inducing interfacial complexation between a mixture of negatively charged SiO2 NP and PSS in the external (PEG) phase with an oppositely charged PE, PDADMAC, in the droplet (dextran) phase,

as described in Chapter 5.[127] These compound AWE-somes enable the same rapid, single-step structure formation as the PE/NP AWE-somes, while enabling PE/PE microcapsule shell-like toughness making them resistant to rupture against mechanical and osmotic stresses. As shown in Figure 5.3, the inclusion of even a small amount of PE in the continuous phase results in the incorporation of both anionic species in the mebrane. Moreover, these compound AWE-somes are able to maintain their structure in high ionic strength solutions unlike PE/NP AWE-somes that disintegrate in such an environment. These features are important especially for the application of AWE-somes as protocells in which the shell may be exposed to varying temperature, pH, and ionic strength.

6.2.3 Stabilized ATPS droplets as cell mimics

Artificial cells or protocells are materials designed to recapitulate key features of biological cells, including selective partitioning of components, supporting reactions in sub-cellular compartments, and selective and controlled permeability through the encapsulating membrane.[155,156] The AWE-somes highlighted above have a significant potential to achieve many of these features. Within the AWE-somes, small molecules can diffuse and partition within the different compartments, as evidenced by selective partitioning of small fluorescent molecules, Rhodamine and fluorescein (Figure 4.9). Furthermore, a simple quenching experiment has shown that these structures are excellent candidates to induce reactions while enabling phase selectivity, Figure 4.9. These simple demonstrations show some of the basic processes of selective partitioning and reaction within sub-cellular organelles that occur within the cell and are recapitulated within these structures. The membrane is permeable to macromolecules of moderate size; thus,

sequential addition of reactive materials is possible, which would be essential in simulating the dynamic nature of biological cells. Significant potential to further enhance AWE-some functionality could be achieved via a layer-by-layer approach, as has been demonstrated for PE/PE microcapsules, which were imbued with additional PE layers[91] and for NP/PE shells, which were decorated with lysozyme, a known antibacterial agent (Figure 4.10). Cellular processes such as recognition and internalization of molecules and materials indeed depend on the membrane-associated proteins and macromolecules. The incorporation of functional molecules that can communicate across the membrane is a step in the direction of imparting such functions to AWE-some cell mimics.

6.3 Cellular-scale confinement: Cellular (micro)niches

While Section 6.2.3 addresses how AWE-some presents basic structure and functionality that are inspired by sub-cellular compartments and organelles, confinement of biological cells plays important roles at other, larger length scales. The confinement and environment of growing cells play important roles in cell fate. One example includes stem cells that respond to environmental cues that affect their differentiation pathway and function;[157] the stem cell environment is known as the cell niche. Environmental cues also impact bacterial cells; microbial miconiches within biofilms influence community dynamics and survival.[158] Artificial systems that mimic cell niche and bacterial microniche studies must allow control and manipulation of the cell environment and means to probe cell response.

Although there are successful examples of microbial microniches within oil-water systems,[72,96] structures comprising ATPS like those discussed in this thesis can be versatile vehicles as cell niches or microbial microniches. Such systems can sequester cells, allow partitioning and exchange of biomolecules between multiple compartments, and allow for controlled environment. Indeed, driven in part by the need to pattern and localize cell growth for applications in niche studies and tissue engineering,[159–163] there is now significant understanding of how cells and cell materials partition within ATPSs (Figure 6.6).[11,164] During equilibration of an ATPS made of PEG and dextran, mammalian cells partition to either the PEG-rich or dextran-rich phase, or the interface (Figure 10a). The differential partitioning of cells is a function of interfacial tension, controlled by ATPS composition, and cell type, which affects the cell surface chemistry (Figure 10b-c). Similarly, studies have demonstrated that ATPS can be used to pattern cells into (micro)niches to enable investigation of cell interactions.[14,16]

The structures formed via interfacial complexation in ATPS described in this thesis may be particularly interesting as niches or microniches for cell encapsulation, as they allow for rapid exchange of media or solvent while protecting their cargo from external forces. PE/PE microcapsules have been shown to successfully encapsulate bacteria and maintain moderate growth with minimal media. Moreover, the cellular function, in this case the cell viability, could be probed by adding a fluorescent probe in the external phase and letting it permeate into the PE/PE capsule lumen as shown in Figure 3.9. The growth of the cells can be improved upon by including non-bacteriocidal membrane forming components, such as polypeptides.

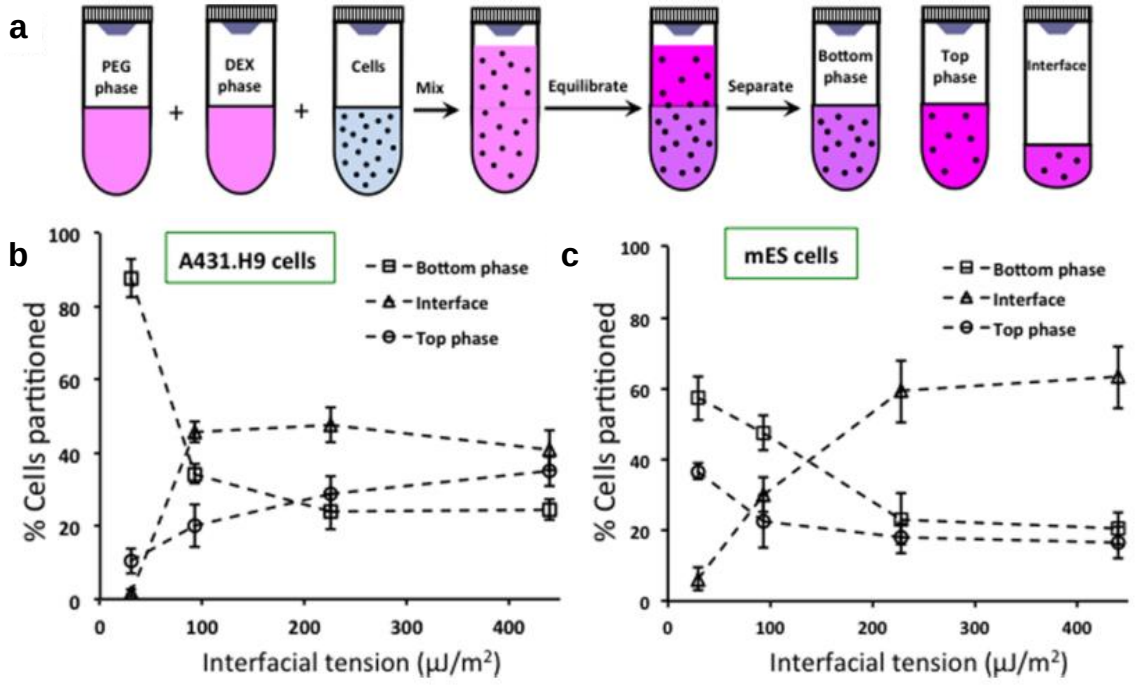

Figure 6.6. Cell partitioning as a function of interfacial tension in the PEG/dex ATPS. (a) Schematic of experimental setup. (b)-(c) Cell partitioning behavior for two different cell types as a function of interfacial tension. Reprinted with permission from Ref 11.

Mammalian cells have been successfully encapsulated in unstable ATPS droplets,[149] therefore stable ATPS structures should be able to support mammalian cells and also enable long-term study of cell dynamics. In this case, compound AWE-somes are extremely promising candidates because of their stability against changes in the salt and pH conditions. Additionally, the possibility of imparting new functionality through the incorporation of synthetic nanoparticles with unique properties and functional proteins provides an exciting and yet-to-be explored potential to control the cellular fate within the cellular niche.

6.4 Conclusions and Outlook

ATPSs provide numerous attributes, in particular biocompatibility, making them a versatile platform to produce compartments that can form the basis for cell mimicry and (micro)niche studies. This chapter highlighted the recent advances in understanding and exploiting interfacial complexation in ATPS to enable the production of microcapsules and all water emulsion bodies (AWE-somes). The thermodynamics as well as transport and interfacial phenomena in ATPS must be taken into consideration to enable control over the resulting structures in this approach. Results summarized here clearly demonstrate that there is a significant potential for using these ATPS-derived structures for more complex biomimicry and biological studies.

Moreover, new opportunities to create systems with functionality and properties that go beyond those of the living cell exist. Inclusion of weak PEs whose degree of ionization depends strongly on the local pH, for example, will enable AWE-somes with pH-sensitive structure and properties. Inclusion of canonical and non-canonical biomacromolecules such as proteins, DNA, or polypeptides will imbue ATPS-derived AWE-somes with additional biological functionality and responsiveness. Also, the burgeoning field of intrinsically disordered proteins and their phase behaviors presents new opportunities to build membrane-less organelles in AWE-somes.[138,139,165] Another potential variation on the capsules highlighted in this article is to include hydrogel-like droplet phases, analogous to the alginate-complex systems.[65,166–170] Such high viscosity microenvironments are important for stem cell niche applications in which the mechanobiology of cells plays a major role in determining the cell fate.[171] Synthetic

nanoparticles can also imbue these AWE-somes with useful functionality. Once biomolecules such as proteins and enzymes are incorporated into AWE-somes, these capsules can serve as an unloading vessel, in which a stimulus can induce the release of the complexed materials. To enable such applications, it will be imperative to study the impact of interfacial complexation on the activity of enzymes or proteins.[117,172,173] Another intriguing possibility that has been barely explored is the potential of inducing interfacial complexation in aqueous mixtures that are out-of-equilibrium or that are triggered to undergo phase separations. Quenching of phase separating system via interfacial complexation could potentially lead to bicontinuous structures akin to those recently developed based on bicontinuous interfacially jammed emulsion gels.[51]

To fully realize these potentials, more detailed studies in various fundamental aspects involving interfacial complexation in ATPS are necessary. The growth mechanism of these interfacial complex layers is yet to be understood. Results thus far indicate that these interfacial complex layers can grow to be quite thick (> 100s' of nm), suggesting that there is continued complexation of the two oppositely charged species beyond the first few molecular layers. Such a process must accompany the diffusion of PEs within the growing layer. Whether this process is thermodynamically or kinetically limited remains an open question. Also more detailed understanding on the effect of assembly conditions and materials on the mechanical and transport properties is currently lacking and warrants future investigation. One of the key features that various biological membranes exhibit is their fluidity. In fact, fluidity is an essential property that enables various cellular functions such as focal adhesion formation and regulation of membrane

permeability.[174,175] Thus, efforts to understand and engineer the fluidity of the interfacial complex membranes in ATPS would be extremely valuable. The field of layer-by-layer (LbL) assembly has accumulated a tremendous amount of knowledge and understanding that is likely to be highly relevant.[176] However, it will be also important to discern the differences between LbL-based complexes and those prepared via interfacial complexation. All these efforts would also substantially benefit from recent advances in understanding the charge-based interactions and complexation based on computational and modeling-based efforts.

To extend on the structures built in Chapters 3-5, a few different strategies may be employed. First, experimenting with different compositions of PEG and dextran (rather than only 10% and 15%) closer to the critical point will enable phase transitions within the microcapsule lumen, as an alternative route to inducing multiple compartments. Additionally, pre-equilibrating the solutions with their respective complexing agents will reduce the osmotic imbalance between the two phases, which may be an important consideration for including living cells.

An important extension of the AWE-somes is to create capsules with a PEG continuous phase and a dextran droplet. Swapping the phases is important for protocell studies in which selective reactions will take place in droplet (nucleus) phase as DNA, RNA and many proteins natively prefer the dextran phase. To accomplish this swap, the main system characteristics to consider are that the droplet phase viscosity must be greater than the continuous phase and the interfacial tension between the two phases must

remain enough to keep the droplet stable during film formation. Lower molecular weight dextran will be useful in accomplishing this goal.

Although there is work to be done to further develop these systems into the aforementioned spaces, interfacial complexation in ATPS is a powerful platform upon which biomimetic and biofunctional structures may be built. Extending the functionality with some of these future directions will enable the design of even more sophisticated studies to elucidate the complex structure dependent properties in nature.

Appendix 1. Experimental Methods: Extra Information

A1. All-Aqueous Electrospray

The All-Aqueous Electrospray (AAE) technique was developed in Anderson Shum's Lab at the University of Hong Kong.[98] This appendix section is meant to supplement the experimental details from Chapters 3-5 to provide tips for setting up and running the AAE setup. The AAE setup requires one steel ring stand, two clamps, capillary device, copper ring, high voltage power source, two electrodes, syringe pump, syringe filled with droplet fluid, and a collecting dish filled with continuous phase fluid.

To assembly the capillary device, 1 mm outer diameter capillaries are pulled with the micropuller and sanded with 220 grit sandpaper to 150-200 μm capillary diameter opening. The capillary tips are examined under a microscope to ensure the tip is not cracked or dramatically asymmetric. Multiple capillary tips are then soaked in a 1 wt% OTS in toluene solution for 30 min. After soaking, the capillaries are heated on a hot plate (held up by a glass slide) at 70°C for 1 hour. This hydrophobic treatment aids in the droplet formation as it prevents the droplet fluid from wetting the outside of the capillary. The treated capillaries are then attached to individual glass slides with UV curable glue, at the spots indicated in Figure A1.1, and cured for at least 5 min with UV light. Next, a small notch is cut into one side of a yellow needle and the needle is centered over the blunt end of the capillary. Epoxy glue is used to hold the needle in place, Figure A1.2. After the epoxy is fully dried, the edges of the glue can be further reinforced by adding the UV glue on top, and curing with UV light once more.

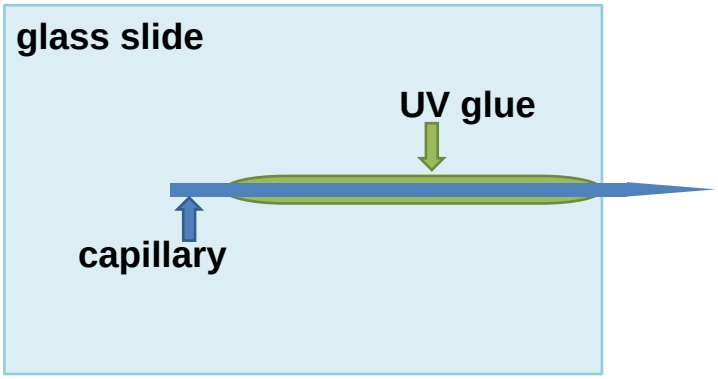

Figure A1.1. First assembly step of capillary device (top view).

Figure A1.2. Second assembly step of capillary device (side view).

This completed capillary device is attached to the higher clamp on the ring stand such that the capillary tip is facing downward. The copper ring is placed ~1 mm below the capillary tip. The collection dish (containing the continuous phase) should sit only a few cm below the capillary tip. The distance of the collection dish will affect the droplet shape, however if the dish is too far away, the electrostatic repulsion of the continuous phase can repel the droplet and redirect it outside of the collection dish. For small collections, the dish can be swirled by hand. For larger collections, the dish is placed on a stir plate with a magnetic stirrer at a rate not to exceed 200 rpm.

To start the AAE system, charge the capillary device by pushing through the syringe until the syringe fluid starts to come out of the capillary tip. Then, turn the syringe pump

and voltage source on. If a droplet gets stuck to the tip and does not start dripping out, give the syringe pump a little push (to momentarily increase the flow rate) and once the flow rate reestablishes, the droplets should drip out nicely.

For a given syringe pump fluid (15% dextran in this thesis), the size of dispersed droplets depends on the flowrate of the syringe pump, the diameter of the capillary tip, and the applied voltage. To demonstrate a change in flowrate and voltage, see Figure A1.3 and Figure A1.4.

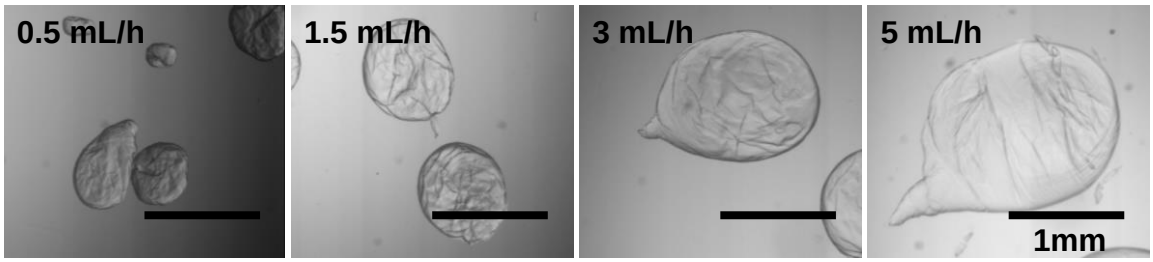

Figure A1.3. Optical micrographs of PE/PE microcapsules made at different syringe pump flowrates. Capillary tip diameter 150 μm, applied voltage 3500 V. Larger flowrates result in larger droplets, all else constant.

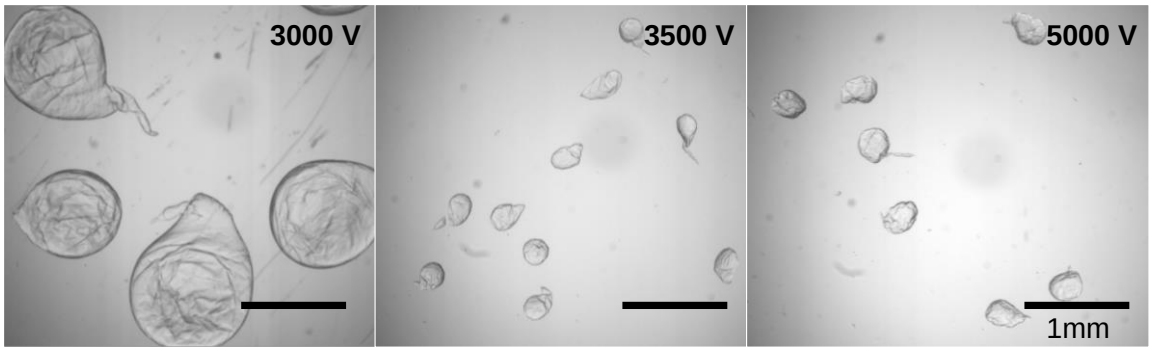

Figure A1.4. Optical micrographs of PE/PE microcapsules made at different voltages. Capillary tip diameter 150 μm, syringe flow rate 1 mL/h. In this system setup, flowrates above 3500 V are in the jetting regime, resulting in little change in droplet size above this voltage.

A2. Minimalist Media

The Minimalist Media used to supplement bacterial growth in Chapter 3 is a special composition of media used due to the low salt content. Typical medias, such as Phosphate Buffered Saline (PBS) contain near physiological salt concentrations, which at elevated temperature, destabilize the PE/PE microcapsule films. The MMS media components are listed below in Table A1.1 and Table A1.2.

Table A1.1. Components in Minimum Media Supplement (MMS) used as vitamin source in bacterial encapsulation.

Chemical	**per 1L (g)**	**Supplier**
L-Ascorbic acid	0.035	Sigma, Cat.# A92902
Sodium acetate	0.07	Sigma, Cat.# S7545
Sodium thiosulfate	0.1	Sigma, Cat.# S7026
Sodium nitrate	0.12	Sigma, Cat.# 221341
Succinic acid	0.37	Sigma, Cat.# 398055
L-Tartaric acid	0.37	Sigma, Cat.# T109
Potassium phosphate monobasic	0.68	Sigma, Cat.# P9791
Wolfe's Mineral solution	5 mL	"Home-made"

Table A1.2. Wolfe's Mineral solution components used to make MMS.

Chemical	**Cat. #**	**per 1L**
Nitrilotriacetic acid	N0128	1.5 g
$MgSO_4$	M7506	1.465 g
$MnSO_4 \cdot H_2O$	M7634	0.5 g
NaCl	S6191	1.0 g
$CoCl_2 \cdot 6\ H_2O$	255599	0.1 g
$CaCl_2 \cdot 2\ H_2O$	C5080	0.1 g
$ZnSO_4 \cdot 7\ H_2O$	Z4750	0.1 g
$CuSO_4 \cdot 5\ H_2O$	C7631	0.01 g
$AlK(SO_4)_2 \cdot 12\ H_2O$	A7210	0.01 g
H_3BO_3	B0394	0.01 g
$Na_2MoO_4 \cdot 2\ H_2O$	M1003	0.01 g

Bibliography

(1) Pickering, S. U. Emulsions. *J. Chem. Soc. Trans.* **1907**, *91*, 2001–2021.

(2) *Partitioning in Aqueous Two-Phase Systems: Theory, Methods, Uses, and Applications to Biotechnology*; Walter, H., Brooks, D. E., Fisher, D., Eds.; Academic Press, Inc: Orlando, FL, 1985.

(3) Albertsson, P.-A. *Partition of Cell Particles and Macromolecules*, 3rd ed.; Wiley-Interscience: New York, 1986.

(4) Albertsson, P.-A. Chromatography and Partition of Cells and Cell Fragments. *Nature* **1956**, *177* (4513), 771–774.

(5) Ryden, J.; Albertsson, P.-A. Interfacial Tension of Dextran-Polyethylene Glycol-Water Two-Phase Systems. *J. Colloid Interface Sci.* **1971**, *37* (1), 219–222.

(6) Van Puyvelde, P.; Antonov, Y. .; Moldenaers, P. Rheo-Optical Measurement of the Interfacial Tension of Aqueous Biopolymer Mixtures. *Food Hydrocoll.* **2002**, *16* (5), 395–402.

(7) Atefi, E.; Mann, J. A.; Tavana, H. Ultralow Interfacial Tensions of Aqueous Two-Phase Systems Measured Using Drop Shape. *Langmuir* **2014**, *30*, 9691–9699.

(8) Diamond, A. D.; Hsu, J. T. Phase Diagrams for Dextran-PEG Aqueous Two-Phase Systems at 22C. *Biotechnol. Tech.* **1989**, *3* (2), 119–124.

(9) Esquena, J. Water-in-Water (W/W) Emulsions. *Curr. Opin. Colloid Interface Sci.* **2016**, *25*, 109–119.

(10) Tromp, R. H.; Vis, M.; Erné, B. H.; Blokhuis, E. M. Composition, Concentration and Charge Profiles of Water–water Interfaces. *J. Phys. Condens. Matter* **2014**, *26* (46), 464101.

(11) Atefi, E.; Joshi, R.; Mann, J. A.; Tavana, H. Interfacial Tension Effect on Cell Partition in Aqueous Two-Phase Systems. *ACS Appl. Mater. Interfaces* **2015**, *7* (38), 21305–21314.

(12) Byun, C. K.; Hwang, H.; Choi, W. S.; Yaguchi, T.; Park, J.; Kim, D.; Mitchell, R. J.; Kim, T.; Cho, Y. K.; Takayama, S. Productive Chemical Interaction between a Bacterial Microcolony Couple Is Enhanced by Periodic Relocation. *J. Am. Chem. Soc.* **2013**, *135* (6), 2242–2247.

(13) Tavana, H.; Jovic, A.; Mosadegh, B.; Lee, Q. Y.; Liu, X.; Luker, K. E.; Luker, G. D.; Weiss, S. J.; Takayama, S. Nanolitre Liquid Patterning in Aqueous Environments for Spatially Defined Reagent Delivery to Mammalian Cells. *Nat. Mater.* **2009**, *8* (9), 736–741.

(14) Tavana, H.; Mosadegh, B.; Takayama, S. Polymeric Aqueous Biphasic Systems for Non-Contact Cell Printing on Cells: Engineering Heterocellular Embryonic Stem Cell Niches. *Adv. Mater.* **2010**, *22* (24), 2628–2631.

(15) Yaguchi, T.; Lee, S.; Choi, W. S.; Kim, D.; Kim, T.; Mitchell, R. J.; Takayama, S. Micropatterning Bacterial Suspensions Using Aqueous Two Phase Systems. *Analyst* **2010**, *135* (11), 2848–2852.

(16) Yaguchi, T.; Dwidar, M.; Byun, C. K.; Leung, B.; Lee, S.; Cho, Y. K.; Mitchell, R. J.; Takayama, S. Aqueous Two-Phase System-Derived Biofilms for Bacterial Interaction Studies. *Biomacromolecules* **2012**, *13* (9), 2655–2661.

(17) Buzza, D. M. A.; Fletcher, P. D. I.; Georgiou, T. K.; Ghasdian, N. Water-in-Water Emulsions Based on Incompatible Polymers and Stabilized by Triblock Copolymers-Templated Polymersomes. *Langmuir* **2013**, *29* (48), 14804–14814.

(18) Vis, M.; Opdam, J.; van 't Oor, I. S. J.; Soligno, G.; Van Roij, R.; Tromp, R. H.; Erné, B. H. Water-in-Water Emulsions Stabilized by Nanoplates. *ACS Macro Lett.* **2015**, *4* (9), 965–968.

(19) Peddireddy, K. R.; Nicolai, T.; Benyahia, L.; Capron, I. Stabilization of Water-in-Water Emulsions by Nanorods. *ACS Macro Lett.* **2016**, *5*, 283–286.

(20) Nguyen, B. T.; Nicolai, T.; Benyahia, L. Stabilization of Water-in-Water Emulsions by Addition of Protein Particles. *Langmuir* **2013**, *29* (34), 10658–10664.

(21) Dewey, D. C.; Strulson, C. A.; Cacace, D. N.; Bevilacqua, P. C.; Keating, C. D. Bioreactor Droplets from Liposome-Stabilized All-Aqueous Emulsions. *Nat. Commun.* **2014**, *5*, 4670.

(22) Balakrishnan, G.; Nicolai, T.; Benyahia, L.; Durand, D. Particles Trapped at the Droplet Interface in Water-in-Water Emulsions. *Langmuir* **2012**, *28* (14), 5921–5926.

(23) Choi, J.; Rubner, M. F. Influence of the Degree of Ionization on Weak Polyelectrolyte Multilayer Assembly. *Macromolecules* **2005**, *38* (1), 116–124.

(24) Fu, J.; Schlenoff, J. B. Driving Forces for Oppositely Charged Polyion Association in Aqueous Solutions: Enthalpic, Entropic, but Not Electrostatic. *J. Am. Chem. Soc.* **2016**, *138* (3), 980–990.

(25) Gao, C.; Leporatti, S.; Moya, S.; Donath, E.; Mohwald, H. Stability and Mechanical Properties of Polyelectrolyte Capsules Obtained by Stepwise Assembly of Poly (Styrenesulfonate Sodium Salt) and Poly (Diallyldimethyl Ammonium) Chloride onto Melamine Resin Particles. *Thin Solid Films* **2001**, *17* (11), 3491–3495.

(26) Zhang, R.; Zhang, Y.; Antila, H. S.; Lutkenhaus, J. L.; Sammalkorpi, M. Role of Salt and Water in the Plasticization of PDAC/PSS Polyelectrolyte Assemblies. *J. Phys. Chem. B* **2017**, *121* (1), 322–333.

(27) Ibarz, G.; Dähne, L.; Donath, E.; Möhwald, H. Controlled Permeability of Polyelectrolyte Capsules via Defined Annealing. *Chem. Mater.* **2002**, *14* (10), 4059–4062.

(28) Ferreira, M.; Cheung, J. H.; Rubner, M. F. Molecular Self-Assembly of Conjugated Polyions: A New Process for Fabricating Multilayer Thin Film Heterostructures. *Thin Solid Films* **1994**, *244*, 806–809.

(29) Kotov, N. A.; Dekany, I.; Fendler, J. Layer-by-Layer Self-Assembly of Polyelectrolyte-Semiconductor Nanoparticle Composite Films. *J. Phys.* **1995**, *99*, 13065–13069.

(30) Lee, D.; Rubner, M. F.; Cohen, R. E. All-Nanoparticle Thin-Film Coatings. *Nano Lett.* **2006**, *6* (10), 2305–2312.

(31) Richardson, J. J.; Cui, J.; Björnmalm, M.; Braunger, J. A.; Ejima, H.; Caruso, F. Innovation in Layer-by-Layer Assembly. *Chem. Rev.* **2016**, *116* (23), 14828–14867.

(32) Kaufman, G.; Boltyanskiy, R.; Nejati, S.; Thiam, A. R.; Loewenberg, M.; Dufresne, E. R.; Osuji, C. O. Single-Step Microfluidic Fabrication of Soft Monodisperse Polyelectrolyte Microcapsules by Interfacial Complexation. *Lab Chip* **2014**, *14* (18), 3494–3497.

(33) Kaufman, G.; Nejati, S.; Sarfati, R.; Boltyanskiy, R.; Loewenberg, M.; Dufresne, E. R.; Osuji, C. O. Soft Microcapsules with Highly Plastic Shells Formed by Interfacial Polyelectrolyte–nanoparticle Complexation. *Soft Matter* **2015**, *11* (38), 7478–7482.

(34) Kim, M.; Yeo, S. J.; Highley, C. B.; Burdick, J. A.; Yoo, P. J.; Doh, J.; Lee, D. One-Step Generation of Multifunctional Polyelectrolyte Microcapsules via Nanoscale Interfacial Complexation in Emulsion (NICE). *ACS Nano* **2015**, *9* (8), 8269–8278.

(35) Tettey, K. E.; Yee, M. Q.; Lee, D. Layer-by-Layer Assembly of Charged Particles in Nonpolar Media. *Langmuir* **2010**, *26* (12), 9974–9980.

(36) Hann, S. D.; Goulian, M.; Lee, D.; Stebe, K. J. Trapping and Assembly of Living Colloids at Water-Water Interfaces. *Soft Matter* **2015**, *11* (9), 1733–1738.

(37) Kralchevsky, P.; Paunov, V.; Ivanov, I.; Nagayama, K. Capillary Meniscus Interaction between Colloidal Particles Attached to a Liquid—fluid Interface. *J. Colloid Interface Sci.* **1992**, *151*, 79–94.

(38) Bowden, N. Self-Assembly of Mesoscale Objects into Ordered Two-Dimensional Arrays. *Science* **1997**, *276* (5310), 233–235.

(39) Stamou, D.; Duschl, C.; Johannsmann, D. Long-Range Attraction between Colloidal Spheres at the Air-Water Interface: The Consequence of an Irregular Meniscus. *Phys. Rev. E* **2000**, *62* (4), 5263–5272.

(40) Loudet, J. C.; Alsayed, A. M.; Zhang, J.; Yodh, A. G. Capillary Interactions Between Anisotropic Colloidal Particles. *Phys. Rev. Lett.* **2005**, *94* (1), 18301.

(41) Domínguez, A.; Oettel, M.; Dietrich, S. Force Balance of Particles Trapped at Fluid Interfaces. *J. Chem. Phys.* **2008**, *128* (11), 114904.

(42) Lewandowski, E. P.; Cavallaro, M.; Botto, L.; Bernate, J. C.; Garbin, V.; Stebe, K. J. Orientation and Self-Assembly of Cylindrical Particles by Anisotropic Capillary Interactions. *Langmuir* **2010**, *26* (19), 15142–15154.

(43) Cavallaro, M.; Botto, L.; Lewandowski, E. P.; Wang, M.; Stebe, K. J. Curvature-Driven Capillary Migration and Assembly of Rod-like Particles. *Proc. Natl. Acad. Sci.* **2011**, *108* (52), 20923–20928.

(44) Pieranski, P. Two-Dimensional Interfacial Colloidal Crystals. *Phys. Rev. Lett.* **1980**, *45* (7).

(45) Bowden, N.; Choi, I. S.; Grzybowski, B. A.; Whitesides, G. M. Mesoscale Self-Assembly of Hexagonal Plates Using Lateral Capillary Forces : Synthesis Using the " Capillary Bond ." *J. Am. Chem. Soc.* **1999**, *121*, 5373–5391.

(46) Brugarolas, T.; Tu, F.; Lee, D. Directed Assembly of Particles Using Microfluidic Droplets and Bubbles. *Soft Matter* **2013**, *9* (38), 9046.

(47) Williams, J. M.; Wrobleski, D. A. Spatial Distribution of the Phases in Water-in-Oil Emulsions. Open and Closed Microcellular Foams from Cross-Linked Polystyrene. *Langmuir* **1988**, *4*, 656–662.

(48) Subramaniam, A. B.; Abkarian, M.; Mahadevan, L.; Stone, H. A. Colloid Science: Non-Spherical Bubbles. *Nature* **2005**, *438* (7070), 930.

(49) Binks, B. P.; Horozov, T. S. *Colloidal Particles at Liquid Interfaces*; 2008.

(50) Herzig, E. M.; White, K. A.; Schofield, A. B.; Poon, W. C. K.; Clegg, P. S. Bicontinuous Emulsions Stabilized Solely by Colloidal Particles. *Nat. Mater.* **2007**, *6* (12), 966–971.

(51) Cates, M. E.; Clegg, P. S. Bijels: A New Class of Soft Materials. *Soft Matter* **2008**, *4* (11), 2132.

(52) Bhat, S.; Tuinier, R.; Schurtenberger, P. Spinodal Decomposition in a Food Colloid-Biopolymer Mixture: Evidence for a Linear Regime. *J. Phys. Condens.*

Matter **2006**, *18* (26), L339-46.

(53) DiLuzio, W. R.; Turner, L.; Mayer, M.; Garstecki, P.; Weibel, D. B.; Berg, H. C.; Whitesides, G. M. Escherichia Coli Swim on the Right-Hand Side. *Nature* **2005**, *435* (7046), 1271–1274.

(54) Galajda, P.; Keymer, J.; Chaikin, P.; Austin, R. A Wall of Funnels Concentrates Swimming Bacteria. *J. Bacteriol.* **2007**, *189* (23), 8704–8707.

(55) Tuval, I.; Cisneros, L.; Dombrowski, C.; Wolgemuth, C. W.; Kessler, J. O.; Goldstein, R. E. Bacterial Swimming and Oxygen Transport near Contact Lines. *Proc. Natl. Acad. Sci.* **2005**, *102* (7), 2277–2282.

(56) Lemelle, L.; Palierne, J. F.; Chatre, E.; Place, C. Counterclockwise Circular Motion of Bacteria Swimming at the Air-Liquid Interface. *J. Bacteriol.* **2010**, *192* (23), 6307–6308.

(57) Frymier, P. D.; Ford, R. M. Analysis of Bacterial Swimming Speed Approaching a Solid-Liquid Interface. *Bioeng. Food, Nat. Prod.* **1997**, *43* (5), 1341–1347.

(58) Dahbi, L.; Alexander, M.; Trappe, V.; Dhont, J. K. G.; Schurtenberger, P. Rheology and Structural Arrest of Casein Suspensions. *J. Colloid Interface Sci.* **2010**, *342*, 564–570.

(59) van Gruijthuijsen, K.; Herle, V.; Tuinier, R.; Schurtenberger, P.; Stradner, A. Origin of Suppressed Demixing in Casein/xanthan Mixtures. *Soft Matter* **2012**, *8* (5), 1547.

(60) Hemar, Y.; Tamehana, M.; Munro, P. A.; Singh, H. Viscosity, Microstructure and Phase Behavior of Aqueous Mixtures of Commercial Milk Protein Products and Xanthan Gum. *Food Hydrocoll.* **2001**, *15*, 565–574.

(61) Goeddel, D. V; Kleid, D. G.; Bolivar, F.; Heyneker, H. L.; Yansura, D. G.; Crea, R.; Hirose, T.; Kraszewski, A.; Itakura, K.; Riggs, A. D. Expression in Escherichia Coli of Chemically Synthesized Genes for Human Insulin. *Proc. Natl. Acad. Sci.* **1979**, *76* (1), 106–110.

(62) Berg, H. C. Chemotaxis in Bacteria. *Annu. Rev. Biophys. Bioeng.* **1975**, *4*, 119–136.

(63) Firoozmand, H.; Rousseau, D. Tailoring the Morphology and Rheology of Phase-Separated Biopolymer Gels Using Microbial Cells as Structure Modifiers. *Food Hydrocoll.* **2014**, 1–11.

(64) Hann, S. D.; Niepa, T. H. R.; Stebe, K. J.; Lee, D. One-Step Generation of Cell-Encapsulating Compartments via Polyelectrolyte Complexation in an Aqueous Two Phase System. *ACS Appl. Mater. Interfaces* **2016**, *8* (38), 25603–25611.

(65) Mazutis, L.; Vasiliauskas, R.; Weitz, D. A. Microfluidic Production of Alginate

Hydrogel Particles for Antibody Encapsulation and Release. *Macromol. Biosci.* **2015**, *15*, 1641–1646.

(66) Zhou, J.; Pishko, M. V; Lutkenhaus, J. L. Thermoresponsive Layer-by-Layer Assemblies for Nanoparticle-Based Drug Delivery. *Langmuir* **2014**, *30*, 5903–5910.

(67) Delcea, M.; Mohwald, H.; Skirtach, A. G. Stimuli-Responsive LbL Capsules and Nanoshells for Drug Delivery. *Adv. Drug Deliv. Rev.* **2011**, *63* (9), 730–747.

(68) Orive, G.; Hernández, R. M.; Gascón, A. R.; Calafiore, R.; Chang, T. M. S.; De Vos, P.; Hortelano, G.; Hunkeler, D.; Lacík, I.; Shapiro, A. M. J.; Pedraz, J. L. Cell Encapsulation: Promise and Progress. *Nat. Med.* **2003**, *9* (1), 104–107.

(69) Rabanel, J. M.; Banquy, X.; Zouaoui, H.; Mokhtar, M.; Hildgen, P. Progress Technology in Microencapsulation Methods for Cell Therapy. *Biotechnol. Prog.* **2009**, *25* (4), 946–963.

(70) Wessel, A. K.; Hmelo, L.; Parsek, M. R.; Whiteley, M. Going Local: Technologies for Exploring Bacterial Microenvironments. *Nat. Rev. Microbiol.* **2013**, *11* (5), 337–348.

(71) Connell, J. L.; Wessel, A. K.; Parsek, M. R. Probing Prokaryotic Social Behaviors with Bacterial "Lobster Traps." *MBio* **2010**, *1* (4), 1–8.

(72) Chang, C. B.; Wilking, J. N.; Kim, S. H.; Shum, H. C.; Weitz, D. A. Monodisperse Emulsion Drop Microenvironments for Bacterial Biofilm Growth. *Small* **2015**, *11* (32), 3954–3961.

(73) Tiruvannamalai-Annamalai, R.; Armant, D. R.; Matthew, H. W. T. A Glycosaminoglycan Based, Modular Tissue Scaffold System for Rapid Assembly of Perfusable, High Cell Density, Engineered Tissues. *PLoS One* **2014**, *9* (1), 1–15.

(74) Velasco, D.; Tumarkin, E.; Kumacheva, E. Microfluidic Encapsulation of Cells in Polymer Microgels. *Small* **2012**, *8* (11), 1633–1642.

(75) Zhao, L. B.; Pan, L.; Zhang, K.; Guo, S. S.; Liu, W.; Wang, Y.; Chen, Y.; Zhao, X. Z.; Chan, H. L. W. Generation of Janus Alginate Hydrogel Particles with Magnetic Anisotropy for Cell Encapsulation. *Lab Chip* **2009**, *9* (20), 2981–2986.

(76) Leal-Calderon, F.; Schmitt, V. Solid-Stabilized Emulsions. *Curr. Opin. Colloid Interface Sci.* **2008**, *13* (4), 217–227.

(77) Kalashnikova, I.; Bizot, H.; Cathala, B.; Capron, I. New Pickering Emulsions Stabilized by Bacterial Cellulose Nanocrystals. *Langmuir* **2011**, *27* (12), 7471–7479.

(78) Lam, S.; Velikov, K. P.; Velev, O. D. Pickering Stabilization of Foams and

Emulsions with Particles of Biological Origin. *Curr. Opin. Colloid Interface Sci.* **2014**, *19* (5), 490–500.

(79) Scott, C.; Wu, D.; Ho, C.-C.; Co, C. C. Liquid-Core Capsules via Interfacial Polymerization: A Free-Radical Analogy of the Nylon Rope Trick. *J. Am. Chem. Soc.* **2005**, *127* (12), 4160–4161.

(80) Zhang, L.; Liu, P.; Ju, L.; Wang, L.; Zhao, S. Polypyrrole Nanocapsules via Interfacial Polymerization. *Macromol. Res.* **2010**, *18* (7), 648–652.

(81) Tian, J.; Yuan, L.; Zhang, M.; Zheng, F.; Xiong, Q.; Zhao, H. Interface-Directed Self-Assembly of Gold Nanoparticles and Fabrication of Hybrid Hollow Capsules by Interfacial Cross-Linking Polymerization. *Langmuir* **2012**, *28* (25), 9365–9371.

(82) Wu, C. B.; Wu, G.; Yang, X.; Liu, Y. J.; Gao, C. X.; Ji, Q. H.; Wang, M.; Chen, H. Z. Preparation of Mannitol@Silica Core-Shell Capsules via an Interfacial Polymerization Process from Water-in-Oil Emulsion. *Colloids Surfaces A Physicochem. Eng. Asp.* **2014**, *457* (1), 487–494.

(83) Antipov, A. A.; Sukhorukov, G. B.; Leporatti, S.; Radtchenko, I. L.; Donath, E.; Möhwald, H. Polyelectrolyte Multilayer Capsule Permeability Control. *Colloids Surfaces A Physicochem. Eng. Asp.* **2002**, *198–200*, 535–541.

(84) Peyratout, C. S.; Dahne, L. Tailor-Made Polyelectrolyte Microcapsules: From Multilayers to Smart Containers. *Angew. Chemie - Int. Ed.* **2004**, *43* (29), 3762–3783.

(85) Antipov, A. A.; Sukhorukov, G. B. Polyelectrolyte Multilayer Capsules as Vehicles with Tunable Permeability. *Adv. Colloid Interface Sci.* **2004**, *111*, 49–61.

(86) Sukhorukov, G.; Fery, A.; Möhwald, H. Intelligent Micro- and Nanocapsules. *Prog. Polym. Sci.* **2005**, *30*, 885–897.

(87) Johnston, A. P. R.; Cortez, C.; Angelatos, A. S.; Caruso, F. Layer-by-Layer Engineered Capsules and Their Applications. *Curr. Opin. Colloid Interface Sci.* **2006**, *11* (4), 203–209.

(88) Wang, Q.; Schlenoff, J. B. Single- and Multicompartment Hollow Polyelectrolyte Complex Microcapsules by One-Step Spraying. *Adv. Mater.* **2015**, *27* (12), 2077–2082.

(89) Koga, S.; Williams, D. S.; Perriman, A. W.; Mann, S. Peptide?nucleotide Microdroplets as a Step towards a Membrane-Free Protocell Model. *Nat. Chem.* **2011**, *3* (9), 720–724.

(90) Williams, D. S.; Koga, S.; Hak, C. R. C.; Majrekar, A.; Patil, A. J.; Perriman, A. W.; Mann, S. Polymer/nucleotide Droplets as Bio-Inspired Functional Micro-Compartments. *Soft Matter* **2012**, *8* (22), 6004–6014.

(91) Ma, Q.; Song, Y.; Kim, J. W.; Choi, H. S.; Shum, H. C. Affinity Partitioning-Induced Self-Assembly in Aqueous Two-Phase Systems: Templating for Polyelectrolyte Microcapsules. *ACS Macro Lett.* **2016**, *5*, 666–670.

(92) Epherre, R.; Goglio, G.; Mornet, S.; Duguet, E. *Hybrid Magnetic Nanoparticles for Targeted Delivery*; Elsevier Ltd., 2011.

(93) Lewis, K. Platforms for Antibiotic Discovery. *Nat. Rev. Drug Discov.* **2013**, *12* (5), 371–387.

(94) Nichols, D.; Cahoon, N.; Trakhtenberg, E. M.; Pham, L.; Mehta, A.; Belanger, A.; Kanigan, T.; Lewis, K.; Epstein, S. S. Use of Ichip for High-Throughput In Situ Cultivation of "Uncultivable" Microbial Species. *Appl. Environ. Microbiol.* **2010**, *76* (8), 2445–2450.

(95) Augustin, M. A.; Hemar, Y. Nano- and Micro-Structured Assemblies for Encapsulation of Food Ingredients. *Chem. Soc. Rev.* **2009**, *38* (4), 902–912.

(96) Niepa, T. H. R.; Hou, L.; Jiang, H.; Goulian, M.; Koo, H.; Stebe, K. J.; Lee, D. Microbial Nanoculture as an Artificial Microniche. *Sci. Rep.* **2016**, 1–9.

(97) Sehgal, A.; Seery, T. A. P. Polyelectrolyte Self-Diffusion: Fluorescence Recovery after Photobleaching of Sodium Poly(styrenesulfonate) in N-Methylformamide. *Macromolecules* **2003**, *36* (26), 10056–10062.

(98) Song, Y.; Chan, Y. K.; Ma, Q.; Liu, Z.; Shum, H. C. All-Aqueous Electrosprayed Emulsion for Templated Fabrication of Cytocompatible Microcapsules. *ACS Appl. Mater. Interfaces* **2015**, *7* (25), 13925–13933.

(99) Pozrikidis, B. C. The Instability of a Moving Viscous Drop. *J. Fluid Mech.* **1990**, *210*, 1–21.

(100) Koh, C. J.; Leal, L. G. The Stability of Drop Shapes for Translation at Zero Reynolds Number through a Quiescent Fluid. *Phys. Fluids* **1989**, *8* (1), 1309–1313.

(101) Kojima, M.; Hinch, E. J.; Acrivos, A. The Formation and Expansion of a Toroidal Drop Moving in a Viscous Fluid. *Phys. Fluids* **1984**, *19* (27), 19–32.

(102) Carmona-Ribeiro, A. M.; de Melo Carrasco, L. D. Cationic Antimicrobial Polymers and Their Assemblies. *Int. J. Mol. Sci.* **2013**, *14* (5), 9906–9946.

(103) Zhao, X.; Zhang, Y. Bacteria-Removing and Bactericidal Efficiencies of PDADMAC Composite Coagulants in Enhanced Coagulation Treatment. *Clean Soil Air Water* **2013**, *41* (1), 37–42.

(104) Hann, S. D.; Stebe, K. J.; Lee, D. All Water Emulsion-Bodies (AWE-Somes) with Permeable Shells and Selective Compartments. *ACS Appl. Mater. Interfaces* **2017**, acsami.7b05800.

(105) Brangwynne, C. P. Phase Transitions and Size Scaling of Membrane-Less Organelles. *J. Cell Biol.* **2013**, *203* (6), 875–881.

(106) Mitrea, D. M.; Kriwacki, R. W. Phase Separation in Biology; Functional Organization of a Higher Order. *Cell Commun. Signal.* **2016**, *14* (1), 1.

(107) Long, M. S.; Jones, C. D.; Helfrich, M. R.; Mangeney-Slavin, L. K.; Keating, C. D. Dynamic Microcompartmentation in Synthetic Cells. *Proc. Natl. Acad. Sci.* **2005**, *102* (17), 5920–5925.

(108) Strulson, C. A.; Molden, R. C.; Keating, C. D.; Bevilacqua, P. C. RNA Catalysis through Compartmentalization. *Nat. Chem.* **2012**, *4* (11), 941–946.

(109) Dominak, L. M.; Gundermann, E. L.; Keating, C. D. Microcompartmentation in Artificial Cells: PH-Induced Conformational Changes Alter Protein Localization. *Langmuir* **2010**, *26* (8), 5697–5705.

(110) Song, Y.; Shum, H. C. Monodisperse W/w/w Double Emulsion Induced by Phase Separation. *Langmuir* **2012**, *28* (33), 12054–12059.

(111) Ziemecka, I.; van Steijn, V.; Koper, G. J. M.; Kreutzer, M. T.; van Esch, J. H. All-Aqueous Core-Shell Droplets Produced in a Microfluidic Device. *Soft Matter* **2011**, *7* (21), 9878–9880.

(112) Clegg, P. S.; Tavacoli, J. W.; Wilde, P. J. One-Step Production of Multiple Emulsions: Microfluidic, Polymer-Stabilized and Particle-Stabilized Approaches. *Soft Matter* **2016**, *12* (4), 998–1008.

(113) Chu, L. Y.; Utada, A. S.; Shah, R. K.; Kim, J. W.; Weitz, D. A. Controllable Monodisperse Multiple Emulsions. *Angew. Chemie - Int. Ed.* **2007**, *46* (47), 8970–8974.

(114) Asenjo, J. A.; Andrews, B. A. Aqueous Two-Phase Systems for Protein Separation: A Perspective. *J. Chromatogr. A* **2011**, *1218* (49), 8826–8835.

(115) Sandrou, D. K.; Arvanitoyannis, I. S. Low-Fat/Calorie Foods: Current State and Perspectives. *Crit. Rev. Food Sci. Nutr.* **2000**, *40* (5), 427–447.

(116) de Graaf, C. Texture and Satiation: The Role of Oro-Sensory Exposure Time. *Physiol. Behav.* **2012**, *107* (4), 496–501.

(117) Zhang, L.; Cai, L.-H.; Lienemann, P. S.; Rossow, T.; Polenz, I.; Vallmajo-Martin, Q.; Ehrbar, M.; Na, H.; Mooney, D. J.; Weitz, D. A. One-Step Microfluidic Fabrication of Polyelectrolyte Microcapsules in Aqueous Conditions for Protein Release. *Angew. Chemie - Int. Ed.* **2016**, *55* (43), 13470–13474.

(118) Ow, H.; Larson, D. R.; Srivastava, M.; Baird, B. A.; Webb, W. W.; Wiesnert, U. Bright and Stable Core-Shell Fluorescent Silica Nanoparticles. *Nano Lett.* **2005**, *5* (1), 113–117.

(119) Caruso, F.; Lichtenfeld, H.; Giersig, M.; Mohwald, H. Electrostatic Self-Assembly of Silica Nanoparticle - Polyelectrolyte Multilayers on Polystyrene Latex Particles. *J. Am. Chem. Soc.* **1998**, No. 120, 8523–8524.

(120) Ling, M. M.; Wang, K. Y.; Chung, T. S. Highly Water-Soluble Magnetic Nanoparticles as Novel Draw Solutes in Forward Osmosis for Water Reuse. *Ind. Eng. Chem. Res.* **2010**, *49* (12), 5869–5876.

(121) Quant, C. A.; Marla, K. T.; Meredith, J. C. Osmotic Pressure and Chemical Potential of Silica Nanoparticles in Aqueous Poly(ethyleneoxide) Solution. *Colloids Surfaces A Physicochem. Eng. Asp.* **2008**, *317* (1–3), 129–135.

(122) Cebeci, F. Ç.; Wu, Z.; Zhai, L.; Cohen, R. E.; Rubner, M. F. Nanoporosity-Driven Superhydrophilicity: A Means to Create Multifunctional Antifogging Coatings. *Langmuir* **2006**, *22* (6), 2856–2862.

(123) Zeng, X.; Osseo-Asare, K. Partitioning Behavior of Silica in the PEG/dextran/water Aqueous Biphasic System. *Colloids Surfaces A Physicochem. Eng. Asp.* **2003**, *226*, 45–54.

(124) Yang, H.; Zhou, T.; Zhang, W. A Strategy for Separating and Recycling Solid Catalysts Based on the pH-Triggered Pickering-Emulsion Inversion. *Angew. Chemie - Int. Ed.* **2013**, *52* (29), 7455–7459.

(125) Zhang, M.; Wei, L.; Chen, H.; Du, Z.; Binks, B. P.; Yang, H. Compartmentalized Droplets for Continuous Flow Liquid-Liquid Interface Catalysis. *J. Am. Chem. Soc.* **2016**, *138* (32), 10173–10183.

(126) Tostanoski, L. H.; Chiu, Y. C.; Andorko, J. I.; Guo, M.; Zeng, X.; Zhang, P.; Royal, W.; Jewell, C. M. Design of Polyelectrolyte Multilayers to Promote Immunological Tolerance. *ACS Nano* **2016**, *10* (10), 9334–9345.

(127) Hann, S. D.; Lee, D.; Stebe, K. J. Tuning Interfacial Complexation in Aqueous Two Phase Systems with Polyelectrolytes and Nanoparticles for Compound All Water Emulsion Bodies (AWE-Somes). *Phys. Chem. Chem. Phys.* **2017**.

(128) Prosser, J. H.; Brugarolas, T.; Lee, S.; Nolte, A. J.; Lee, D. Avoiding Cracks in Nanoparticle Films. *Nano Lett.* **2012**, *12* (10), 5287–5291.

(129) Zhang, L.; Feng, G.; Zeravcic, Z.; Brugarolas, T.; Liu, A. J.; Lee, D. Using Shape Anisotropy to Toughen Disordered Nanoparticle Assemblies. *ACS Nano* **2013**, *7* (9), 8043–8050.

(130) Song, Y.; Sauret, A.; Shum, H. C. All-Aqueous Multiphase Microfluidics. *Biomicrofluidics* **2013**, *7* (6), 61301.

(131) Iqbal, M.; Tao, Y.; Xie, S.; Zhu, Y.; Chen, D.; Wang, X.; Huang, L.; Peng, D.; Sattar, A.; Shabbir, M. A. B.; Hussain, H. I.; Ahmed, S.; Yuan, Z. Aqueous Two-

Phase System (ATPS): An Overview and Advances in Its Applications. *Biol. Proced. Online* **2016**, *18* (1), 18.

(132) Jue, E.; Yamanishi, C. D.; Chiu, R. Y. T.; Wu, B. M.; Kamei, D. T. Using an Aqueous Two-Phase Polymer-Salt System to Rapidly Concentrate Viruses for Improving the Detection Limit of the Lateral-Flow Immunoassay. *Biotechnol. Bioeng.* **2014**, *111* (12), 2499–2507.

(133) Banani, S. F.; Lee, H. O.; Hyman, A. A.; Rosen, M. K. Biomolecular Condensates: Organizers of Cellular Biochemistry. *Nat. Rev. Mol. Cell Biol.* **2017**.

(134) Discher, B. M.; Won, Y.-Y.; Ege, D. S.; Lee, J. C.-M.; Bates, F. S.; Discher, D. E.; Hammer, D. A. Polymersomes : Tough Vesicles Made from Diblock Copolymers. *Science* **1999**, *284* (5417), 1143–1146.

(135) Kamat, N. P.; Katz, J. S.; Hammer, D. A. Engineering Polymersome Protocells. *J. Phys. Chem. Lett.* **2011**, *2* (13), 1612–1623.

(136) Tsumoto, K.; Nomura, S.-I. M.; Nakatani, Y.; Yoshikawa, K. Giant Liposome as a Biochemical Reactor: Transcription of DNA and Transportation by Laser Tweezers. *Langmuir* **2001**, *17* (23), 7225–7228.

(137) Dominak, L. M.; Keating, C. D. Polymer Encapsulation within Giant Lipid Vesicles. *Langmuir* **2007**, *23*, 7148–7154.

(138) Brangwynne, C. P.; Tompa, P.; Pappu, R. V. Polymer Physics of Intracellular Phase Transitions. *Nat. Phys.* **2015**, *11* (11), 899–904.

(139) Elbaum-Garfinkle, S.; Kim, Y.; Szczepaniak, K.; Chen, C. C.-H.; Eckmann, C. R.; Myong, S.; Brangwynne, C. P. The Disordered P Granule Protein LAF-1 Drives Phase Separation into Droplets with Tunable Viscosity and Dynamics. *Proc. Natl. Acad. Sci.* **2015**, *112* (23), 7189–7194.

(140) Qin, J.; Priftis, D.; Farina, R.; Perry, S. L.; Leon, L.; Whitmer, J.; Hoffmann, K.; Tirrell, M.; De Pablo, J. J. Interfacial Tension of Polyelectrolyte Complex Coacervate Phases. *ACS Macro Lett.* **2014**, *3* (6), 565–568.

(141) Black, K. A.; Priftis, D.; Perry, S. L.; Yip, J.; Byun, W. Y.; Tirrell, M. Protein Encapsulation via Polypeptide Complex Coacervation. *ACS Macro Lett.* **2014**, *3* (10), 1088–1091.

(142) Aumiller, W. M.; Davis, B. W.; Keating, C. D. Phase Separation as a Possible Means of Nuclear Compartmentalization. In *International Review of Cell and Molecular Biology*; 2014; Vol. 307, pp 109–149.

(143) Keating, C. D. Aqueous Phase Separation as a Possible Route to Compartmentalization of Biological Molecules. *Acc. Chem. Res.* **2012**, *45* (12), 2114–2124.

(144) Atefi, E.; Fyffe, D.; Kaylan, K. B.; Tavana, H. Characterization of Aqueous Two-Phase Systems from Volume and Density Measurements. *J. Chem. Eng. Data* **2016**, *61* (4), 1531–1539.

(145) Simeone, M.; Alfani, a.; Guido, S. Phase Diagram, Rheology and Interfacial Tension of Aqueous Mixtures of Na-Caseinate and Na-Alginate. *Food Hydrocoll.* **2004**, *18* (3), 463–470.

(146) Anna, S. L. Droplets and Bubbles in Microfluidic Devices. *Annu. Rev. Fluid Mech.* **2016**, *48* (1), 285–309.

(147) Garstecki, P.; Gitlin, I.; DiLuzio, W.; Whitesides, G. M.; Kumacheva, E.; Stone, H. A. Formation of Monodisperse Bubbles in a Microfluidic Flow-Focusing Device. *Appl. Phys. Lett.* **2004**, *85* (13), 2649–2651.

(148) Utada, A. S.; Fernandez-Nieves, A.; Stone, H. A.; Weitz, D. A. Dripping to Jetting Transitions in Coflowing Liquid Streams. *Phys. Rev. Lett.* **2007**, *99* (9), 94502.

(149) Moon, B.-U.; Abbasi, N.; Jones, S. G.; Hwang, D. K.; Tsai, S. S. H. Water-in-Water Droplets by Passive Microfluidic Flow Focusing. *Anal. Chem.* **2016**, *88* (7), 3982–3989.

(150) Moon, B.-U.; Jones, S. G.; Hwang, D. K.; Tsai, S. S. H. Microfluidic Generation of Aqueous Two-Phase System (ATPS) Droplets by Controlled Pulsating Inlet Pressures. *Lab Chip* **2015**, *15* (11), 2437–2444.

(151) Sauret, A.; Shum, H. C. Forced Generation of Simple and Double Emulsions in All-Aqueous Systems. *Appl. Phys. Lett.* **2012**, *100* (15), 154106.

(152) Shum, H. C.; Varnell, J.; Weitz, D. A. Microfluidic Fabrication of Water-in-Water (W/w) Jets and Emulsions. *Biomicrofluidics* **2012**, *6* (1), 12808–128089.

(153) Geschiere, S. D.; Ziemecka, I.; van Steijn, V.; Koper, G. J. M.; van Esch, J. H.; Kreutzer, M. T. Slow Growth of the Rayleigh-Plateau Instability in Aqueous Two Phase Systems. *Biomicrofluidics* **2012**, *6* (2).

(154) de Freitas, R. A.; Nicolai, T.; Chassenieux, C.; Benyahia, L. Stabilization of Water-in-Water Emulsions by Plysaccharide-Coated Protein Particles. *Langmuir* **2016**, *32*, 1227–1232.

(155) Dzieciol, A. J.; Mann, S. Designs for Life: Protocell Models in the Laboratory. *Chem. Soc. Rev.* **2012**, *41* (1), 79–85.

(156) Huang, X.; Li, M.; Green, D. C.; Williams, D. S.; Patil, A. J.; Mann, S. Interfacial Assembly of Protein–polymer Nano-Conjugates into Stimulus-Responsive Biomimetic Protocells. *Nat. Commun.* **2013**, *4* (22), 6004–6014.

(157) Scadden, D. T. The Stem-Cell Niche as an Entity of Action. *Nature* **2006**, *441* (7097), 1075–1079.

(158) Hall-Stoodley, L.; Costerton, J. W.; Stoodley, P. Bacterial Biofilms: From the Natural Environment to Infectious Diseases. *Nat. Rev. Microbiol.* **2004**, *2* (2), 95–108.

(159) Fang, Y.; Frampton, J. P.; Raghavan, S.; Sabahi-Kaviani, R.; Luker, G.; Deng, C. X.; Takayama, S. Rapid Generation of Multiplexed Cell Cocultures Using Acoustic Droplet Ejection Followed by Aqueous Two-Phase Exclusion Patterning. *Tissue Eng. Part C Methods* **2012**, *18* (9), 647–657.

(160) Tavana, H.; Kaylan, K.; Bersano-Begey, T.; Luker, K. E.; Luker, G. D.; Takayama, S. Rehydration of Polymeric, Aqueous, Biphasic System Facilitates High Throughput Cell Exclusion Patterning for Cell Migration Studies. *Adv. Funct. Mater.* **2011**, *21* (15), 2920–2926.

(161) Frampton, J. P.; White, J. B.; Abraham, A. T.; Takayama, S. Cell Co-Culture Patterning Using Aqueous Two-Phase Systems. *J. Vis. Exp.* **2013**, No. 73, 16–20.

(162) Atefi, E.; Lemmo, S.; Fyffe, D.; Luker, G. D.; Tavana, H. High Throughput, Polymeric Aqueous Two-Phase Printing of Tumor Spheroids. *Adv. Funct. Mater.* **2014**, *24* (41), 6509–6515.

(163) Frampton, J. P.; Leung, B. M.; Bingham, E. L.; Lesher-Perez, S. C.; Wang, J. D.; Sarhan, H. T.; El-Sayed, M. E. H.; Feinberg, S. E.; Takayama, S. Rapid Self-Assembly of Macroscale Tissue Constructs at Biphasic Aqueous Interfaces. *Adv. Funct. Mater.* **2015**, *25* (11), 1694–1699.

(164) Madeira, P. P.; Reis, C. A.; Rodrigues, A. E.; Mikheeva, L. M.; Zaslavsky, B. Y. Solvent Properties Governing Solute Partitioning in Polymer/polymer Aqueous Two-Phase Systems: Nonionic Compounds. *J. Phys. Chem. B* **2010**, *114* (1), 457–462.

(165) Quiroz, F. G.; Chilkoti, A. Sequence Heuristics to Encode Phase Behaviour in Intrinsically Disordered Protein Polymers. *Nat. Mater.* **2015**, *14* (11), 1164–1171.

(166) Cheow, W. S.; Hadinoto, K. Biofilm-Like Lactobacillus Rhamnosus Probiotics Encapsulated in Alginate and Carrageenan Microcapsules Exhibiting Enhanced Thermotolerance and Freeze Drying Resistance. *Biomacromolecules* **2013**, *14* (9), 3214–3222.

(167) Park, J. Il; Tumarkin, E.; Kumacheva, E. Small, Stable, and Monodispersed Bubbles Encapsulated with Biopolymers. *Macromol. Rapid Commun.* **2009**, *31* (2).

(168) Anselmo, A. C.; McHugh, K. J.; Webster, J.; Langer, R.; Jaklenec, A. Layer-by-Layer Encapsulation of Probiotics for Delivery to the Microbiome. *Adv. Mater.* **2016**, *28* (43), 9486–9490.

(169) Correia, C. R.; Pirraco, R. P.; Cerqueira, M. T.; Marques, A. P.; Reis, R. L.; Mano,

J. F. Semipermeable Capsules Wrapping a Multifunctional and Self-Regulated Co-Culture Microenvironment for Osteogenic Differentiation. *Sci. Rep.* **2016**, *6* (1), 21883.

(170) Correia, C. R.; Santos, T. C.; Pirraco, R. P.; Cerqueira, M. T.; Marques, A. P.; Reis, R. L.; Mano, J. F. In Vivo Osteogenic Differentiation of Stem Cells inside Compartmentalized Capsules Loaded with Co-Cultured Endothelial Cells. *Acta Biomater.* **2017**, *53*, 483–494.

(171) Engler, A. J.; Sen, S.; Sweeney, H. L.; Discher, D. E. Matrix Elasticity Directs Stem Cell Lineage Specification. *Cell* **2006**, *126* (4), 677–689.

(172) Pippa, N.; Meristoudi, A.; Pispas, S.; Demetzos, C. Lysozyme Complexes with Thermo- and pH-Responsive PNIPAM-B-PAA Block Copolymer. *J. Nanoparticle Res.* **2017**, *19* (2), 76.

(173) Vertegel, A. A.; Siegel, R. W.; Dordick, J. S. Silica Nanoparticle Size Influences the Structure and Enzymatic Activity of Adsorbed Lysozyme. *Langmuir* **2004**, *20* (16), 6800–6807.

(174) Houk, A. R.; Jilkine, A.; Mejean, C. O.; Boltyanskiy, R.; Dufresne, E. R.; Angenent, S. B.; Altschuler, S. J.; Wu, L. F.; Weiner, O. D. Membrane Tension Maintains Cell Polarity by Confining Signals to the Leading Edge during Neutrophil Migration. *Cell* **2012**, *148* (1–2), 175–188.

(175) Gennis, R. B. Physiological Relevance of Membrane Fluidity. In *Biomembranes: Molecular Structure and Function*; Gennis, Ro. B., Ed.; Springer Science & Business Media, 2013; p 173.

(176) *Multilayer Thin Films: Sequential Assembly of Nanocomposite Materials*, 2nd ed.; Decher, G., Schlenoff, J. B., Eds.; Wiley-VCH, 2012.